Mesonic correlations and excitations in the deconfined phase of QCD

UNIVERSITÀ DEGLI STUDI DI TORINO
Dipartimento di Fisica Teorica

DOTTORATO di RICERCA in: Fisica fondamentale, applicata ed astrofisica

XVIII CICLO

TESI PRESENTATA DA:
Andrea Beraudo

TUTORS:
Prof. Wanda Maria Alberico
Prof. Alfredo Molinari

COORDINATORE DEL CICLO:
Prof. Ezio Menichetti

Anni accademici: 2002/03-2003/04-2004/05
Settore specifico-disciplinare di appartenenza: FIS/02

Abstract

In this thesis I address some issues related to the Quark Gluon Plasma (QGP) phase of QCD, i.e. the phase in which chiral symmetry is restored and the active degrees of freedom are the fundamental fields appearing in the QCD lagrangian.

I start with a brief introduction in which I first present what we know about the QCD phase diagram from the lattice data available so far and then I illustrate the main experimental signatures of the onset of deconfinement obtained in the heavy ion experiments.

In the second chapter I discuss in some details the mathematical tools employed to describe the finite temperature behaviour of a Quantum Field Theory (QFT), in particular of QCD. Specifically I discuss the main aspects of the resummation scheme referred to as *Hard Thermal Loop* (HTL) approximation.

In the second part of my thesis I deal with the two topics I addressed in my research.

The first item is the study of correlation functions of (light) mesonic currents in the deconfined phase of QCD. In particular I present the results obtained for the meson spectral functions (which display a peculiar behaviour at low energy) and the correlation functions along the (imaginary-) temporal direction.

The second topic is a quantitative study of the possible presence of $Q\overline{Q}$ (where $Q = c, b$) bound states above the deconfinement temperature. Indeed, till very recently all the $c\overline{c}$ states were supposed to melt above T_c due to the Debye screening of the potential and this fact was proposed as an unambiguous signal of deconfinement. By exploiting the available lattice data on the heavy quark free energies it is now possible to check whether the above assumption is correct. This is the subject of the last chapter of my thesis.

Chapter 1

The onset of deconfinement: lattice data and experimental signatures

1.1 The QCD phase diagram from lattice calculations

The Quantum-Chromo-Dynamic is the gauge theory which describes the strong interactions. Its lagrangian reads:

$$\mathcal{L}_{\mathrm{QCD}} = -\frac{1}{4} F^a_{\mu\nu} F^{\mu\nu}_a + i\overline{\psi}\gamma^\mu \left(\partial_\mu - igt^a A^a_\mu\right)\psi - m\overline{\psi}\psi \; , \tag{1.1}$$

where:

$$F^a_{\mu\nu} = \partial_\mu A^a_\nu - \partial_\nu A^a_\mu + g f_{abc} A^b_\mu A^c_\nu \; . \tag{1.2}$$

As it can be seen in Eq.(1.1) the fundamental fields of QCD are quarks (Ψ) and gluons (A^a_μ). In the above $t^a = \lambda^a/2$ (λ^a being the Gell-Mann matrices) are the generators of the gauge group SU(3) in the fundamental representation and f_{abc} are the structure constants of the corresponding Lie algebra. The most striking feature of strong interactions is that the degrees of freedom contained in the QCD lagrangian are not the ones which are experimentally found in nature or detected in the final stage of a high energy collision. Indeed for ordinary values of the temperature and of the baryon density the eigenstates of the QCD hamiltonian are found to be color-singlet states: mesons and baryons. The fundamental degrees of freedom are frozen, *confined* in such color-singlet states.

QCD should therefore have a non-trivial phase diagram in the temperature-chemical potential plane.

The main tool to investigate such *non perturbative* features of QCD are lattice simulations. The fundamental quantity in finite temperature QCD on the lattice is its partition function given by the following functional integral:

$$\mathcal{Z} = \int \mathcal{D}A_\mu \mathcal{D}\overline{\psi}\mathcal{D}\psi\, e^{-S_E[A_\mu, \overline{\psi}, \psi]}, \tag{1.3}$$

where S_E is the *euclidean action* associated to a certain field configuration. The whole problem is then reduced to randomly generate field configurations weighted according to the statistical distribution e^{-S_E} and to evaluate the expectation values of the operators of interest over this ensemble.

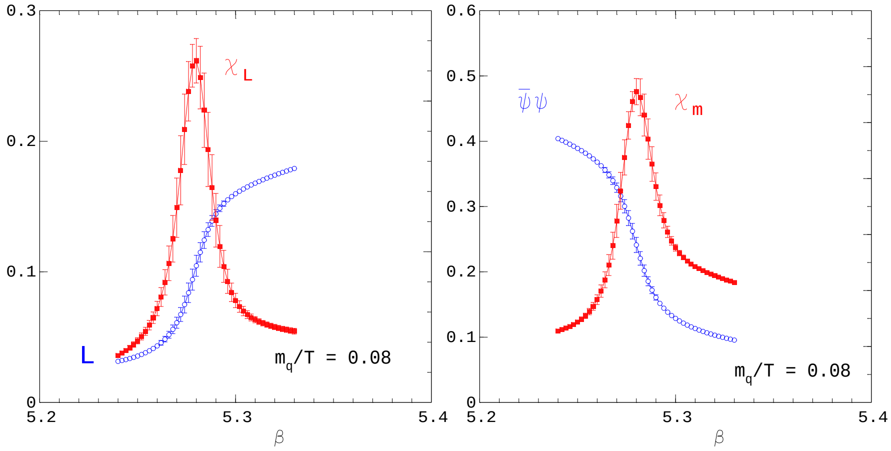

Figure 1.1: Deconfinement and chiral symmetry restoration in 2-flavour QCD from Ref. [1]: The figure shows $\langle L \rangle$ (left), which is the order parameter for deconfinement in the pure gauge limit ($m_q \to \infty$), and $\langle \bar{\psi}\psi \rangle$ (right), which is the order parameter for chiral symmetry breaking in the chiral limit ($m_q \to 0$). Also shown are the corresponding susceptibilities as a function of the coupling $\beta = 6/g^2$ (not to be confused with the inverse temperature $1/T$).

In order to signal the occurrence of a phase transition an order parameter has to be introduced and identified.

The order parameter for the deconfinement phase transition is usually assumed to be the Polyakov loop operator which is defined as:

$$L(\mathbf{x}) = \frac{1}{3}\mathrm{Tr}\left(\mathcal{P} e^{ig\int_0^\beta A_0(\mathbf{x},\tau)d\tau}\right) , \tag{1.4}$$

where $A_0(\mathbf{x}, \tau) = A_0^a(\mathbf{x}, \tau)t^a$, $\beta = 1/T$ is the size of the imaginary temporal direction and $\mathcal{P}$ denotes path-ordering (being the theory non-abelian). In the case of a pure SU(3) theory it turns out that:

$$\langle L\rangle = \frac{1}{V}\langle\sum_{\mathbf{x}} L(\mathbf{x})\rangle \begin{cases} \langle L\rangle = 0\ , & \text{when} \quad T < T_c^{\rm dec} \\ \langle L\rangle \neq 0\ , & \text{when} \quad T > T_c^{\rm dec}\ . \end{cases} \tag{1.5}$$

In the above V is the lattice volume and the sum runs over all the lattice sites. Thus above $T_c^{\rm dec}$ the Polyakov loop operator acquires a non-zero expectation value leading to the breaking of the global Z_3 symmetry. Actually in presence of light dynamical fermions, as can be seen from Fig. 1.1, $\langle L\rangle \neq 0$ even at low temperature, hence it cannot be considered a genuine order parameter. However the associated *susceptibility* (namely the variance of the operator L)

$$\chi_L = V\left(\langle L^2\rangle - \langle L\rangle^2\right) \tag{1.6}$$

still displays a narrow peak for a particular value of the gauge coupling which one uses to signal the phase transition.

A second kind of phase transition occurring in QCD is the chiral symmetry breaking. For N_f massless quarks the QCD lagrangian is invariant under global transformations of the group $SU(N_f)_A$ acting in flavour space as follows:

$$q \ \rightarrow \ e^{i\theta^a t^a \gamma^5} q\ . \tag{1.7}$$

Such a symmetry is not shared by the ground state of the theory: scalar and pseudoscalar (vector and pseudovector) mesons have different masses. In particular the masses of the pseudoscalar mesons are found to be much lighter than the others: this reflects their nature of *Goldstone boson* in the limit $m_q \to 0$. The two important objects for the study of the chiral phase transition are the *chiral condensate* and the *chiral susceptibility* which are defined as

$$\langle\overline{\psi}_f\psi_f\rangle = -\frac{T}{V}\frac{\partial}{\partial m_f}\ln\mathcal{Z}(T,V,\mu_f) \tag{1.8a}$$

$$\chi_m = -\sum_{f=1}^{N_f}\frac{\partial}{\partial m_f}\langle\overline{\psi}_f\psi_f\rangle = \frac{T}{V}\frac{\partial^2}{\partial m_f^2}\ln\mathcal{Z}(T,V,\mu_f)\ , \tag{1.8b}$$

respectively. In the above $\mathcal{Z}(T,V,\mu_f)$ is the euclidean QCD partition function introduced in Eq. (1.3) and μ_f is the chemical potential related to the flavour f. For large values of the gauge coupling (for $T < T_c^{\chi}$) the chiral condensate develops a finite expectation value leading to the breaking of the $SU(N_f)_A$ symmetry; for small coupling ($T > T_c^{\chi}$) the chiral condensate drops to zero (for massless quarks) and chiral symmetry is restored. Indeed for massive quarks, as can be seen from Fig. 1.1, the chiral condensate is not a well defined order parameter and, as for the Polyakov loop operator, one should better use its susceptibility to identify the phase transition.

Quite surprisingly the two susceptibilities χ_L and χ_m turn out to have a peak at the same value of the coupling. Hence the two critical temperatures do coincide: $T_c = T_c^{\rm dec} = T_c^{\chi}$.

The most recent lattice calculations manage to treat also the case of finite chemical potential. Hence it is nowadays possible to draw a reliable phase diagram of QCD in which two different regimes are displayed: a high temperature-density phase in which quarks and gluons are deconfined and chiral symmetry is restored and a low temperature-density phase in which quark and gluons are confined and chiral symmetry is spontaneously broken. The findings of the lattice simulations are displayed in Fig. 1.2.

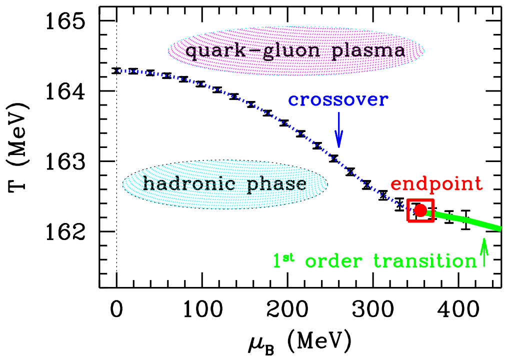

Figure 1.2: The QCD phase diagram (from Ref. [2]) in the realistic case $N_f = 2+1$. The hadronic and QGP phases for low baryon density are separated by a cross-over. Then, when the density is large enough, the cross-over becomes a first order phase transition.

From the partition function (1.3) all the thermodynamical quantities are straightforwardly evaluated. In Fig. (1.3) the behaviour of the energy density and the pressure versus the temperature, for different numbers of dynamical fermions, is given. From the results of the lattice simulations it appears that the ideal gas (Stephan-Boltzmann) limit is far not reached even at the highest temperatures accessible in the heavy-ion experiments.

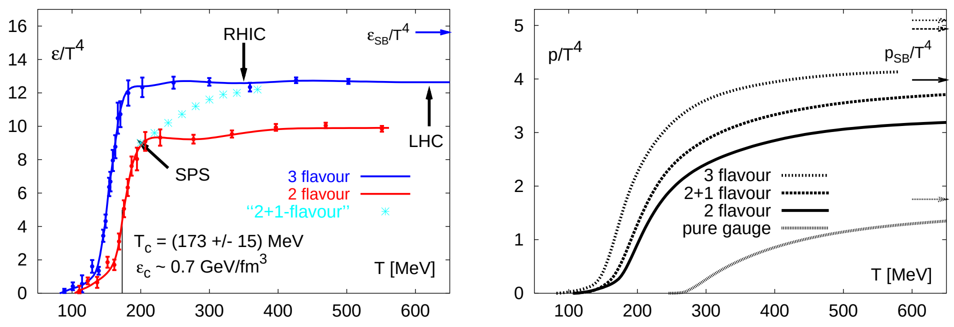

Figure 1.3: The QCD equation of state from Ref. [3] with different numbers of dynamical fermions. The arrows point to the Stephan-Boltzmann limit.

1.2 The experimental signatures of deconfinement

In the collisions of two heavy nuclei at very high energy one tries to create a medium in which quarks and gluons are no longer bound in color-singlet states, namely a QGP. After a time scale of order $\tau \sim 0.5$ fm/c a thermalized QGP is formed. Then the system expands and cools till the temperature gets small enough that matter undergoes hadronization.

Since all the strongly interacting particles reaching the detectors are hadrons, one of the trickiest theoretical and experimental challenges is to propose and identify signals of the onset of deconfinement which are not washed-out by the subsequent hadronization process.

In the following an overview of the main experimental signatures of the formation of the QGP is given.

1.2.1 The J/Ψ suppression

One of the first signals of deconfinement, proposed long time ago by Matsui and Satz [10], is the occurrence of an *anomalous suppression* (with respect to the normal nuclear matter absorption) of the J/Ψ meson yield in the final state. The argument given in [10] is that, in the presence of a deconfined medium, the large number of free color charges leads to the screening of the Coulomb $Q\overline{Q}$ potential and, consequently, favours the melting of the J/Ψ mesons.

In the experiments the J/Ψ multiplicity is reconstructed through the branching ratio of its decay into $\mu^+\mu^-$ pairs, which are experimentally de-

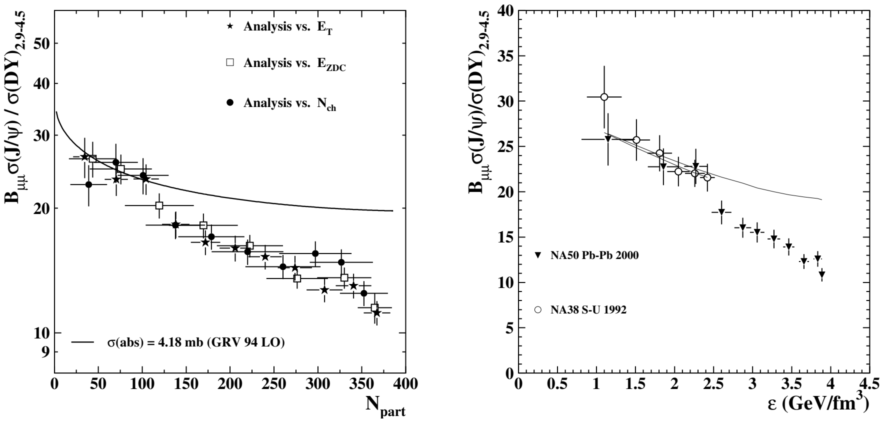

Figure 1.4: The J/Ψ production cross section in Pb-Pb collisions vs. the number of participants (left) and the energy density (right) from Ref. [5]. The solid curve refers to normal nuclear absorption.

tected. Experimental results can be found, for instance, in Refs. [4, 5] and are displayed in Fig. 1.4.

More quantitative details on the problem of heavy quarkonia spectroscopy in the QGP together with some recent criticism on the simple argument of Ref. [10] will be given in Chapter 4.

1.2.2 Jet-quenching and high p_T hadron suppression

In the elementary collisions described by pQCD (e^+e^-, pp...) hard partons are produced in back-to-back pairs in their center of mass frame. The most probable event which may occur is that each hard parton gives rise to a *jet*, i.e. a set of hadrons contained into a cone centered around the parent parton. Then in most collisions hadrons emerge from two cones oriented in opposite directions (three or more jets events are suppressed by powes of α_s).

In heavy-ion collisions the situation is different. Let us consider a central high energy nucleus-nucleus collision in which one expects deconfinement to occur. If a hard parton pair is produced near the surface of the fireball, the parton pointing outward will move toward the detectors without interacting significantly with the thermal bath and it will give rise to a well-defined jet. On the contrary the second hard parton has to travel a long distance through the medium, hence suffering a large energy loss, mainly due to multiple gluon emmission. The energy of the original hard parton will be then distributed among the other thermal soft particles and *no jet will be detected in the*

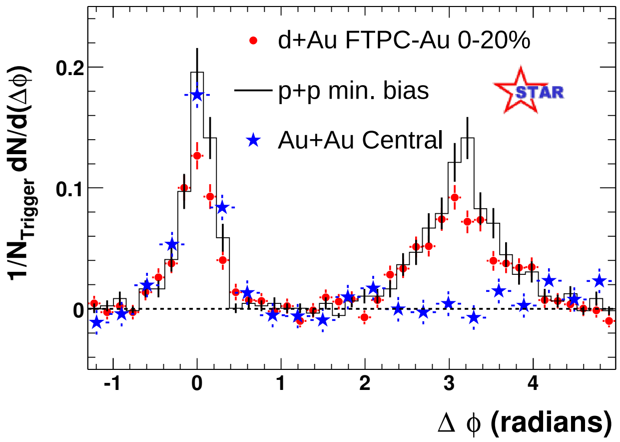

Figure 1.5: The jet quenching observed at RHIC in Au-Au collisions by the STAR collaboration compared to the "reference" experiments p-p and d-Au [6].

opposite direction.

In order to distinguish this scenario from the normal nuclear matter energy loss d-Au collision experiments (where one does not expect deconfinement to occur) have been performed too.

The main experimental results are summarized in Fig. 1.5.

A further experimental signature of the strong radiative energy loss suffered by a parton crossing the hot/dense medium produced in the high energy nucleus nucleus collisions is given by the suppression of high p_T hadron spectra. This effect can be quantified considering the ratio

$$R_{AA} = \frac{d^2N_{AA}/dydp_T}{N_{\rm coll}d^2N_{pp}/dydp_T} \ . \tag{1.9}$$

$R_{AA} = 1$ corresponds to the case of no final state interaction (binary collision scaling), while $R_{AA} < 1$ signals medium suppression of the produced hadrons due to the energy loss suffered by the parent partons.

The experimental results obtained at RHIC are summarized in Fig. (1.6) and indicate *strong medium effects* leading to a factor ~ 5 of suppression with respect to the case of an incoherent sum of proton-proton collisions. The fact that direct photons (which do not interact with the hot/dense QCD medium) seem to follow binary collisions scaling signals that the high p_T hadron suppression is not an initial state effect but arises from parton energy loss.

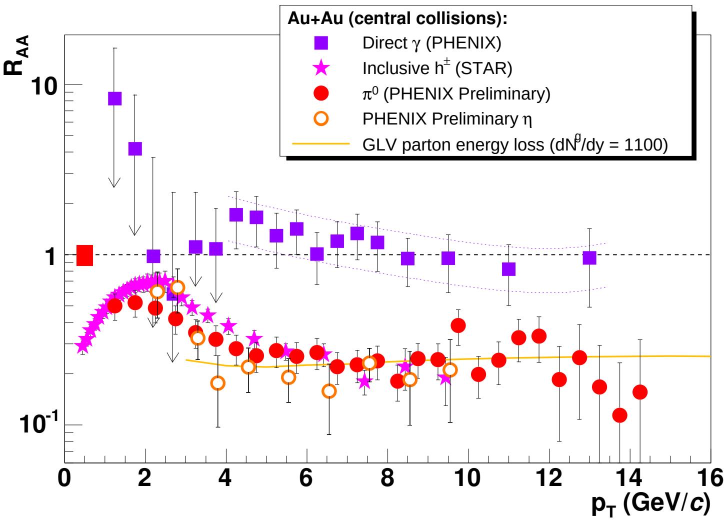

Figure 1.6: High p_T hadron suppression pattern observed at RHIC for different hadron species [7]. Photons appear to follow the binary collision scaling ($R_{AA} \sim 1$).

1.2.3 Statistical hadronization models: particle multiplicities and strangeness enhancement

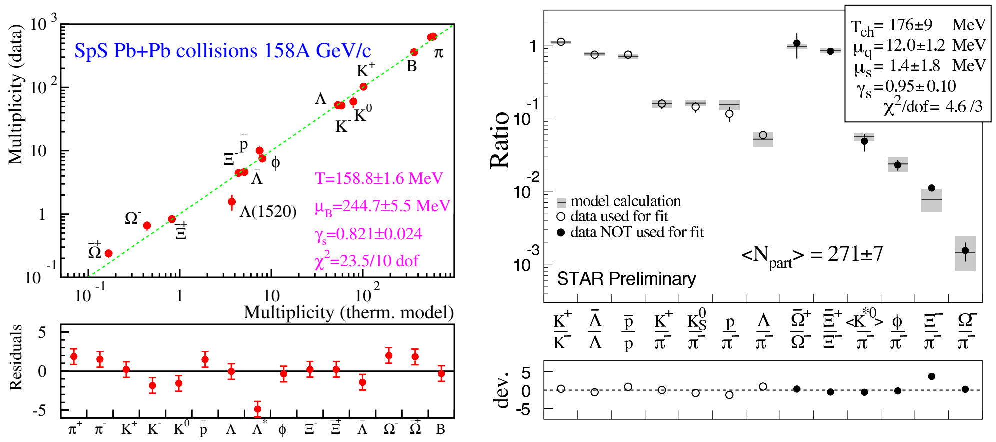

Figure 1.7: Chemical equilibrium fits to the hadron abundances from Pb+Pb collisions at SPS (left) and from Au+Au collisions at RHIC (right) ([8] and references therein).

The measurement of particle multiplicities in the final state can shed light on the features of hadronization, probably one of the most non-perturbative processes occurring in nature. A statistical approach (first proposed by Fermi, Landau and Hagedorn) is considered nowadays one of the best theoretical tools to deal with the hadronization process, independently on the nature of the colliding particles (e^+e^-, pp, AA).

In the statistical hadronization models hadrons are produced maximizing the entropy, with the constraints of the conservation of energy, baryon number and strangeness. If the volume of the system is large enough and only a fraction of the produced hadrons are detected (and this is the case for AA collisions) one is allowed to treat the problem in the gran-canonical ensemble: the conservation of the above quantities is not imposed exactly but only to their mean values. Three independent *Lagrange multipliers* ($\beta = 1/KT$, μ_B and μ_S) are then introduced (associated with the conservation of energy, baryon number and strangeness, respectively[1]).

In the simplest version of the statistical model only two parameters (T and μ_B) suffice to nicely reproduce all the particle multiplicities in nucleus-nucleus collisions. In more refined treatments the statistical factors of the different hadrons are multiplied by a third independent fit parameter, the strangeness undersaturation factor γ_s, which is applied to the abundances of all hadrons containing a strange valence quark (or antiquark), once for each strange valence quark (or antiquark) of the hadron.

The quality of the results obtained in such approaches can be appreciated in Fig. 1.7.

The values of the fit parameters T and μ_B are the ones assumed by the latter at the *chemical freeze-out*, i.e. at the time after which the particle multiplicities don't change any more. The fact that, as can be seen from the RHIC data in Fig. 1.7, the freeze-out temperature pratically coincides with the critical temperature measured on the lattice indicates that *the maximization of the entropy by the final particle multiplicities is not related to inelastic rescattering occurring in the hadronic phase, but reflects the nature itself of the hadronization process, which is a statistical one.*

An enhanced production of strange particles and of multistrange hadrons in high energy nucleus-nucleus collisions with respect to more elementary processes (like e^+e^-, pp, p$\bar{\text{p}}$) was proposed long time ago as a possible signature of the formation of QGP [11]. The argument given in [11] is that inelastic reactions leading to the production of strange particles are much more efficient in the QGP than in the hadronic phase. Hence an enhanced

[1]Indeed μ_S is not a free fit parameter, but its value has to be fixed in order to give overall strangeness neutrality.

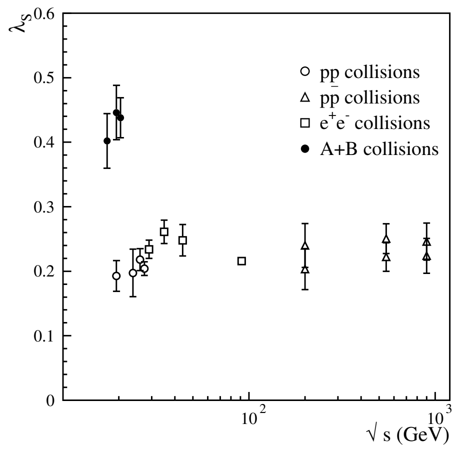

Figure 1.8: The strangeness suppression factor $\lambda_s = 2\langle s\bar{s}\rangle/(\langle u\bar{u}\rangle + \langle d\bar{d}\rangle)$ as a function of the centre of mass energy (nucleon-nucleon c.m. in the case of heavy-ion collisions) for different kind of high energy collisions [9]. The huge increase of strangeness production in nucleus nucleus collisions appears evident.

multiplicity of strange hadrons in the final state should reflect a primordial deconfined phase.

In central AA collisions, in which one expects QGP to be formed, such an enhancement of strangeness production is experimentally observed, as it appears from Fig. 1.8.

Actually, in the framework of the statistical hadronization models the interpretation of the large yields of strange particles is not so direct: indeed it relates to the fact that, in the gran-canonical ensemble, the constraint of strangeness conservation is not imposed exactly, but only on the mean value $\langle S\rangle$. The possibility of adopting the gran canonical statistics in heavy-ion collisions, in contrast to what happens in more elementary processes (like e^+e^-, pp, p$\bar{\text{p}}$) which require a canonical (or micro-canonical) treatment, stems from the production of an extended fireball which can be possibly identified with a thermalized QGP.

1.2.4 Hydrodynamical expansion: radial and elliptic flow

The expansion of the fireball resulting from the heavy ion collision and consequently the p_T (transverse momentum) spectra of the observed hadrons are nicely reproduced by the hydrodynamics of an ideal (i.e. with negligible viscosity) fluid.

The energy momentum tensor of the latter reads

$$T^{\mu\nu}(x) = (e(x) + p(x))\, u^\mu(x) u^\nu(x) - p(x) g^{\mu\nu} \ , \tag{1.10}$$

and the baryon number current is given by

$$j_B^\mu(x) = n_B(x) u^\mu(x) \ , \tag{1.11}$$

where in the above $e(x)$, $p(x)$, $u^\mu(x)$ and $n_B(x)$ are the energy density, pressure, 4-velocity and baryon density of the fluid element in the space-time point x.

The evolution of the fireball is obtained through the solution of 6 equations. The conservation of energy, momentum and baryon number is encoded in the continuity equations:

$$\partial_\mu T^{\mu\nu}(x) = 0 \qquad (\nu = 0, \ldots 3) \tag{1.12a}$$
$$\partial_\mu j_B^\mu(x) = 0 \ . \tag{1.12b}$$

The last equation required to close the system is the *Equation of State* (EOS) which allows to express the pressure as a function of the energy and baryon density. In principle it is provided by lattice calculation. In practice a schematic model of EOS is often employed: it corresponds to a hadron-resonance gas below T_c and to an ideal gas of quarks and gluons above T_c.

Results of hydro calculations are compared to the experimental data in Fig. 1.9.

The fact that ideal hydrodynamics works well at RHIC is not at all obvious. A hydrodynamical description of a many-body system requires the *mean free path* $\lambda_{\rm mfp}$ of the constituents to be much smaller than the linear size L of the system itself. Since $\lambda_{\rm mfp} \sim 1/(n\sigma)$, where n is the density and σ is the total cross section, the condition $\lambda_{\rm mfp} \ll L$ entails large values of σ in order to be satisfied. Elementary partonic cross sections are too small to explain why hydro works so well.

The matter obtained at RHIC is nowadays often described [12] as a strongly interacting QGP (sQGP) whose behaviour is more similar to an ideal liquid than to a weakly interacting gas of quarks and gluons.

The fact that, for temperatures slightly exceeding T_c, the QGP behaves like a liquid whose expansion is driven by pressure gradients results particulary evident from the *elliptic flow* observed in the non central collisions. In non central events the initial shape of the fireball looks like an almond and the expansion occurs mainly along the direction of larger pressure gradient. This reflects into the p_T distribution of the observed hadrons, which is no

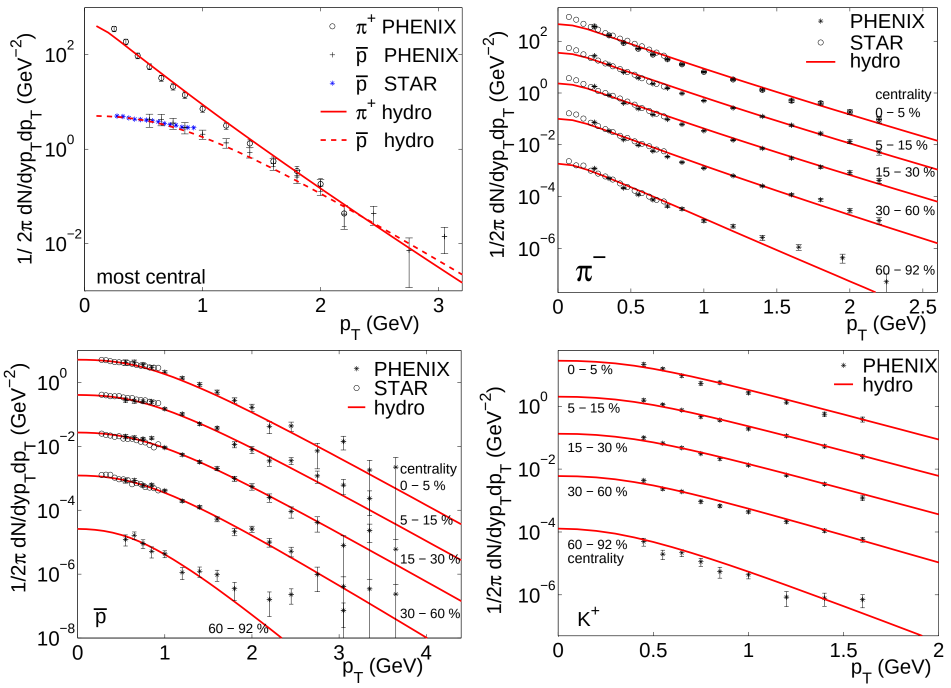

Figure 1.9: Identified pion, antiproton and kaon spectra for $\sqrt{s_{\mathrm{NN}}} = 130$ GeV from the PHENIX and STAR collaborations in comparison with results from hydrodynamic calculations ([8] and references therein).

longer azimuthally symmetric. This occurrence can be quantified through the introduction of the Fourier expansion

$$\frac{dN}{d\phi} = N_0 \left\{ 1 + \sum_n 2v_n \cos\left(n(\phi - \psi_{RP})\right) \right\} \ , \tag{1.13}$$

where N_0 is a normalization constant, ϕ is the azimuthal angle and ψ_{RP} is the angle of the nuclear impact parameter (reaction plane).

The experimental values for the first non zero Fourier coefficient $v_2(p_T)$ are given in Fig. 1.10 and compared with the results of hydrodynamical calculations.

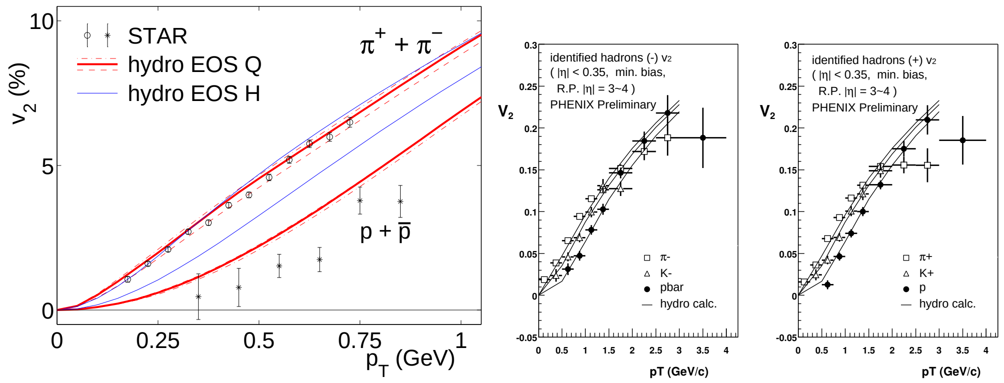

Figure 1.10: The elliptic flow coefficient v_2 measured at STAR (left) and PHENIX (right) compared to hydrodinamic calculations ([8] and references therein).

Chapter 2

QCD at finite temperature: general introduction and some resummation schemes

In this chapter we first present the basic formalism required to treat a Quantum Field Theory like QCD at finite temperature (in the Matsubara imaginary-time approach). In accord with Ref. [13] we employ in doing the scalar products an ordinary Minkowskian metric $g^{\mu\nu} = \mathrm{diag}(1, -1, -1, -1)$ simply letting, where necessary, $t \to -i\tau$, with $\tau \in [0, \beta]$. Also the Dirac matrices satisfy the ordinary anticommutation relation $\{\gamma^\mu, \gamma^\nu\} = 2g^{\mu\nu}$.

After discussing the non interacting theory we introduce a *separation of momentum scales* in the QCD plasma and present a *resummation scheme* called *Hard Thermal Loop* (HTL) approximation, allowing to study the effects of the interaction with the thermal bath on the propagation of *soft momentum* (long wavelength) excitations.

We finally present a many-body technique referred to in the literature as Φ-derivable approximation which can be employed in the study of the thermodynamics of a QFT. In the literature such an approach has been employed to obtain an Equation Of State (EOS) for the QGP which can be eventually compared and checked with the lattice findings. The results obtained within this scheme are quite satisfactory and can be found for example in Refs. [23, 26]. In order to access the meaning of the above results, here we simply display the main features of this many-body scheme by applying it (as a toy model) to the case of a scalar field theory: this is indeed enough to illustrate how different contributions to the entropy and the pressure may arise.

2.1 The free theory at finite temperature

2.1.1 The quark propagator

In configuration space the Matsubara fermionic propagator is defined as follows:

$$\begin{aligned} S_{\alpha\beta}(\tau,\boldsymbol{x};\tau',\boldsymbol{x'}) &= \langle T_\tau(\psi_\alpha(-i\tau,\boldsymbol{x})\bar{\psi}_\beta(-i\tau',\boldsymbol{x'}))\rangle \\ &= \theta(\tau-\tau')\langle\psi_\alpha(-i\tau,\boldsymbol{x})\bar{\psi}_\beta(-i\tau',\boldsymbol{x'})\rangle \\ &\quad -\theta(\tau'-\tau)\langle\bar{\psi}_\beta(-i\tau',\boldsymbol{x'})\psi_\alpha(-i\tau,\boldsymbol{x})\rangle \ , \end{aligned} \tag{2.1}$$

whereas in Fourier space, for the non interacting Dirac field, it reads:

$$S_F(i\omega_n,\boldsymbol{p}) = -\frac{\not{P}+m}{P^2-m^2} = \frac{\not{P}+m}{\omega_n^2+E_p^2} = (\not{P}+m)\widetilde{\Delta}(P) \ . \tag{2.2}$$

Of course the quark propagator is diagonal in the flavour and colour indices. In the above $E_p^2 = \boldsymbol{p}^2+m^2$ and $p_0 = i\omega_n$, with $\omega_n = (2n+1)\pi/\beta$, due to the finite size of the imaginary temporal direction and to the antiperiodic boundary conditions

$$S_{\alpha\beta}(\tau-\beta,\boldsymbol{x};\tau',\boldsymbol{x'}) = -S_{\alpha\beta}(\tau,\boldsymbol{x};\tau',\boldsymbol{x'}) \ . \tag{2.3}$$

In terms of the free fermionic spectral function

$$\rho_F(P) = \epsilon(p_0)(\not{P}+m)\delta(P^2-m^2) \equiv (\not{P}+m)\rho_0(P) \ , \tag{2.4}$$

$\rho_0(P)$ being the free scalar spectral function, the following representation holds for the free thermal propagator:

$$S_F(z,\boldsymbol{p}) = -\int_{-\infty}^{+\infty} dp_0 \frac{\rho_F(p_0,\boldsymbol{p})}{z-p_0} \quad , \tag{2.5}$$

with z off the real axis.

It may be useful, in some computations, to use the following expression for the fermionic propagator in the mixed representation:

$$S_F(\tau>0,\boldsymbol{p}) = \int_{-\infty}^{+\infty} dp_0\, e^{-p_0\tau}\rho_F(p_0,\boldsymbol{p})(1-\tilde{n}(p_0)) \ , \tag{2.6}$$

where $\tilde{n}(p_0)$ is a Fermi distribution.
It is easily verified that Eq. (2.6) leads to the proper spectral representation

(2.5). In fact:

$$
\begin{aligned}
S_F(i\omega_n, \boldsymbol{p}) &= \int_0^\beta d\tau e^{i\omega_n \tau} S_F(\tau, \boldsymbol{p}) = \int_0^\beta d\tau e^{i\omega_n \tau} \int_{-\infty}^{+\infty} dp_0\, e^{-p_0 \tau} \rho_F(p)(1 - \tilde{n}(p_0)) \\
&= \int_{-\infty}^{+\infty} dp_0 \rho_F(p_0, \boldsymbol{p})(1 - \tilde{n}(p_0)) \int_0^\beta d\tau e^{(i\omega_n - p_0)\tau} = -\int_{-\infty}^{+\infty} dp_0 \frac{\rho_F(p_0, \boldsymbol{p})}{i\omega_n - p_0} \,.
\end{aligned} \tag{2.7}
$$

2.1.2 The gluon and ghost propagators

Here we give the expressions of the tree level gluon and ghost propagators, which clearly depend on the choice of the gauge. In the Feynman gauge the latters reads:

$$
\Delta^{ab}_{\mu\nu}(K) = \frac{\delta^{ab} g_{\mu\nu}}{K^2} = -\frac{\delta^{ab} g_{\mu\nu}}{\omega_l^2 + k^2} = -\delta^{ab} g_{\mu\nu} \Delta(K) \tag{2.8a}
$$

$$
\Delta^{ab}(K) = \delta^{ab} \Delta(K) \,, \tag{2.8b}
$$

where $K = (i\omega_l, \boldsymbol{k})$ and we have isolated the scalar propagator $\Delta(K)$. The *bosonic Matsubara frequencies* are given by:

$$
\omega_l = \frac{(2l)\pi}{\beta}, \tag{2.9}
$$

because of the periodic boundary conditions.

Given the scalar spectral function

$$
\rho_0(K) = \rho_0(k_0, k) = \epsilon(k_0)\delta(K^2) \tag{2.10}
$$

and the spectral representation

$$
\Delta(z, \boldsymbol{k}) = -\int_{-\infty}^{+\infty} dk_0 \frac{\rho_0(k_0, \boldsymbol{k})}{z - k_0} \,, \tag{2.11}
$$

the scalar propagator $\Delta(K)$ can be conveniently written in the mixed form:

$$
\Delta(\tau > 0, \boldsymbol{k}) = \int_{-\infty}^{+\infty} dk_0\, e^{-k_0 \tau} \rho_0(k_0, \boldsymbol{k})(1 + n(p_0)) \,, \tag{2.12}
$$

where $n(p_0)$ is a Bose distribution. The proof is analogous to the one holding for the fermionic case.

Though working in the Feynman gauge is very convenient in performing calculations, other gauges can be used, in which the physical degrees of freedom appear more transparently. Since the physical results must not depend on the choice of the gauge one should check that the approximation schemes employed in the calculations respect gauge invariance.

2.2 HTL approximation for a QCD plasma

Let us consider an ultrarelativistic plasma, i.e. at a temperature $T \gg m_i$ (m_i being the masses of the constituents), so that we are allowed to work in the massless limit.
For a gauge theory the coupling with the gauge field occurs through the *covariant derivative*:

$$D_\mu \equiv \partial_\mu - i\, g\, A_\mu = \partial_\mu - i\, g\, A_\mu^a\, t^a \quad , \tag{2.13}$$

where t^a are the generators of the gauge group and g is the coupling constant. If g is sufficiently small (for QED this is always the case, while for QCD we have to go to large enough temperatures beyond T_c) we can describe our system at the zeroth order as a gas of massless non interacting particles for which the Stephan Boltzmann results hold:

$$E \sim T^4 \,, \qquad\qquad N \sim T^3 \,. \tag{2.14}$$

Hence, being the particles ultrarelativistic, the typical components of their quadrimomenta behaves like $k \sim T$. Thus we have identified a scale of *hard momenta* $k \sim T$ whose corresponding *degrees of freedom* are the *plasma particles*: quarks, antiquarks and transverse gluons for a QCD plasma.
We can define also a *soft scale of momenta* $k \sim gT$ which is associated to collective, long wavelength phenomena (like screening masses).
The Hard Thermal Loop (HTL) approximation gives us a recipe to treat the interaction of the soft modes with the hard degrees of freedom yielding *resummed propagators* for the soft fields.

2.2.1 Gluon self-energy

In this section we compute the gluon polarization tensor in the HTL approximation, which gives us the leading term of $\Pi^{ab}_{\mu\nu}$ when the incoming gluon is *soft*. There are four diagrams which contribute: the quark loop, the gluon loop, the gluon tadpole and the ghost loop. Differently from QED, even at the one-loop level the computation involves gauge field propagators, thus a gauge must be fixed from the beginning. We will evaluate the gluon polarization tensor in Feynman gauge: however the final result for the HTL computation will be gauge-independent. As usual the computations are done in the *imaginary-time* formalism, but once the sum over the Matsubara modes has been performed, we can analytically continue the result to real frequencies.

We first perform the exact calculation for the quark loop contribution which involves also a divergent (temperature-independent) piece. Then we

verify that, when the incoming gluon momentum is soft, the dominant contribution to the loop integral comes from momenta $k\sim T$. This fact allows us to perform some kinematical approximations which simplify the evaluation of the integral. At the end of the computation we give a general recipe that allows one to single out , from the beginning, the leading term which contributes to the loop.
Then, through this recipe, we briefly sketch how one can get the HTL contribution for the other diagrams.
Since the colour structure of the polarization tensor is trivial $\Pi^{ab}_{\mu\nu}=\delta^{ab}\Pi_{\mu\nu}$, in the following we shall drop the colour indices.

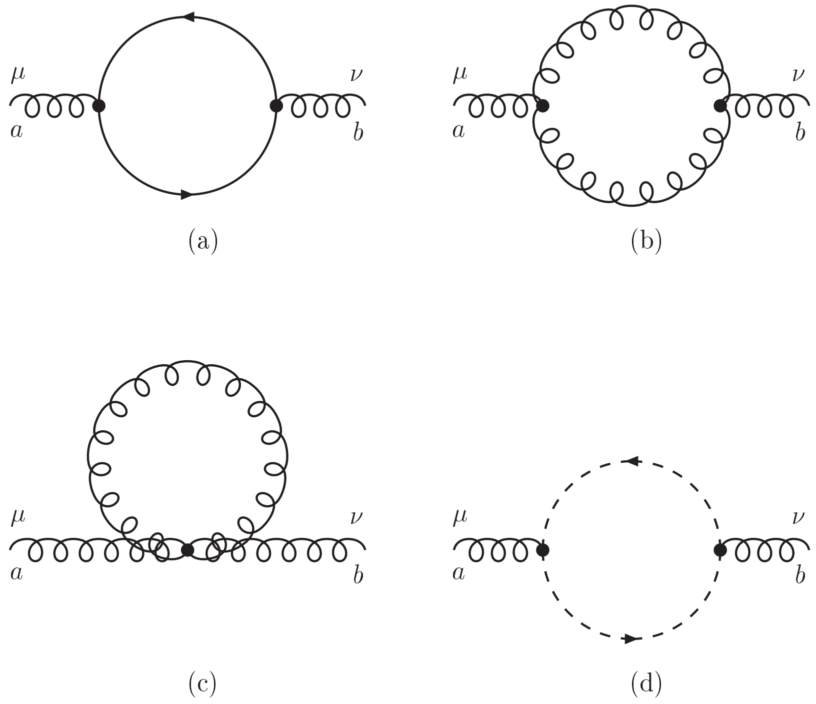

Figure 2.1: Diagrams contributing to the gluon polarization tensor in the HTL approximation.

Let us then consider the expression for the quark loop:

$$\Pi^{(a)}_{\mu\nu}(i\omega_l,\boldsymbol{p}) = \frac{g^2 N_f}{2}\int\{dK\}\mathrm{Tr}[\gamma_\mu S_F(i\omega_n,\boldsymbol{k})\gamma_\nu S_F(i\omega_n - i\omega_l,\boldsymbol{k}-\boldsymbol{p})] \ , \quad (2.15)$$

where ω_l is even while ω_n is odd, the factor $1/2$ comes from $\mathrm{Tr}(t^a t^b) = \frac{1}{2}\delta^{ab}$, N_f is the number of flavours and we use the compact notation for the fermionic loop-integral (the curly brackets meaning a sum over odd frequencies):

$$\int \{dK\} = \frac{1}{\beta} \sum_{n=-\infty}^{+\infty} \int \frac{d^3k}{(2\pi)^3} \quad . \tag{2.16}$$

We can immediately perform the sum over the Matsubara frequencies with the following procedure: let us write the fermionic propagators in mixed representation

$$S_F(i\omega_n, \boldsymbol{k}) = \int_0^\beta d\tau_1 e^{i\omega_n \tau_1} S_F(\tau_1, \boldsymbol{k}) \tag{2.17a}$$

$$S_F(i\omega_n - i\omega_l, \boldsymbol{k} - \boldsymbol{p}) = \int_0^\beta d\tau_2 e^{i(\omega_n - \omega_l)\tau_2} S_F(\tau_2, \boldsymbol{k} - \boldsymbol{p}) \quad . \tag{2.17b}$$

The dependence on ω_n appears now only in the arguments of the exponentials. We can now sum over the *odd* frequencies ω_n by exploiting the identity:

$$\frac{1}{\beta} \sum_{n=-\infty}^{+\infty} e^{i\omega_n \tau} = \sum_{l=-\infty}^{+\infty} (-1)^l \delta(\tau - l\beta) \ . \tag{2.18}$$

Hence the contribution of the quark loop to the gluon polarization tensor becomes:

$$\Pi^{(a)}_{\mu\nu}(i\omega_l, \boldsymbol{p}) = -\frac{g^2 N_f}{2} \int \frac{d^3k}{(2\pi)^3} \int_0^\beta d\tau e^{-i\omega_l \tau} \mathrm{Tr}[\gamma_\mu S_F(\beta - \tau, \boldsymbol{k}) \gamma_\nu S_F(\tau, \boldsymbol{k} - \boldsymbol{p})] \ . \tag{2.19}$$

In the above the fermionic propagators can be expressed more conveniently in terms of the free spectral functions, as in eq. (2.6). The integration over τ is then easily performed (we consider here massless quarks) yielding:

$$\Pi^{(a)}_{\mu\nu}(i\omega_l, \boldsymbol{p}) = \frac{g^2 N_f}{2} \int \frac{d^3k}{(2\pi)^3} \int_{-\infty}^{+\infty} dk_0 \int_{-\infty}^{+\infty} dq_0 \, \rho_0(k) \, \rho_0(q) \times$$
$$\times \, \mathrm{Tr}[\gamma_\mu \not{k} \gamma_\nu \not{q}] \, \frac{\tilde{n}(k_0) - \tilde{n}(q_0)}{k_0 - q_0 - i\omega_l} \ , \tag{2.20}$$

where $k^\mu = (k_0, \boldsymbol{k})$, $q^\mu = (q_0, \boldsymbol{q})$ with $\boldsymbol{q} \equiv \boldsymbol{k} - \boldsymbol{p}$ and ρ_0 is the free scalar spectral function, namely $\rho_0(k) = \epsilon(k_0)\delta(k^2)$.

Once we have summed over the Matsubara frequencies we can analytically continue our result to the whole complex plane letting $i\omega_l \to p_0$ with p_0 off the real axis. Thus we get:

$$\Pi^{(a)}_{\mu\nu}(p_0,\boldsymbol{p}) = 2g^2 N_f \int \frac{d^3k}{(2\pi)^3}\int_{-\infty}^{+\infty} dk_0 \int_{-\infty}^{+\infty} dq_0 \rho_0(k)\rho_0(q)\times \\ \times \left[k_\mu q_\nu + q_\mu k_\nu - g_{\mu\nu}(k\cdot q)\right]\frac{\tilde{n}(k_0)-\tilde{n}(q_0)}{k_0-q_0-p_0}\ . \quad (2.21)$$

Let us focus on the spatial components. The integration over k_0 and q_0 can be done by exploiting the explicit form of the free spectral functions. Hence we have:

$$\Pi^{(a)}_{ij}(p_0,\boldsymbol{p}) = \frac{g^2 N_f}{2}\int \frac{d^3k}{(2\pi)^3}\frac{1}{\epsilon_k\epsilon_q}\times \\ \times\Bigg\{(k_iq_j + q_ik_j + \delta_{ij}(\epsilon_k\epsilon_q - \boldsymbol{k}\cdot\boldsymbol{q}))\left(\frac{\tilde{n}(\epsilon_k)-\tilde{n}(\epsilon_q)}{\epsilon_k-\epsilon_q+p_0}+\frac{\tilde{n}(\epsilon_k)-\tilde{n}(\epsilon_q)}{\epsilon_k-\epsilon_q-p_0}\right)+ \\ +(k_iq_j + q_ik_j - \delta_{ij}(\epsilon_k\epsilon_q + \boldsymbol{k}\cdot\boldsymbol{q}))\left(\frac{1-\tilde{n}(\epsilon_k)-\tilde{n}(\epsilon_q)}{\epsilon_k+\epsilon_q+p_0}+\frac{1-\tilde{n}(\epsilon_k)-\tilde{n}(\epsilon_q)}{\epsilon_k+\epsilon_q-p_0}\right)\Bigg\} \quad (2.22)$$

We can notice that in eq. (2.22) the temperature dependent part is UV finite, because the statistical factors exponentially vanish for large values of k. Thus, in order to evaluate its contribution, we don't need any regularization of the integral.
On the other hand in the limit $T\to 0$ the only surviving term is the *vacuum part*

$$\Pi^{(a)T=0}_{ij}(P) = \frac{g^2 N_f}{2}\int \frac{d^3k}{(2\pi)^3}\,\frac{k_iq_j + q_ik_j - \delta_{ij}(\epsilon_k\epsilon_q + \boldsymbol{k}\cdot\boldsymbol{q})}{\epsilon_k\epsilon_q}\times \\ \times\left(\frac{1}{\epsilon_k+\epsilon_q+p_0}+\frac{1}{\epsilon_k+\epsilon_q-p_0}\right)\ , \quad (2.23)$$

where $P=(p_0,\boldsymbol{p})$. This integral develops UV divergences and requires renormalization (it corresponds to the diagram which, in QED, is responsible for the renormalization of the electron charge).
Now, after imposing *retarded boundary conditions* setting $p_0 = \omega + i\eta$ (with real ω), we perform explicitly, although approximately, the integration. We wish to isolate the leading contribution to $\Pi_{\mu\nu}$ in the case of *soft external momenta*, i.e. $\omega, p\sim gT$.
We notice that, when P is soft, the finite part of $\Pi_{T=0}(P)\sim g^2P^2$ gives a subleading correction of order g^4T^2.

For what concerns the temperature dependent part the major contribution to the integral comes from the region of hard momenta $k \sim T$, which is, as pointed out in section (2.3), the typical momentum of a quark (or an anti-quark) of the plasma. Higher values of k are in fact suppressed due to the Fermi distributions. On the other hand the contribution coming from the region of soft momenta $k \sim gT$ behaves as

$$g^2 \int^{gT} dk\,(gT)^2 \frac{1}{(gT)^2}(gT)^2 \frac{\tilde{n}(gT)}{gT} \sim g^4 T^2 \ . \tag{2.24}$$

For the region of *hard momenta* $k \sim T \gg p$ the following kinematical approximations for the energy

$$\epsilon_q \equiv |\boldsymbol{k} - \boldsymbol{p}| \simeq k - \hat{\boldsymbol{k}} \cdot \boldsymbol{p} \tag{2.25a}$$

$$\epsilon_k + \epsilon_q \pm \omega \simeq 2k \ , \quad \epsilon_k - \epsilon_q \pm \omega \simeq \hat{\boldsymbol{k}} \cdot \boldsymbol{p} \pm \omega \tag{2.25b}$$

and for the statistical factors

$$\tilde{n}(\epsilon_k) - \tilde{n}(\epsilon_q) \simeq \hat{\boldsymbol{k}} \cdot \boldsymbol{p} \frac{\mathrm{d}\tilde{n}}{\mathrm{d}k} \ , \quad \tilde{n}(\epsilon_k) + \tilde{n}(\epsilon_q) \simeq 2\tilde{n}(k) \tag{2.26}$$

are allowed. Using the relations:

$$\int_0^{+\infty} dk\, k\, \tilde{n}(k) = -\frac{1}{2} \int_0^{+\infty} dk\, k^2 \frac{\mathrm{d}\tilde{n}}{\mathrm{d}k} = \frac{\pi^2 T^2}{12} \ , \tag{2.27}$$

we get for the spatial components of the quark loop:

$$\Pi_{ij}^{(a)}(\omega, \boldsymbol{p}) = \frac{g^2 T^2 N_f}{6} \int \frac{d\Omega_k}{4\pi} \frac{\omega\, \hat{k}_i \hat{k}_j}{\omega - \hat{\boldsymbol{k}} \cdot \boldsymbol{p} + i\eta} \ . \tag{2.28}$$

Similar considerations hold also for the other components. The complete result for the quark loop at leading order in HTL reads then:

$$\Pi_{\mu\nu}^{(a)}(\omega, \boldsymbol{p}) = \frac{g^2 T^2 N_f}{6} \left\{ -g_{\mu 0} g_{\nu 0} + \omega \int \frac{d\Omega_k}{4\pi} \frac{\widehat{K}_\mu \widehat{K}_\nu}{\omega - \hat{\boldsymbol{k}} \cdot \boldsymbol{p} + i\eta} \right\} \ , \tag{2.29}$$

being $\widehat{K} = (1, \hat{\boldsymbol{k}})$.

Having illustrated in detail the approximations which lead to the LO contribution of the loop integral, we suggest here a recipe which allows to retain, in a Feynman diagram, only the terms which contribute to the HTL result. For this purpose in eq. (2.15) we simply neglect all the soft momenta in the numerator. For example, calling $K=(i\omega_n, \boldsymbol{k})$ and $P=(p_0=i\omega_l, \boldsymbol{p})$, we write

$$S_F(K) = -\frac{\not{K}}{K^2} = \frac{\not{K}}{\omega_n^2+\boldsymbol{k}^2} \equiv \not{K}\widetilde{\Delta}(K) \ , \tag{2.30}$$

for the first propagator, while the second one can be approximated by:

$$S_F(K-P) \approx \not{K}\widetilde{\Delta}(K-P) \ . \tag{2.31}$$

Thus one arrives at the expression:

$$\Pi^{(a)}_{\mu\nu}(P) \approx 2g^2 N_f \int dK \left\{ 2K_\mu K_\nu \widetilde{\Delta}(K)\widetilde{\Delta}(K-P) + g_{\mu\nu}\widetilde{\Delta}(K) \right\} \ . \tag{2.32}$$

One may wonder whether the above approximation is justified at this level since $p_0 = i\omega_l$ is at least of order T for $l \neq 0$. Actually this does not affect the evaluation of the sum over the Matsubara frequencies and at the end of the calculation one is allowed to analytically continue the result to real *soft* values of $\omega \sim gT$.

The previous considerations allow us to evaluate in a quite straightforward way the gluon and the ghost loops which would require otherwise tedious calculations, since they involve momentum dependent vertices. If one is just interested in isolating the HTL contribution to $\Pi_{\mu\nu}$ one can safely keep only the *hard internal momenta* and drop all the other terms.
At this point one has to fix a gauge: choosing the Feynman gauge the gluon and ghost propagators $[K=(i\omega_l, \boldsymbol{k})]$ read, as already quoted in Sec. (2.1.2):

$$\Delta^{ab}_{\mu\nu}(K) = \frac{\delta^{ab} g_{\mu\nu}}{K^2} = -\frac{\delta^{ab} g_{\mu\nu}}{\omega_l^2 + k^2} = -\delta^{ab} g_{\mu\nu}\Delta(K) \tag{2.33a}$$

$$\Delta^{ab}(K) = \delta^{ab}\Delta(K) \quad . \tag{2.33b}$$

We get then the following expressions for the gluon loop (b), the gluon tadpole (c) and the ghost loop (d) contributions to the polarization tensor (N is the number of colours, while the notation $\int [dK]$ means that we are summing over bosonic frequencies):

$$\Pi^{(b)}_{\mu\nu}(P) \approx -\frac{g^2 N}{2} \int [dK] \left((4d-6)K_\mu K_\nu + 2g_{\mu\nu}K^2 \right) \Delta(K)\Delta(P-k) \tag{2.34a}$$

$$\Pi^{(c)}_{\mu\nu}(P) = -g_{\mu\nu} g^2 (d-1) N \int [dK]\Delta(K) \tag{2.34b}$$

$$\Pi^{(d)}_{\mu\nu}(P) \approx g^2 N \int [dK] K_\mu K_\nu \Delta(K)\Delta(P-k) \ , \tag{2.34c}$$

where $d = 4 - 2\epsilon$. The choice of working in dimensional regularization is particularly convenient since some integrals, which would diverge in other schemes, here exactly vanish (for massless particles). Moreover, since:

$$\int \frac{d^{d-1}k}{(2\pi)^{d-1}} \frac{1}{2k} = 0 \,, \tag{2.35}$$

we have

$$\int [dK]\Delta(K) = \int \frac{d^{d-1}k}{(2\pi)^{d-1}} \frac{1+2n(k)}{2k} = \int \frac{d^3k}{(2\pi)^3} \frac{n(k)}{k} = \frac{T^2}{12} \,, \tag{2.36a}$$

$$\int \{dK\}\Delta(K) = \int \frac{d^{d-1}k}{(2\pi)^{d-1}} \frac{1-2\tilde{n}(k)}{2k} = -\int \frac{d^3k}{(2\pi)^3} \frac{\tilde{n}(k)}{k} = -\frac{T^2}{24} \tag{2.36b}$$

respectively in the bosonic and fermionic case.
In analogy with what previously done for the quark loop one arrives to the following complete result for the gluon polarization propagator in HTL (which can be proved to be gauge independent):

$$\Pi^{HTL}_{\mu\nu}(\omega, \boldsymbol{p}) = m_D^2 \left\{ -g_{\mu 0} g_{\nu 0} + \omega \int \frac{d\Omega_k}{4\pi} \frac{\widehat{K}_\mu \widehat{K}_\nu}{\omega - \hat{\boldsymbol{k}} \cdot \boldsymbol{p} + i\eta} \right\} \,. \tag{2.37}$$

Here we have adopted retarded boundary conditions and we have factorized the *Debye mass* m_D which is given by:

$$m_D = gT\sqrt{\frac{N}{3} + \frac{N_f}{6}} \,. \tag{2.38}$$

This is the *leading order* expression for the mass which *screens* the electric colour interaction between quarks. Actually, as can be found in the literature [14], it receives large NLO corrections.
For *space-like momenta* the denominator in eq. (2.37) can vanish. Thus $\Pi_{\mu\nu}$ develops an imaginary part:

$$\mathrm{Im}\Pi_{\mu\nu} = -\pi m_D^2 \omega \int \frac{d\Omega_k}{4\pi} \widehat{K}_\mu \widehat{K}_\nu \, \delta(\omega - \hat{\boldsymbol{k}} \cdot \boldsymbol{p}) \,. \tag{2.39}$$

Furthermore at the one loop level the gluon polarization tensor is transverse:

$$P^\mu \Pi_{\mu\nu}(P) = 0 \quad . \tag{2.40}$$

This outcome makes life easier when we want to invert the Dyson equation (we omit the colour indices)

$$^\star G^{-1}_{\mu\nu} = G^{-1}_{0\,\mu\nu} + \Pi_{\mu\nu} \tag{2.41}$$

in order to get a HTL resummed gluon propagator.

While in calculating $\Pi_{\mu\nu}$ we worked in a covariant gauge (Feynman gauge), obtaining at the end a gauge invariant result, at this point it is convenient to operate another choice of the gauge. Here it is more suggestive to choose the Coulomb gauge, where the particle content of the theory is more transparent. In this gauge the only non trivial components of ${}^\star G_{\mu\nu}$ are:

$$
\begin{aligned}
{}^\star G_{00}(p_0,\boldsymbol{p}) &\equiv\ {}^\star\Delta_L(p_0,p) \quad \text{(electric)} &\text{(2.42a)}\\
{}^\star G_{ij}(p_0,\boldsymbol{p}) &\equiv\ (\delta_{ij}-\hat{p}_i\hat{p}_j)\,{}^\star\Delta_T(p_0,p) \quad \text{(magnetic)}\ . &\text{(2.42b)}
\end{aligned}
$$

At the tree level we have:

$$
\begin{aligned}
\Delta_L(p_0,p) &= \frac{-1}{p^2} &\text{(2.43a)}\\
\Delta_T(p_0,p) &= \frac{-1}{p_0^2-p^2}\ , &\text{(2.43b)}
\end{aligned}
$$

where one immediately recognizes that, at the tree level, the electric (longitudinal) propagator corresponds to the instantaneous Coulomb interaction (a feature that is peculiar of the Coulomb gauge), while the magnetic (transverse) propagator describes the propagation of massless transverse gluons.
It is easily found that the different components of $\Pi_{\mu\nu}$ can be conveniently written in terms of two functions Π_L and Π_T in the following way:

$$
\Pi_{00}(p_0,\boldsymbol{p}) = -\Pi_L(p_0,p)\ , \qquad \Pi_{0i}(p_0,\boldsymbol{p}) = -\frac{p_0 p_i}{p^2}\Pi_L(p_0,p)\ ,
$$
$$
\Pi_{ij}(p_0,\boldsymbol{p}) = (\delta_{ij}-\hat{p}_i\hat{p}_j)\Pi_T(p_0,p) - \hat{p}_i\hat{p}_j\frac{p_0^2}{p^2}\Pi_L(p_0,p)\ . \quad (2.44)
$$

Combining eq. (2.37) with the definitions reported in (2.44) one gets the following expression for Π_L and Π_T:

$$
\begin{aligned}
\Pi_L(p_0,p) &= m_D^2\,(1-Q(p_0/p)) &\text{(2.45a)}\\
\Pi_T(p_0,p) &= \frac{m_D^2}{2}\frac{p_0^2}{p^2}\left(1-\frac{p_0^2-p^2}{p_0^2}\,Q(p_0/p)\right)\ , &\text{(2.45b)}
\end{aligned}
$$

where

$$
Q(x) \equiv \frac{x}{2}\ln\frac{x+1}{x-1} \qquad (2.46)
$$

is the Legendre polynomial of second kind.
Because of the prescription $p_0=\omega+i\eta$ (ω real) we have that:

$$
\mathrm{Im}Q(p_0/p) = -\frac{\pi\omega}{2p}\theta(p-|\omega|)\quad . \qquad (2.47)
$$

The longitudinal and transverse gluon propagators in HTL thus read:

$$
{}^\star\Delta_L(p_0,p) = \frac{-1}{p^2+\Pi_L(p_0,p)} \,, \qquad {}^\star\Delta_T(p_0,p) = \frac{-1}{p_0^2-p^2-\Pi_T(p_0,p)} \,. \quad (2.48)
$$

The two dressed propagators admit the following *spectral representation*:

$$
{}^\star\Delta_L(z,p) = -\frac{1}{p^2} - \int_{-\infty}^{+\infty} dp_0 \, \frac{{}^\star\rho_L(p_0,p)}{z-p_0} \qquad (2.49a)
$$

$$
{}^\star\Delta_T(z,p) = - \int_{-\infty}^{+\infty} dp_0 \, \frac{{}^\star\rho_T(p_0,p)}{z-p_0} \,, \qquad (2.49b)
$$

with z in the complex energy plane. The spectral densities are then given by:

$$
{}^\star\rho_{L/T}(\omega,p) = \frac{1}{\pi}\mathrm{Im}{}^\star\Delta_{L/T}(\omega+i\eta,p) \,. \qquad (2.50)
$$

The following inverse energy weighted sum rules are immediately proved:

$$
{}^\star\Delta_L(0,p) = \frac{-1}{p^2+m_D^2} \quad \Rightarrow \quad \int_{-\infty}^{+\infty} \frac{dp_0}{p_0} {}^\star\rho_L(p_0,p) = \frac{1}{p^2} - \frac{1}{p^2+m_D^2} \qquad (2.51a)
$$

$$
{}^\star\Delta_T(0,p) = \frac{1}{p^2} \quad \Rightarrow \quad \int_{-\infty}^{+\infty} \frac{dp_0}{p_0} {}^\star\rho_T(p_0,p) = \frac{1}{p^2} \,. \qquad (2.51b)
$$

The HTL gluon spectral functions receive two kinds of contributions. For time-like momenta ($|\omega| > p$) $\mathrm{Im}\Pi_{L/T} = 0$, thus the solutions of the equation $\mathrm{Re}({}^\star\Delta_{L/T}^{-1}) = 0$ correspond to quasi-particle poles. On the other hand for space-like momenta ($|\omega| < p$) the spectral function has a continuum support coming from the imaginary part of $\Pi_{L/T}$.

Let us now consider the dispersion relations of the quasi-particle excitations. For what concern the transverse part the dispersion relation which yields the position of the quasi-particle pole as a function of the spatial momentum is given by the solution $\omega_T = \omega_T(p)$ of the equation:

$$
\omega_T^2 - p^2 - \frac{m_D^2}{2}\frac{\omega_T^2}{p^2}\left(1 - \frac{\omega_T^2-p^2}{\omega_T^2} Q(\omega_T/p)\right) = 0 \,. \qquad (2.52)
$$

Eq. (2.52) leads to the following asymptotic behaviour:

$$
p \ll m_D \quad \omega_T^2 \simeq \frac{m_D^2}{3} + \frac{6}{5}p^2 = \omega_p^2 + \frac{6}{5}p^2 \,, \qquad (2.53a)
$$

$$
p \gg m_D \quad \omega_T^2 \simeq p^2 + \frac{m_D^2}{2} = p^2 + m_\infty^2 \qquad (2.53b)
$$

where we have introduced the *plasma frequency* $\omega_p = m_D/\sqrt{3}$ and the *asymptotic mass* of the transverse gluon $m_\infty = m_D/\sqrt{2}$.

The longitudinal dispersion relation comes instead from the solution $\omega_L = \omega_L(p)$ of the equation:

$$p^2 + \mathrm{Re}\left[m_D^2\left(1 - Q(\omega_L/p)\right)\right] = 0, \tag{2.54}$$

which leads to the asymptotic expressions:

$$p \ll m_D \quad \omega_L^2 \simeq \omega_p^2 + \frac{3}{5}p^2\ , \tag{2.55a}$$

$$p \gg m_D \quad \omega_L^2 \simeq p\left(1 + 2\exp\left(-\frac{p^2 + m_\infty^2}{m_\infty^2}\right)\right). \tag{2.55b}$$

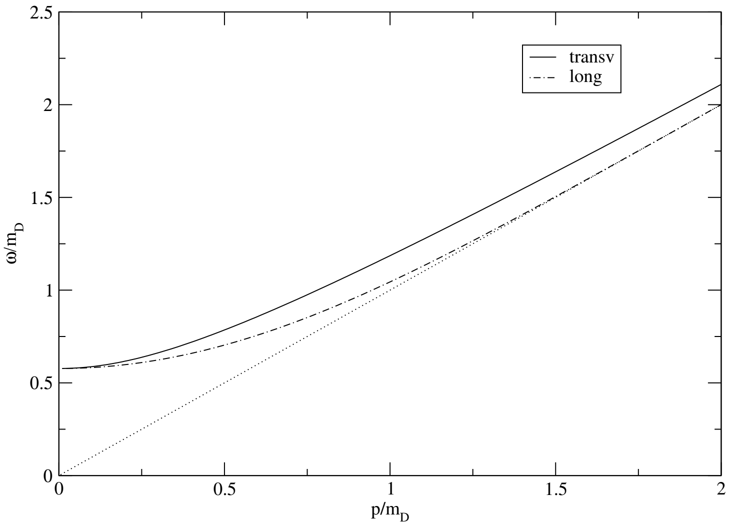

Figure 2.2: Transverse and longitudinal dispersion relations corresponding to the quasiparticle poles of the HTL gluon propagator. We use the dimensionless units p/m_D and ω/m_D.

We notice that at $p = 0$ both curves approach the same value ω_p, which is different from zero. Thus the spectrum presents a *gap*, called *plasma frequency*: one has to spend a finite amount of energy to add to the system a zero momentum excitation. In a classical plasma it corresponds to the frequency of spatially uniform oscillations.

On the other hand the behaviour for large values of p is very different. The longitudinal mode exponentially approaches the light cone, while the dispersion relation for the transverse gluons becomes the one of a relativistic particle of mass m_∞ (note that this asymptotic mass depends on temperature). Such an occurrence seems to justify the description of the thermodynamics of an SU(3) plasma in terms of a gas of *massive transverse gluons* [15].

One can obtain other useful *sum rules* in the following way. Let us consider the spectral representation (2.49a) for the gluon longitudinal propagator. At a fixed value of p the support of the spectral function is compact: it consists of two peaks at $\pm\omega_L(p)$ and a continuum part in the region $p_0 \in (-p, p)$. This makes it simpler to consider the limit $\omega \to \infty$. In fact we can write eq. (2.49a) in the following way:

$$\begin{aligned} {}^\star\Delta_L(\omega, p) &= -\frac{1}{p^2} - \frac{1}{\omega}\int_{-\infty}^{+\infty} dp_0 \frac{{}^\star\rho_L(p_0, p)}{1 - \left(\frac{p_0}{\omega}\right)} \\ &= -\frac{1}{p^2} - \frac{1}{\omega}\int_{-\infty}^{+\infty} dp_0 \sum_{n=0}^{+\infty} \left(\frac{p_0}{\omega}\right)^n {}^\star\rho_L(p_0, p)\ . \end{aligned} \tag{2.56}$$

Since $\rho_L(-p_0) = -\rho_L(p_0)$ only the odd powers contributes to the series. Thus we can write, for $\omega \to \infty$:

$${}^\star\Delta_L(\omega, p) = -\frac{1}{p^2} - \frac{1}{\omega}\sum_{n=0}^{+\infty}\int_{-\infty}^{+\infty} dp_0 \left(\frac{p_0}{\omega}\right)^{2n+1} {}^\star\rho_L(p_0, p). \tag{2.57}$$

Since the support of ${}^\star\rho_L$ is compact all the above moments exist and, for $\omega \to \infty$, just the first few terms of the series contribute. We can compare them with what we get expanding in powers of ω^{-1} the explicit expression of the longitudinal propagator:

$${}^\star\Delta_L(\omega, p) = \frac{-1}{p^2 + \Pi_L(\omega, p)} \simeq -\frac{1}{p^2} - \frac{m_D^2}{3p^2} + \dots \quad . \tag{2.58}$$

For $n = 0$ one gets the *energy weighted* sum rule:

$$\int_{-\infty}^{+\infty} dp_0\, p_0\, {}^\star\rho_L(p_0, p) = \frac{m_D^2}{3p^2} = \frac{\omega_p^2}{p^2} \tag{2.59}$$

One can follow the same steps for the transverse case obtaining:

$$\int_{-\infty}^{+\infty} dp_0\, p_0\, {}^\star\rho_T(p_0, p) = 1 \quad . \tag{2.60}$$

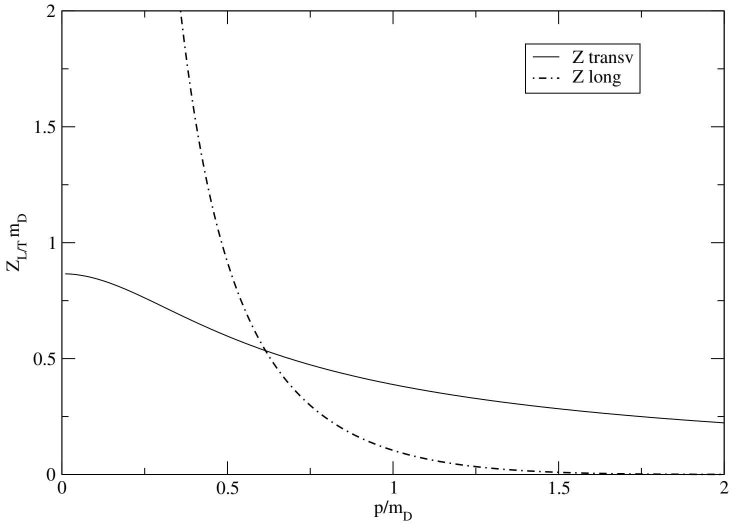

Figure 2.3: Residues of the transverse and longitudinal modes as a function of p/m_D. For dimensional reasons the residues $Z_{T/L}$ are multiplied by m_D.

To obtain the residues of the quasi-particle excitations the propagators should be expanded around their poles.
For the longitudinal propagator we get (we consider the positive energy excitation and retarded boundary conditions):

$$ {}^{\star}\Delta_L(\omega + i\eta, p) \underset{\omega\to\omega_L(p)}{\sim} \frac{\omega_L(p)(\omega_L^2(p) - p^2)}{p^2(p^2 + m_D^2 - \omega_L^2(p))} \frac{-1}{\omega - \omega_L(p) + i\eta} \; . \tag{2.61} $$

Hence the longitudinal residue is:

$$ Z_L(p) = \frac{\omega_L(p)(\omega_L^2(p) - p^2)}{p^2(p^2 + m_D^2 - \omega_L^2(p))} \quad , \tag{2.62} $$

which has the asymptotic behaviour:

$$ p \ll m_D \quad Z_L(p) \simeq \frac{\omega_p}{2p^2}\left(1 - \frac{3}{10}\frac{p^2}{\omega_p^2}\right) \tag{2.63a} $$

$$ p \gg m_D \quad Z_L(p) \simeq \frac{2p}{m_\infty^2}\exp\left(-\frac{p^2 + m_\infty^2}{m_\infty^2}\right) \; . \tag{2.63b} $$

We see that the longitudinal mode (which would correspond to an unphysical polarization for the gluon) tends to disappear very rapidly from the spectrum

for large enough momenta: it is a purely collective excitation which is relevant only at a *soft scale*. Instead, for *hard momenta* the relevant degrees of freedom are the physical particles (in this case the transverse gluons).
The full longitudinal spectral function in HTL approximation reads then:

$$ {}^*\rho_L(\omega,p) = Z_L(p)[\delta(\omega-\omega_L(p)) - \delta(\omega+\omega_L(p))] + \beta_L(\omega,p) \ , \tag{2.64} $$

where β_L represents the continuum contribution arising from the imaginary part of Π_L for space-like momenta. It is given by (we set $x = \omega/p < 1$):

$$ \beta_L(\omega,p) = \frac{\frac{m_D^2}{2}\, x\, \theta(1-x^2)}{\left[p^2 + m_D^2\left(1 - \frac{x}{2}\ln\left|\frac{x+1}{x-1}\right|\right)\right]^2 + \left[\pi\frac{m_D^2}{2}x\right]^2} \ . \tag{2.65} $$

Following the same steps for the transverse propagator we get for the residue of the quasi-particle

$$ Z_T(p) = \frac{\omega_T(p)(\omega_T^2(p) - p^2)}{m_D^2\omega_T^2(p) - (\omega_T^2(p) - p^2)^2} \ , \tag{2.66} $$

whose asymptotic expressions read:

$$ p \ll m_D \quad Z_T(p) \simeq \frac{1}{2\omega_p}\left(1 - \frac{4}{5}\frac{p^2}{\omega_p^2}\right) \tag{2.67a} $$

$$ p \gg m_D \quad Z_T(p) \simeq \frac{1}{2p} \ . \tag{2.67b} $$

We finally get for the transverse spectral function in HTL approximation:

$$ {}^*\rho_T(\omega,p) = Z_T(p)[\delta(\omega-\omega_T(p)) - \delta(\omega+\omega_T(p))] + \beta_T(\omega,p) \ , \tag{2.68} $$

where the continuum contribution, coming from $\mathrm{Im}\Pi_T$, reads:

$$ \beta_T(\omega,p) = \frac{\frac{m_D^2}{4}\, x(1-x^2)\theta(1-x^2)}{\left[p^2(x^2-1) - \frac{m_D^2}{2}\left(x^2 + \frac{x(1-x^2)}{2}\ln\left|\frac{x+1}{x-1}\right|\right)\right]^2 + \left[\pi\frac{m_D^2}{4}x(1-x^2)\right]^2} \ . \tag{2.69} $$

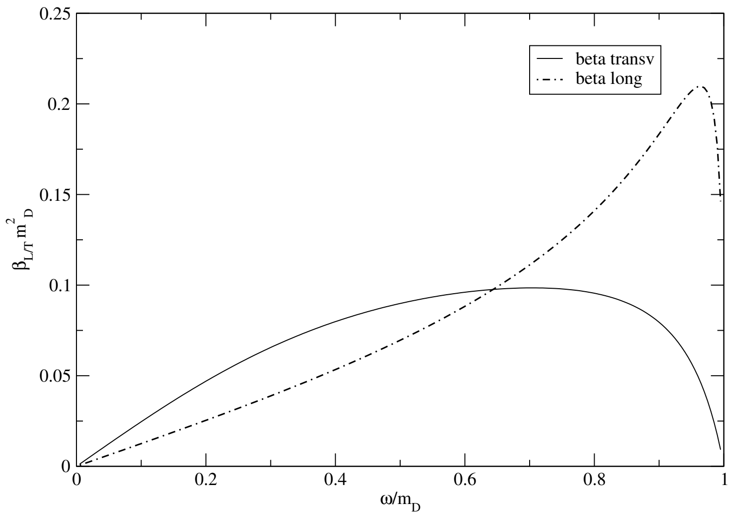

Figure 2.4: Dimensionless spectral function $m_D^2 \rho_{T/L}$ for space-like momenta at $p = m_D$ as a function of ω/m_D. The maximum of β_L comes from a second solution of the equation (2.54) in the space-like region, but in this case, due to the imaginary part of Π_L, it does not give rise to a well defined peak corresponding to a quasi-particle excitation.

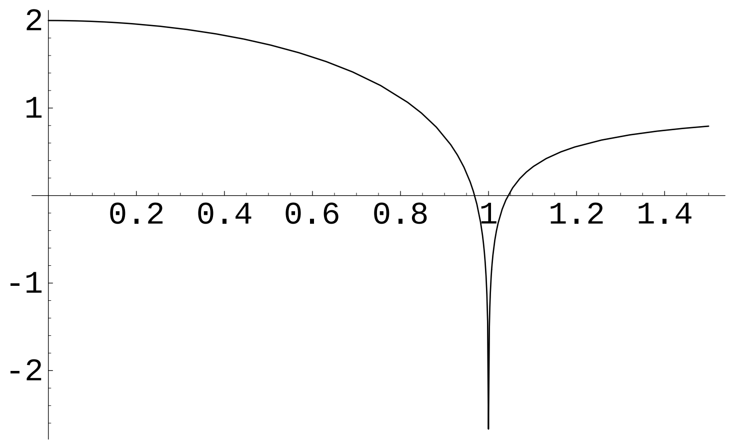

Figure 2.5: Real part of the denominator of the longitudinal gluon propagator at $p = m_D$ in suitable dimensionless units. We see that there is also a value of ω in the space-like domain for which it vanishes.

2.2.2 Quark self-energy

The Dyson equation provides a convenient recipe to get a resummed propagator, once a certain approximation for the sum of all the one particle irreducible (1PI) diagrams is made. In fact, starting from the free (massless) quark propagator, reported in eq. (2.2), we can easily resum the series:

$$\frac{-1}{\not p} + \frac{-1}{\not p}(-\Sigma)\frac{-1}{\not p} + \frac{-1}{\not p}(-\Sigma)\frac{-1}{\not p}(-\Sigma)\frac{-1}{\not p} + \dots \quad , \tag{2.70}$$

obtaining:

$$^\star S(P) = \frac{-1}{\not p - \Sigma(p)} \quad . \tag{2.71}$$

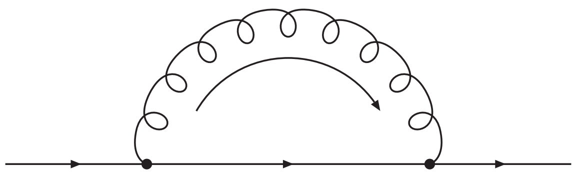

Figure 2.6: The diagram contributing to the quark self-energy in the HTL approximation.

The HTL approximation consists in keeping into account for Σ just the one-loop diagram in fig (2.6). Like in the case of the gluon self-energy the main contribution to the integral is assumed to arise from the interaction between a soft external quark ($P \sim gT$) and the hard momenta in the loop ($K \sim T$ or larger). Note that in order to express the resummed propagator as in Eq. (2.71), the diagram in Fig. (2.6) is equal to $-\Sigma(P)$. As usual we start working in the imaginary time formalism. We define the four-vectors $P = (i\omega_n, \boldsymbol{p})$, $K = (i\omega_l, \boldsymbol{k})$ and $\widehat{K} = (1, \hat{\boldsymbol{k}})$, where ω_n is a fermionic frequency while ω_l is a bosonic one. The propagators entering in the diagram (we work in Feynman gauge) are defined, in accord with Secs. 2.1.1 and 2.1.2, as follows:

$$\Delta^{ab}_{\mu\nu}(K) = -\delta^{ab} g_{\mu\nu}\Delta(K) \ , \quad S(P-K) = (\not P - \not K)\widetilde{\Delta}(P-K) \ . \tag{2.72}$$

Thus we can write:

$$\Sigma(P) = +g^2(t^a t^a)\int [dK][\gamma^\mu(\not P - \not K)\gamma_\mu]\Delta(K)\widetilde{\Delta}(P-K) \ . \tag{2.73}$$

The matrices t^a belong to the fundamental representation of SU(3) and the repeated indices a are meant to be summed. Moreover the compact notation

$$\int [dK] = \frac{1}{\beta}\sum_{l=-\infty}^{+\infty}\int \frac{d^3k}{(2\pi)^3} \tag{2.74}$$

has been introduced (the square brackets mean that we are summing over *even* frequencies).
As above stated in the HTL approximation one assumes that the integral is dominated by hard momenta and thus the "external" $\not{P}$ in the numerator is ignored. Since $t^a t^a = 4/3$, applying Dirac algebra one gets:

$$\begin{aligned}\Sigma(P) &= 2g^2\frac{4}{3}\int [dK]\not{K}\Delta(K)\widetilde{\Delta}(P-K)\\ &= 2g^2\frac{4}{3}\int [dK](i\gamma^0\omega_l - \gamma^i k^i)\Delta(K)\widetilde{\Delta}(P-K) \quad .\end{aligned} \tag{2.75}$$

The frequency sum can be performed with standard techniques (see for example [16]). Aiming at evaluating explicitly the leading dependence of the quark self-energy on the temperature and since, as already stressed, the leading order effect is assumed to be the interaction of a soft quark ($P \sim gT$) with the hard degrees of freedom of the plasma ($K \sim T \gg P$) one can use the following approximation:

$$\begin{aligned} E_1 &= k & E_2 &= |\boldsymbol{p}-\boldsymbol{k}| \simeq k - p\cos\theta\\ E_1 - E_2 &\simeq p\cos\theta & E_1 + E_2 &\simeq 2k - p\cos\theta \end{aligned} \tag{2.76}$$

Then the leading terms in T should be extracted from the following integrals:

$$\begin{aligned}\int [dK]k^i\Delta(K)\widetilde{\Delta}(P-K) = -\frac{1}{8\pi^2}\int \frac{k^2\,dk\,d\Omega}{4\pi}\,\frac{k^i}{E_1E_2}\times\\ \times\left[\left(\frac{1}{i\omega_n - E_1 - E_2} - \frac{1}{i\omega_n + E_1 + E_2}\right)(1 + n_1 - \tilde{n}_2) + \right.\\ \left. + \left(\frac{1}{i\omega_n + E_1 - E_2} - \frac{1}{i\omega_n - E_1 + E_2}\right)(n_1 + \tilde{n}_2)\right]\end{aligned} \tag{2.77}$$

and

$$\begin{aligned}\int [dK]\omega_n\Delta(K)\widetilde{\Delta}(P-K) = \frac{1}{8\pi^2}\int \frac{k^2\,dk\,d\Omega}{4\pi}\,\frac{i}{E_2}\times\\ \times\left[\left(\frac{1}{i\omega_n - E_1 - E_2} + \frac{1}{i\omega_n + E_1 + E_2}\right)(1 + n_1 - \tilde{n}_2) + \right.\\ \left. - \left(\frac{1}{i\omega_n + E_1 - E_2} + \frac{1}{i\omega_n - E_1 + E_2}\right)(n_1 + \tilde{n}_2)\right] \quad .\end{aligned} \tag{2.78}$$

Using the approximations (2.76) it is easily found that only the second term in the two integrals contributes to order T^2. One obtains:

$$\int [dK]\omega_l \Delta(K)\widetilde{\Delta}(P-K) \simeq \frac{-iT^2}{16}\int \frac{d\Omega_k}{4\pi}\frac{1}{P\cdot\widehat{K}} \tag{2.79a}$$

$$\int [dK]k^i \Delta(K)\widetilde{\Delta}(P-K) \simeq \frac{T^2}{16}\int \frac{d\Omega_k}{4\pi}\frac{\hat{k}^i}{P\cdot\widehat{K}} \quad . \tag{2.79b}$$

As in the case of the gluon self-energy the temperature dependent part of the diagram is UV finite: switching on temperature does not introduce new UV divergences, so we don't care about renormalization. This fact can be interpreted by saying that temperature does not modify the physics at very short scales, i.e. at scales much shorter than the average distance between the partons of the thermal bath.
Inserting the approximate results (2.79a) and (2.79b) into Eq. (2.75) one gets the compact expression

$$\Sigma_{HTL}(P) = m_q^2 \int \frac{d\Omega_k}{4\pi}\frac{\widehat{\not{K}}}{P\cdot\widehat{K}} \tag{2.80}$$

for the HTL quark self-energy, where the *quark thermal mass* $m_q^2 = g^2T^2/6$ has been introduced. In fact we will see in the following that the spectrum of the theory, also in the quark sector, presents a *gap*, which we identify with the thermal mass of the fermion: for time-like quadrimomenta an energy m_q is required to excite the system with zero spatial momentum.
We can now analytically continue our result to real values of the frequency letting $i\omega_n \to \omega + i\eta$ (retarded boundary conditions) obtaining:

$$\Sigma_{HTL}(\omega, \boldsymbol{p}) = m_q^2 \int \frac{d\Omega_k}{4\pi}\frac{\widehat{\not{K}}}{\omega - p\cos\theta + i\eta} \quad , \tag{2.81}$$

$\boldsymbol{p}$ defining the z-axis. The angular integration is immediately done. Thus we get:

$$\Sigma_{HTL}(\omega, \boldsymbol{p}) = a(\omega, p)\gamma^0 + b(\omega, p)\boldsymbol{\gamma}\cdot\hat{\boldsymbol{p}} \quad , \tag{2.82}$$

where:

$$a(\omega, p) \equiv \frac{m_q^2}{\omega}Q(\omega/p), \quad b(\omega, p) \equiv \frac{m_q^2}{p}[1 - Q(\omega/p)]. \tag{2.83}$$

The function $Q(x)$ has been defined in eq. (2.46).
Once we know the self-energy in this approximation (from now on we will drop the subscript HTL) we can obtain the resummed propagator by inverting the Dyson equation:

$$^{\star}S^{-1}(P) = S_0^{-1}(P) + \Sigma(P) \quad . \tag{2.84}$$

In this connection it is particularly useful to introduce the operators

$$h_{\pm}(\hat{\boldsymbol{p}}) = (\gamma^0 \mp \hat{\boldsymbol{p}} \cdot \boldsymbol{\gamma})/2 \; . \tag{2.85}$$

The free propagator and the self-energy can be in fact decomposed in the following way:

$$\begin{aligned}
S_0(\omega, \boldsymbol{p}) &= \frac{-1}{\omega - p} h_+(\hat{\boldsymbol{p}}) + \frac{-1}{\omega + p} h_-(\hat{\boldsymbol{p}}) && (2.86)\\
S_0^{-1}(\omega, \boldsymbol{p}) &= (-\omega - p) h_+(\hat{\boldsymbol{p}}) + (-\omega + p) h_-(\hat{\boldsymbol{p}}) && (2.87)\\
\Sigma(\omega, \boldsymbol{p}) &= (a(\omega,p) + b(\omega,p)) \frac{\gamma^0 + \hat{\boldsymbol{p}} \cdot \boldsymbol{\gamma}}{2} + (a(\omega,p) - b(\omega,p)) \frac{\gamma^0 - \hat{\boldsymbol{p}} \cdot \boldsymbol{\gamma}}{2} \\
&= h_-(\hat{\boldsymbol{p}}) \Sigma_+(\omega, p) - h_+(\hat{\boldsymbol{p}}) \Sigma_-(\omega, p) \quad , && (2.88)
\end{aligned}$$

where $\Sigma_{\pm}(\omega,p) = \pm a(\omega,p) + b(\omega,p)$. Thus the inverse quark propagator can be written as:

$${}^{\star}S(\omega, \boldsymbol{p})^{-1} = \left(-\omega - p - \Sigma_-(\omega,p)\right) h_+(\hat{\boldsymbol{p}}) + \left(-\omega + p + \Sigma_-(\omega,p)\right) h_-(\hat{\boldsymbol{p}}) \quad . \tag{2.89}$$

Let us also introduce the *projection operators*

$$\Lambda_{\pm}(\hat{\boldsymbol{p}}) = h_{\pm}(\hat{\boldsymbol{p}}) \gamma^0 \; . \tag{2.90}$$

One can immediately verify the identities:

$$h_{\pm}(\hat{\boldsymbol{p}}) \cdot h_{\pm}(\hat{\boldsymbol{p}}) = 0 \quad , \quad h_{\pm}(\hat{\boldsymbol{p}}) \cdot h_{\mp}(\hat{\boldsymbol{p}}) = \Lambda_{\pm}(\hat{\boldsymbol{p}}) \; . \tag{2.91}$$

These allow to invert Eq. (2.89) yielding:

$${}^{\star}S(\omega, \boldsymbol{p}) = {}^{\star}\Delta_+(\omega,p) \; h_+(\hat{\boldsymbol{p}}) + {}^{\star}\Delta_-(\omega,p) \; h_-(\hat{\boldsymbol{p}}) \; , \tag{2.92}$$

where:

$$\begin{aligned}
{}^{\star}\Delta_{\pm}(\omega,p) &= \frac{-1}{\omega \mp (p + \Sigma_{\pm}(\omega,p))} && (2.93)\\
&= \frac{-1}{\omega \mp p - \dfrac{m_q^2}{2p}\left[\left(1 \mp \dfrac{\omega}{p}\right) \ln \dfrac{\omega + p}{\omega - p} \pm 2\right]} \; . && (2.94)
\end{aligned}$$

Note that since $\{\Sigma_{HTL}, \gamma^5\} = 0$, the dressed propagator still anticommutes with γ^5. Thus, though a thermal mass appears in the spectrum, the chirality of a quark propagating in the plasma is conserved.

Let us consider in more detail this last point. Using the projection operators $\Lambda_\pm(\hat{\boldsymbol{p}})$ a generic spinor can be decomposed as follows:

$$\psi(P) = \Lambda_+(\hat{\boldsymbol{p}})\psi(P) + \Lambda_-(\hat{\boldsymbol{p}})\psi(P) \quad . \tag{2.95}$$

From the definition of the spin operator $\Sigma^i = \gamma^5\gamma^0\gamma^i$ we then have:

$$\gamma^5\left(\Lambda_+(\hat{\boldsymbol{p}})\psi(P)\right) = \frac{\gamma^5 + \vec{\Sigma}\cdot\hat{p}}{2}\psi(P) \tag{2.96a}$$

$$\gamma^5\left(\Lambda_-(\hat{\boldsymbol{p}})\psi(P)\right) = \frac{\gamma^5 - \vec{\Sigma}\cdot\hat{p}}{2}\psi(P) \quad . \tag{2.96b}$$

Thus we see that the operators $\Lambda_\pm(\hat{\boldsymbol{p}})$ project onto spinors whose helicity over chirality ratio χ is equal respectively to ± 1. While at $T = 0$ the propagating (massless) positive energy excitations are forced to have $\chi = 1$, at $T \neq 0$ also excitation with $\chi = -1$ (antiquark holes) can propagate into the plasma.

The HTL quark propagator is conveniently expressed through its spectral function

$$^\star S(p_0, \boldsymbol{p}) = -\int_{-\infty}^{+\infty} d\omega \frac{\rho_{\mathrm{HTL}}(\omega, \boldsymbol{p})}{p_0 - \omega} \; . \tag{2.97}$$

With the explicit form for $^\star\Delta_\pm$ (2.93) it is easily proved that the HTL quark spectral function

$$\rho_{\mathrm{HTL}}(\omega, \boldsymbol{p}) = \frac{\gamma^0 - \boldsymbol{\gamma}\cdot\hat{\boldsymbol{p}}}{2}\rho_+(\omega, p) \; + \; \frac{\gamma^0 + \boldsymbol{\gamma}\cdot\hat{\boldsymbol{p}}}{2}\rho_-(\omega, p) \; , \tag{2.98}$$

with

$$\rho_\pm(\omega, p) = \frac{1}{\pi}\mathrm{Im}\,^\star\Delta_\pm(\omega + i\eta, p), \tag{2.99}$$

gets contributions both from the imaginary part coming from the logarithm appearing in the self-energy (for space-like momenta) and from the quasi-particle poles (for time-like momenta). We have:

$$\rho_\pm(\omega, p) = \lim_{\eta\to 0^+}\frac{1}{\pi}\frac{\eta \mp \mathrm{Im}\Sigma_\pm(\omega + i\eta, p)}{\left[\omega \mp (p + \mathrm{Re}\Sigma_\pm(\omega + i\eta, p))\right]^2 + \left[\eta \mp \mathrm{Im}\Sigma_\pm(\omega + i\eta, p)\right]^2} \; . \tag{2.100}$$

The $+i\eta$ appearing in the self energies gives us a prescription on how to approach the cut of the function $Q(x)$ defined in eq. (2.46). It is unessential for time-like momenta.

The quasi-particle poles correspond to the zeros of the *real part* of the denominator of $^\star\Delta_\pm$ for $|\omega| > p$. In both cases one gets a positive and a negative energy solution which lead to the *dispersion relations*:

$$\omega = \omega_+(p) \; , \quad \omega = -\omega_-(p) \tag{2.101}$$

for ${}^\star\Delta_+$ and

$$\omega = \omega_-(p)\ , \quad \omega = -\omega_+(p) \tag{2.102}$$

for ${}^\star\Delta_-$. The behaviour of $\omega_\pm$ can be obtained by solving numerically the equation:

$$\omega_\pm = \pm p + \frac{m_q^2}{2p}\left[\left(1 \mp \frac{\omega_\pm}{p}\right)\ln\left|\frac{\omega_\pm + p}{\omega_\pm - p}\right| \pm 2\right] \quad . \tag{2.103}$$

It is important to notice that the condition of setting to zero the real part of the denominator of the fermionic propagator is not sufficient to identify all the solutions of such an equation as quasi-particle poles. In fact eq. (2.103) has solutions also for space-like momenta, but in this case $\mathrm{Im}\Sigma_\pm \neq 0$, thus we don't find any peaks in the spectral function, as can be seen in fig. (2.8).

Expanding eq. (2.103) we find the asymptotic behaviour for small values of

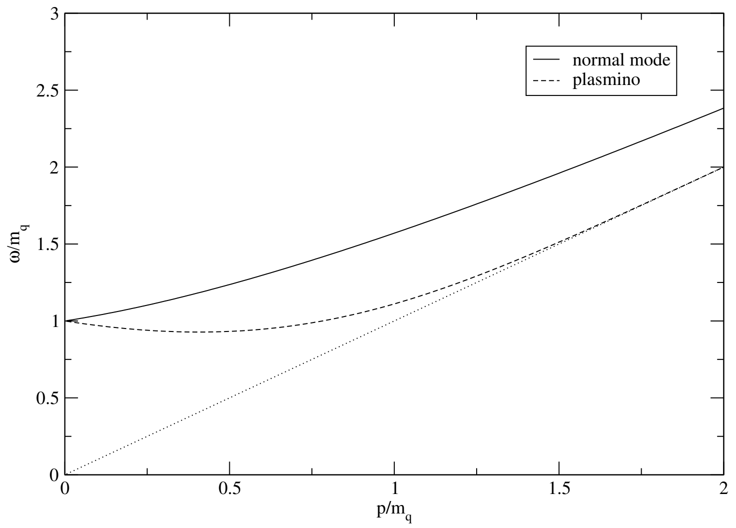

Figure 2.7: Dispersion relations corresponding to the quasiparticle poles of the HTL fermion propagator. We use the dimensionless units p/m_q and ω/m_q.

p ($p \ll m_q$), namely:

$$\omega_\pm(p) \simeq m_q \pm \frac{1}{3}p \quad , \tag{2.104}$$

while for large values of p ($m_q \ll p \ll T$) we have:

$$\omega_+(p) \simeq p + \frac{m_q^2}{p} \qquad \omega_-(p) \simeq p + 2p\,\exp\left(-\frac{2p^2 + m_q^2}{m_q^2}\right) \quad . \tag{2.105}$$

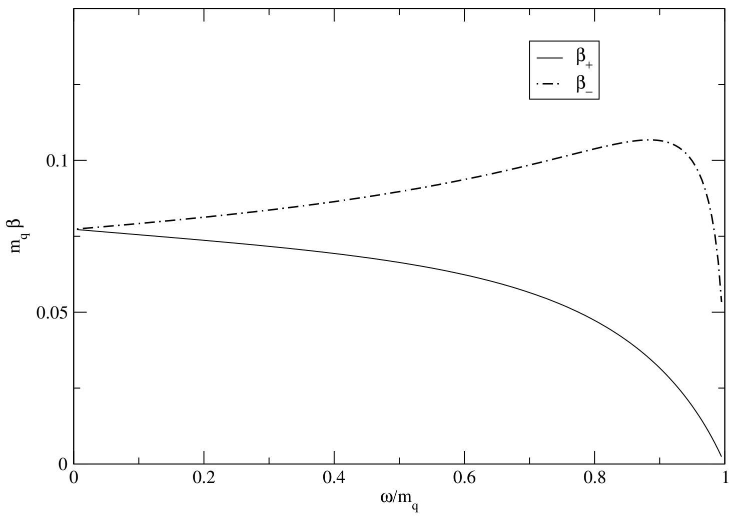

Figure 2.8: Dimensionless spectral function $m_q \rho_\pm$ for space-like momenta at $p = m_q$ as a function of ω/m_q. The maximum of β_- comes from a second value of $\omega_-(p)$ which satisfies eq. (2.103) in the space-like region, but in this case, due to the imaginary part of the self-energy, it does not give rise to a well defined peak corresponding to a quasi-particle excitation

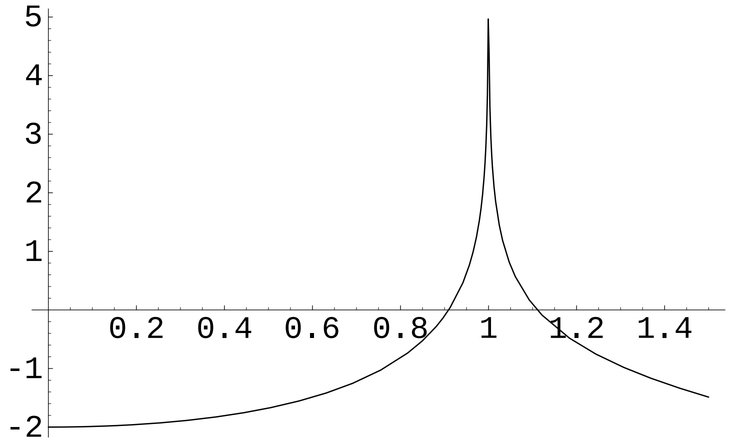

Figure 2.9: Real part of the denominator of ${}^\star\Delta_-$ at $p = m_q$ in suitable dimensionless units. We see that there is also a value of ω in the space-like domain for which it vanishes.

Note that, for high spatial momenta, the normal quark mode behaves like a massive particle:

$$\omega_+(p) \simeq \sqrt{p^2 + \hat{m}_\infty^2} \quad \text{with} \quad \hat{m}_\infty^2 = 2m_q^2 \quad , \tag{2.106}$$

where we have introduced the *asymptotic quark mass* $\hat{m}_\infty$.

It is of interest to calculate the residue of the quasi-particle poles associated with the above mentioned excitations, in order to display the weight of their contribution to the spectrum of the theory. This can be easily done by expanding the denominators of ${}^\star\Delta_\pm$ around the quasi-particle poles. We get, assuming retarded boundary conditions (i.e. the poles lie below the real axis):

$$^\star\Delta_\pm(\omega, p) \underset{\omega\to\omega_\pm}{\sim} \frac{\omega_\pm^2(p) - p^2}{2m_q^2} \frac{-1}{\omega - \omega_\pm(p) + i\eta} \ , \tag{2.107}$$

$$^\star\Delta_\pm(\omega, p) \underset{\omega\to-\omega_\mp}{\sim} \frac{\omega_\mp^2(p) - p^2}{2m_q^2} \frac{-1}{\omega + \omega_\mp(p) + i\eta} \ . \tag{2.108}$$

$$\tag{2.109}$$

Thus the pole contribution to the quark spectral function can be written as:

$$\rho_\pm^{\text{pole}}(\omega, p) = Z_\pm(p)\delta(\omega - \omega_\pm(p)) + Z_\mp(p)\delta(\omega + \omega_\mp(p)) \ , \tag{2.110}$$

the residues $Z_\pm$ being given by:

$$Z_\pm = \frac{\omega_\pm^2(p) - p^2}{2m_q^2} \ . \tag{2.111}$$

Inserting eq. (2.104) and (2.105) into (2.111) the following asymptotic expressions are found

$$p \ll m_q \ : \qquad Z_\pm(p) \simeq \frac{1}{2} \pm \frac{p}{3m_q} \tag{2.112}$$

while for large values of the momentum one gets:

$$p \gg m_q \ : \qquad Z_+(p) \simeq 1 + \frac{m_q^2}{2p^2}\left(1 - \ln\frac{2p^2}{m_q^2}\right) \tag{2.113a}$$

$$Z_-(p) \simeq \frac{2p^2}{m_q^2} \exp\left(-\frac{2p^2 + m_q^2}{m_q^2}\right) \ . \tag{2.113b}$$

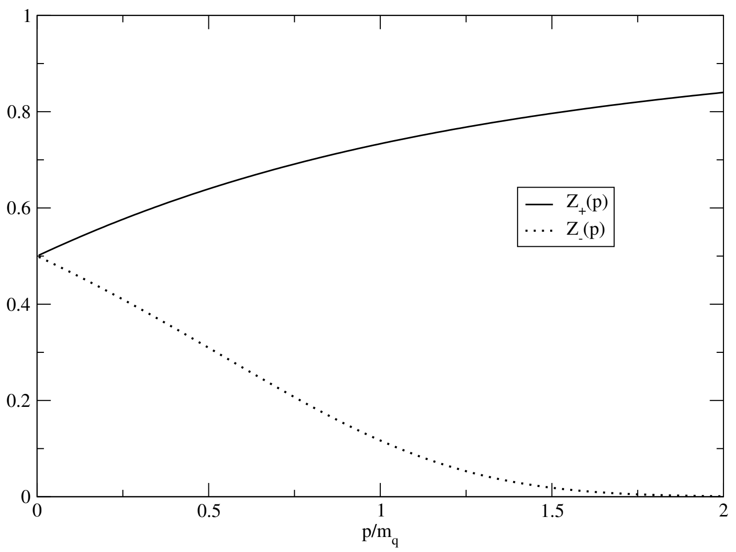

Figure 2.10: Residues of the quasi-particle excitations as a function of p/m_q. We can appreciate that, while at $p = 0$ $Z_\pm$ give the same contribution, for larger values of p the plasmino mode tends to disappear from the spectrum.

We can see that the *plasmino mode*, which is a pure collective excitation and would correspond to the propagation of an unphysical quark mode with helicity over chirality ratio $\chi = -1$, tends to disappear from the spectrum for hard momenta. This agrees with the starting assumption that the *hard degrees of freedom* correspond to the plasma particles (quarks, antiquarks and transverse gluons), while at a *soft scale* the spectrum also contains collective excitations (longitudinal gluons and plasminos) which do not have counterpart at $T = 0$.
Proceeding analogously to what was done in Sec. (2.2.1) it is possible to deduce the following *sum rules*:

$$\int_{-\infty}^{+\infty} dp_0\, \rho_\pm(p_0, p) = 1 \tag{2.114a}$$

$$\int_{-\infty}^{+\infty} dp_0\, p_0\, \rho_\pm(p_0, p) = \pm p \tag{2.114b}$$

$$\int_{-\infty}^{+\infty} dp_0\, p_0^2\, \rho_\pm(p_0, p) = p^2 + m_q^2\ . \tag{2.114c}$$

Eq. (2.114a) can be obtained from the equal-time anticommutation relation:

$$\{\psi(t, \boldsymbol{x}), \psi^\dagger(t, \boldsymbol{x'})\} = \delta(\boldsymbol{x} - \boldsymbol{x'}) \quad , \tag{2.115}$$

whereas the other ones require a more elaborated analysis, similar to the procedure followed in Sec. (2.2.1) for the longitudinal and transverse sum rules. Actually Eq. (2.114a) can be written in a more suggestive way as:

$$Z_+(p) + Z_-(p) + \int_{-p}^{+p} dp_0 \, \rho_\pm(p_0, p) = 1 \quad , \tag{2.116}$$

where the two different contributions, namely the quasi-particle poles and the continuum part (Landau damping), are clearly separated out.
We can see from eq. (2.104) that, for small momenta, the pole part almost saturates the sum rule and an almost equal contribution is given by the two modes $\chi = \pm 1$. On the contrary for large momenta, from Eq. (2.105), we see that the major role is played by the mode with $\chi = +1$. The continuum part gives a significant contribution only for intermediate momenta.

We now want to compare, in a range of temperatures of experimental interest, the HTL (gauge invariant) quark self-energy with the complete one-loop result. Actually the latter turns out to be gauge dependent, but we don't worry about this since the quark self-energy is not directly an observable. Here we adopt the Feynman gauge. It has been checked in the literature that, though the quark self-energy depend on the choice of the gauge, the location of the poles of the quark propagator, which represent physical excitations, results gauge invariant.

We start from the general formula for the one-loop self-energy for a massive quark:

$$\begin{aligned}\Sigma(P) &= -g^2 \frac{1}{\beta} \sum_{l=-\infty}^{+\infty} \int \frac{d^3k}{(2\pi)^3} \gamma^\mu t^a S_F(P-K) \gamma^\nu t^b \Delta^{ab}_{\mu\nu}(K) \\ &= \frac{4}{3} g^2 \frac{1}{\beta} \sum_{l=-\infty}^{+\infty} \int \frac{d^3k}{(2\pi)^3} \gamma^\mu S_F(P-K) \gamma_\mu \Delta(K) \, ,\end{aligned} \tag{2.117}$$

where we labelled the four-momenta as in Eq. (2.73), i.e. $P = (i\omega_n, \boldsymbol{p})$ and $K = (i\omega_l, \boldsymbol{k})$, and for the gluon propagator in Feynman gauge we employed the formula given in Eq. (2.8a).

By introducing the momentum $\boldsymbol{q} = \boldsymbol{p} - \boldsymbol{k}$ and writing the single particle propagators according to Eqs. (2.6) and (2.12) one gets:

$$\begin{aligned}\Sigma(i\omega_n, \boldsymbol{p}) = \frac{4}{3} g^2 \frac{1}{\beta} \sum_{l=-\infty}^{+\infty} \int \frac{d^3k}{(2\pi)^3} \int_0^\beta d\tau_1 \int_0^\beta d\tau_2 \int_{-\infty}^{+\infty} dq_0 \int_{-\infty}^{+\infty} dk_0 \\ e^{i\omega_n \tau_1} e^{i\omega_l(\tau_2 - \tau_1)} e^{-q_0 \tau_1} e^{-k_0 \tau_2} (1 - \tilde{n}(q_0))(1 + n(k_0)) \\ \rho_0(q_0, \boldsymbol{q}) \rho_0(k_0, \boldsymbol{k}) \gamma^\mu (\not{Q} + m) \gamma_\mu \, ,\end{aligned} \tag{2.118}$$

being $Q = (q_0, \boldsymbol{q})$.

The sum over the *even* Matsubara frequencies can be performed by exploiting the identity:

$$\frac{1}{\beta} \sum_{l=-\infty}^{+\infty} e^{i\omega_l(\tau_2 - \tau_1)} = \sum_{m=-\infty}^{+\infty} \delta(\tau - \tau_1 - m\beta) \ . \tag{2.119}$$

The domain of integration selects in the above sum only the $m = 0$ term. The two temporal integrations are immediately done and, after some simple Dirac algebra, we are left with:

$$\begin{aligned} \Sigma(i\omega_n, \boldsymbol{p}) = \frac{4}{3} g^2 \frac{1}{\beta} \sum_{l=-\infty}^{+\infty} \int \frac{d^3k}{(2\pi)^3} \int_{-\infty}^{+\infty} dq_0 \int_{-\infty}^{+\infty} dk_0 \frac{1 + e^{-\beta(q_0 + k_0)}}{i\omega_n - q_0 - k_0} \\ (1 - \tilde{n}(q_0))(1 + n(k_0)) \rho_0(q_0, \boldsymbol{q}) \rho_0(k_0, \boldsymbol{k})(2\not{Q} - 4m) \ . \end{aligned} \tag{2.120}$$

The statistical factors can be cast in the more convenient form:

$$\left(1 + e^{-\beta(q_0 + k_0)}\right)(1 - \tilde{n}(q_0))(1 + n(k_0)) = 1 - \tilde{n}(q_0) + n(k_0) \ . \tag{2.121}$$

As usual, having performed the frequency sum, the result can be continued in the complex energy plane. The retarded self-energy is obtained through the replacement $i\omega_n \to \omega + i\eta$ and reads:

$$\begin{aligned} \Sigma_R(\omega, \boldsymbol{p}) = \frac{4}{3} g^2 \int \frac{d^3k}{(2\pi)^3} \frac{1}{4\epsilon_k \epsilon_q} \times \\ \times \Bigg\{ \left(\epsilon_q \gamma^0 - \boldsymbol{q} \cdot \boldsymbol{\gamma} - 2m\right) \left(\frac{1 + n(\epsilon_k) - \tilde{n}(\epsilon_q)}{\omega - \epsilon_q - \epsilon_k + i\eta} + \frac{\tilde{n}(\epsilon_q) + n(\epsilon_k)}{\omega - \epsilon_q + \epsilon_k + i\eta} \right) + \\ + \left(\epsilon_q \gamma^0 + \boldsymbol{q} \cdot \boldsymbol{\gamma} + 2m\right) \left(\frac{\tilde{n}(\epsilon_q) + n(\epsilon_k)}{\omega + \epsilon_q - \epsilon_k + i\eta} + \frac{1 + n(\epsilon_k) - \tilde{n}(\epsilon_q)}{\omega + \epsilon_q + \epsilon_k + i\eta} \right) \Bigg\} \end{aligned} \tag{2.122}$$

The above equation, as usual, can be separated into a temperature independent term

$$\begin{aligned} \Sigma_R^{T=0}(\omega, \boldsymbol{p}) = \frac{4}{3} g^2 \int \frac{d^3k}{(2\pi)^3} \frac{1}{4\epsilon_k \epsilon_q} \times \\ \times \left(\frac{\epsilon_q \gamma^0 - \boldsymbol{q} \cdot \boldsymbol{\gamma} - 2m}{\omega - \epsilon_q - \epsilon_k + i\eta} + \frac{\epsilon_q \gamma^0 + \boldsymbol{q} \cdot \boldsymbol{\gamma} + 2m}{\omega + \epsilon_q + \epsilon_k + i\eta} \right) \ , \end{aligned} \tag{2.123}$$

related to the *vacuum fluctuations* (a quark splits into a quark and a gluon), and a temperature dependent term

$$\Sigma_R^T(\omega,\boldsymbol{p}) = \frac{4}{3}g^2\int\frac{d^3k}{(2\pi)^3}\frac{1}{4\epsilon_k\epsilon_q}\times$$
$$\times\left\{\left(\epsilon_q\gamma^0-\boldsymbol{q}\cdot\boldsymbol{\gamma}-2m\right)\left(\frac{n(\epsilon_k)-\tilde{n}(\epsilon_q)}{\omega-\epsilon_q-\epsilon_k+i\eta}+\frac{\tilde{n}(\epsilon_q)+n(\epsilon_k)}{\omega-\epsilon_q+\epsilon_k+i\eta}\right)+\right.$$
$$\left.+\left(\epsilon_q\gamma^0+\boldsymbol{q}\cdot\boldsymbol{\gamma}+2m\right)\left(\frac{\tilde{n}(\epsilon_q)+n(\epsilon_k)}{\omega+\epsilon_q-\epsilon_k+i\eta}+\frac{n(\epsilon_k)-\tilde{n}(\epsilon_q)}{\omega+\epsilon_q+\epsilon_k+i\eta}\right)\right\}\ . \quad (2.124)$$

The latter embodies (for positive ω) two further processes: a quark which absorbs a gluon from the thermal bath changing its momentum (second term) and a quark which annihilates with an antiquark from the thermal bath giving a gluon (third term). For large enough temperature these are the dominant contributions to the integral, leading precisely, after neglecting the quark mass and making some kinematical approximation, to the HTL result quoted in Eq. (2.81). We now neglect the quark mass and consider

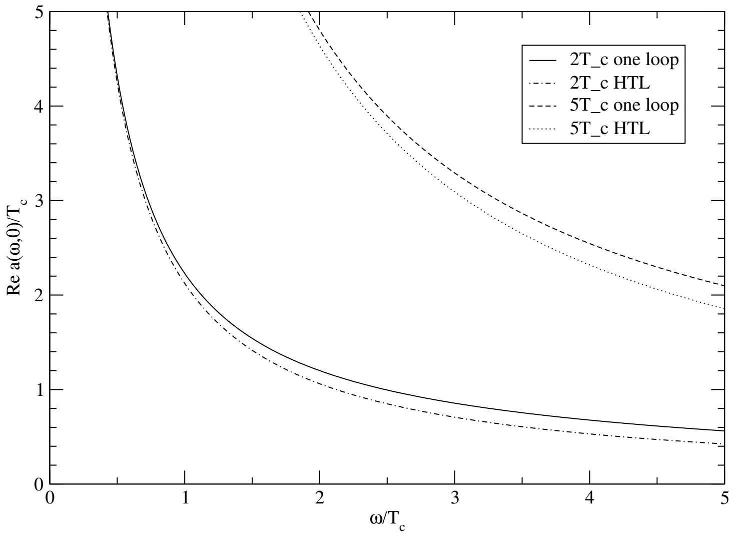

Figure 2.11: Comparison of the behaviour of $\mathrm{Re}\,a(\omega,0)/T_c$ as a function of ω/T_c computed keeping the full one-loop result and in the HTL approximation, for $T=2T_c$ and $T=5T_c$. The plot refers to the case of massless quarks and $N_f=2$.

for simplicity the case of zero spatial momentum. It is possible to compare the HTL approximation with the full one-loop result (for the latter we keep only the thermal contribution). For $\boldsymbol{p}=0$ the self-energy of a massless quark

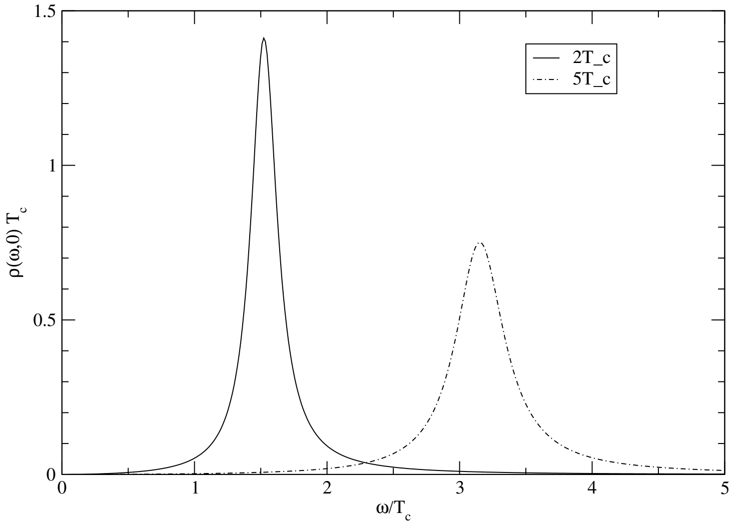

Figure 2.12: Here we plot the full one-loop result for the zero-momentum quark spectral function (multiplied by T_c). The plot is given for positive values of the dimensionless variable ω/T_c for two different temperatures: $T = 2T_c$ and $T = 5T_c$.

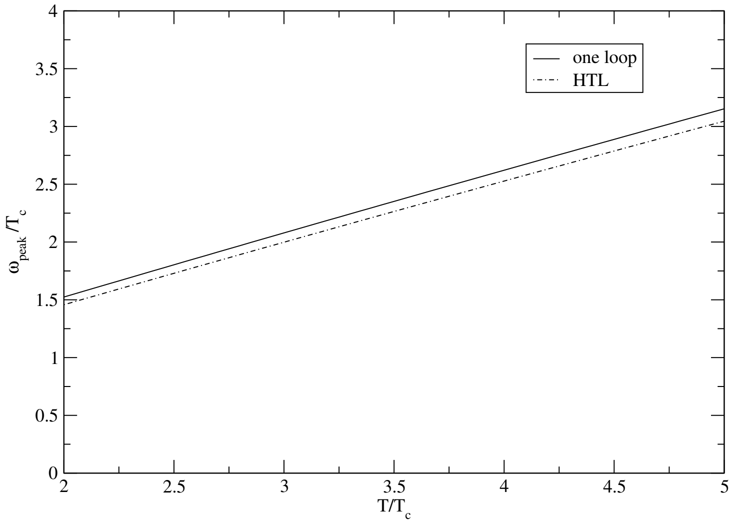

Figure 2.13: Here we display how the position of the peak (in units of T_c) of the *zero momentum* quark spectral function scales with respect to T/T_c. Notice that the HTL result differs from the full one loop calculation by less than 5%.

reduces to

$$\Sigma(\omega, 0) = a(\omega, 0)\gamma^0 \quad . \tag{2.125}$$

In the HTL approximation such a self-energy, being the four-momentum timelike, is purely real. In the full one loop calculation $a(\omega, 0)$ becomes instead complex, the real part arising from the principal value of the loop integral and the imaginary part coming from the poles of the integrand function.

Hence the quark spectral function (which in the HTL case is simply a delta-like peak at the value of the thermal quark mass) acquires a width which, as it can be seen in Fig. (2.12), increases with the temperature. For what concerns the real part of Σ we can appreciate in Fig. (2.11) how the HTL approximation essentially coincides with the full calculation for soft frequencies and still gives the major contribution for higher values of ω. In Fig. (2.13) we display, for both cases, the position of the quasi-particle peak as a function of the temperature. Notice that the HTL result differs from the full calculation just by a few percent.

The running of $\alpha_s(\mu)$ is obtained through the two-loop QCD β-function with $N_f = 2$. In the case of massless quarks the only physical scale is the temperature. Thus we evaluate α_s at the scale $\mu = 2\pi T$ which corresponds to the spacing between the Matsubara frequencies. For the case $N_f = 2$ we take from Ref. [23] the result $T_c/\Lambda_{\overline{MS}} = 0.49$.

We wish to stress that the one-loop self-energy is not gauge invariant. In particular the width of the spectral functions plotted in Fig. (2.12) depends strongly on the choice of the gauge. In order to evaluate the *physical, gauge invariant, decay width* of a quark in the thermal bath one has to employ for the gluon line a *resummed propagator*. For such a calculation we refer the reader to the literature [13].

In the following we will dress the soft fermionic lines with HTL self energy insertions (which account for the most relevant part of the interaction, as illustrated above) obtaining resummed propagators.
For what concerns the hard fermionic modes, NLO effects are taken into account considering their interaction with *soft gluons*, for which the HTL approximation provide us resummed propagators.

2.2.3 Vertex corrections and Ward identities

We now address the issue of evaluating, in the HTL approach, the vertex corrections to the coupling between a quark of the thermal bath and a vector boson (a photon or a gluon). For the sake of illustration, we start with the quark-photon vertex, since it involves just one diagram. Such a vertex is of importance for the evaluation of the dilepton production rate from the QCD

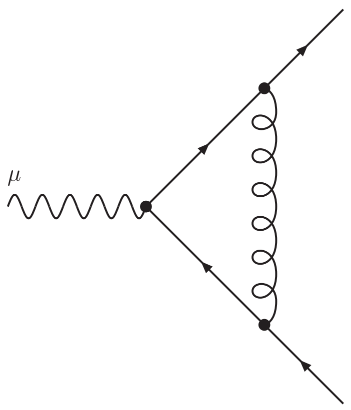

Figure 2.14: Correction to the tree level quark-photon vertex.

plasma. We will also see that the axial coupling receives no correction at the leading order (LO) in HTL.
On the other hand the LO correction to the quark-gluon vertex gets contribution from two diagrams, the second one, which involves a three gluon coupling, arising from the non abelian nature of QCD. At the end of the computation we will verify that, when the quark self-energy and the *effective* quark-gluon vertex are computed in the HTL approximation, then the Ward identities are satisfied.

Let us first consider the lowest order correction to the quark-photon vertex which comes from the diagram in Fig. (2.14). For the internal lines we adopt the notation reported in Eq. (2.33a) and (2.30). The expression for the effective vertex thus reads:

$$\begin{aligned}{}^{\star}\Gamma_\mu(P_1,P_2) &= Q_f\, e\ (\gamma_\mu + \delta\Gamma_\mu(P_1,P_2)) \\ &= Q_f\, e\,\gamma_\mu - Q_f\, e\gamma_\mu\, g^2(t^a t^a)\int [dK][\gamma^\alpha(\not{P}_2 - \not{K})\gamma_\mu(\not{P}_1 - \not{K})\gamma_\alpha]\cdot \\ &\quad \cdot\Delta(K)\widetilde{\Delta}(P_2-K)\widetilde{\Delta}(P_1-K) \quad , \qquad (2.126)\end{aligned}$$

where $P_1 = (i\omega_{n_1}, \boldsymbol{p_1})$, $P_2 = (i\omega_{n_2}, \boldsymbol{p_2})$ and we have used the compact notation already adopted in eq. (2.74).

Let us now concentrate on the correction to the tree level vertex, computing it in the limit of *soft external momenta*. In the HTL approach the dominant part to the integral is supposed to come from *hard* internal momenta. Thus we can drop P_1 and P_2 in the numerator of Eq. (2.126) getting:

$$\delta\Gamma_\mu(P_1,P_2) = -\frac{4}{3}g^2 \int [dK][\gamma^\alpha \not{K}\gamma_\mu \not{K}\gamma_\alpha]\Delta(K)\widetilde{\Delta}(P_2-K)\widetilde{\Delta}(P_1-K) \quad . \tag{2.127}$$

After using some Dirac algebra the above becomes:

$$\begin{aligned}\delta\Gamma_\mu(P_1,P_2) &= -2\,\frac{4}{3}g^2\gamma_\mu \int [dK]K^2\Delta(K)\widetilde{\Delta}(P_2-K)\widetilde{\Delta}(P_1-K) \\ &\quad +4\,\frac{4}{3}g^2\gamma^\alpha \int [dK]K_\mu K_\alpha\Delta(K)\widetilde{\Delta}(P_2-K)\widetilde{\Delta}(P_1-K) \\ &\quad .\end{aligned} \tag{2.128}$$

In our spirit of keeping only the temperature dependent corrections proportional to T^2 we can neglect the first term in eq. (2.128). Such a term is the only one which would be present in the case of a scalar or pseudoscalar coupling: *hence the scalar and axial vertexes receive no correction in the HTL approximation.* Coming back to the quark-photon vertex the expression we have to evaluate is the following one:

$$\delta\Gamma_\mu^{HTL}(P_1,P_2) = 4\,\frac{4}{3}g^2\gamma^\alpha \int [dK]K_\mu K_\alpha\Delta(K)\widetilde{\Delta}(P_2-K)\widetilde{\Delta}(P_1-K) \quad , \tag{2.129}$$

where $K = (i\omega_l, \boldsymbol{k})$. The basic ingredients required to evaluate the above expression are now

$$X_0 = T\sum_{l=-\infty}^{+\infty} \Delta(K)\widetilde{\Delta}(P_2-K)\widetilde{\Delta}(P_1-K) \tag{2.130a}$$

$$X_1 = T\sum_{l=-\infty}^{+\infty} \omega_l\Delta(K)\widetilde{\Delta}(P_2-K)\widetilde{\Delta}(P_1-K) \tag{2.130b}$$

$$X_2 = T\sum_{l=-\infty}^{+\infty} \omega_l^2\Delta(K)\widetilde{\Delta}(P_2-K)\widetilde{\Delta}(P_1-K) \quad . \tag{2.130c}$$

Of course, since $K^2 = -\omega_l^2 - k^2$ and since the term with K^2 gives a subleading contribution, we immediately get that, in HTL:

$$X_2 = -k^2 X_0 \quad . \tag{2.131}$$

For what concerns X_0 and X_1, after doing the same kind of kinematic approximations as in section (2.2.1) and (2.2.2) (see ref. [16] for details) we

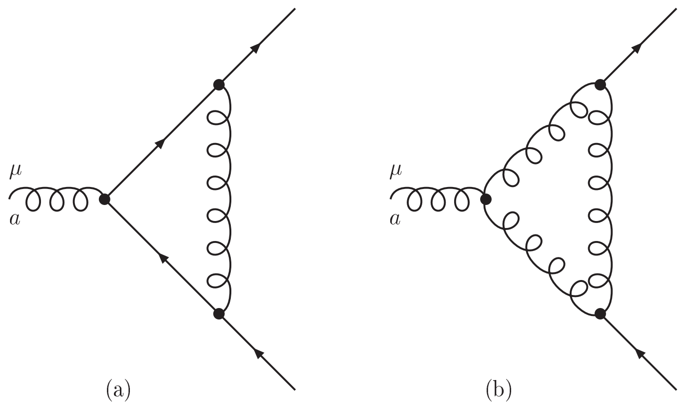

Figure 2.15: Diagrams contributing to the effective quark-gluon vertex in the HTL approximation.

obtain the following results:

$$X_0 = \frac{n(k)+\tilde{n}(k)}{8k^3}\left[\frac{1}{(P_1\cdot\widehat{K})(P_2\cdot\widehat{K})}+\frac{1}{(P_1\cdot\widehat{K}')(P_2\cdot\widehat{K}')}\right] \tag{2.132a}$$

$$X_1 = -i\,\frac{n(k)+\tilde{n}(k)}{8k^2}\left[\frac{1}{(P_1\cdot\widehat{K})(P_2\cdot\widehat{K})}-\frac{1}{(P_1\cdot\widehat{K}')(P_2\cdot\widehat{K}')}\right]\ , \tag{2.132b}$$

where $\widehat{K} = (1, \hat{\boldsymbol{k}})$ and $\widehat{K}' = (1, \hat{\boldsymbol{k}}')$. Then, performing the integration over k, we can express the HTL correction to the quark-photon vertex in the compact form according to

$$\delta\Gamma_\mu^{HTL}(P_1,P_2) = m_q^2\int\frac{d\Omega_k}{4\pi}\frac{\widehat{\not{K}}\,\widehat{K}_\mu}{\left[(P_1\cdot\widehat{K})(P_2\cdot\widehat{K})\right]} \tag{2.133}$$

and the quark-photon effective vertex then reads:

$$^\star\Gamma_\mu(P_1,P_2) = Q_f e\left(\gamma_\mu + m_q^2\int\frac{d\Omega_k}{4\pi}\frac{\widehat{\not{K}}\,\widehat{K}_\mu}{\left[(P_1\cdot\widehat{K})(P_2\cdot\widehat{K})\right]}\right)\quad . \tag{2.134}$$

In the case of the quark-gluon vertex correction one has to sum the two diagrams of fig. (2.15). Using the same approximations as above (i.e. keeping only the leading term in T^2) one gets, in the HTL framework, the following effective vertex,:

$$\begin{aligned} {}^{\star}\Gamma^a_\mu(P_1,P_2) &= g\,t^a(\gamma_\mu + \delta\Gamma^{HTL}_\mu(P_1,P_2)) \\ &= g\,t^a\left(\gamma_\mu + m_q^2\int\frac{d\Omega_k}{4\pi}\frac{\widehat{\not K}\,\widehat{K}_\mu}{\left[(P_1\cdot\widehat{K})(P_2\cdot\widehat{K})\right]}\right)\,. \quad (2.135)\end{aligned}$$

Then from eq. (2.80) one can immediately verify that the Ward identity:

$$(P_1-P_2)^\mu\delta\Gamma^{HTL}_\mu(P_1,P_2) = \Sigma_{HTL}(P_2) - \Sigma_{HTL}(P_1) \quad (2.136)$$

holds.

2.3 Scales and degrees of freedom in a relativistic plasma

In this section we aim at providing a systematic classification of the scales of momenta in a QCD plasma and of their interactions. We will verify *a posteriori* that the HTL approximation accounts for the most relevant part of the interaction for what concerns the *soft modes*.
First of all we need to estimate the behaviour of the *gauge field fluctuations* (which, at the equilibrium, does not depend on the space-time point):

$$\bar{A}^a_\mu = \sqrt{\langle A^a_\mu(t,\boldsymbol{x})A^a_\mu(t,\boldsymbol{x})\rangle}\,. \quad (2.137)$$

As discussed in detail in ([13]) these are given by:

$$\langle A^2\rangle = \int\frac{d^4k}{(2\pi)^4}(1+n(k_0))\,2\pi\,\rho(k) \quad . \quad (2.138)$$

Since we want to consider only the *thermal fluctuation* we can drop the temperature independent term and write:

$$\langle A^2\rangle = \int\frac{d^4k}{(2\pi)^4}n(k_0)\,2\pi\,\rho(k) \quad , \quad (2.139)$$

where $\rho(k)$ is an appropriate spectral function, depending the channel (longitudinal or transverse) and the scale of momenta one is interested in.
As discussed in detail at the beginning of section (2.2) the dominant fluctuations in the plasma have momenta $k\sim T$ and correspond to the partonic degrees of freedom. For this scale we substitute into eq. (2.139) a free (massless)

spectral function $\rho_0(k) = \epsilon(k_0)\delta(k^2)$ (such an assumption will be justified *a posteriori*), thus obtaining:

$$\langle A^2 \rangle_T = \int \frac{d^3k}{(2\pi)^3} \frac{n(k)}{k} \sim T^2 \quad . \tag{2.140}$$

In addressing the *long-wavelength fluctuations* ($k \ll T$) one can approximate the statistical factor according to $n(k_0) \approx T/k_0$. Then:

$$\langle A^2 \rangle_{\text{soft}} \approx T \int d^3k \int \frac{dk_0}{k_0} \rho(k) \quad . \tag{2.141}$$

For this scale of momenta one can substitute into Eq. (2.141) the longitudinal and transverse spectral functions deduced in Sec. (2.2.1). In particular the integral in Eq. (2.141) can be evaluated through the sum rules (2.51a) and (2.51b).
For the longitudinal (electric) sector we get:

$$\langle A^2 \rangle_{gT} \approx T m_D^2 \int \frac{d^3k}{k^2(k^2 + m_D^2)} \sim T m_D \sim gT^2 \quad . \tag{2.142}$$

Indeed the integral over k has to be limited to momenta $k \ll T$; however for the electric sector, thanks to the presence of the *Debye screening mass*, we don't need to insert by hands an upper cutoff.
For the magnetic sector this is no longer possible and we have:

$$\langle A^2 \rangle_{\mu} \approx T \int^{\mu} \frac{d^3k}{k^2} \sim \mu T \quad . \tag{2.143}$$

Thus for the *soft* ($\mu \sim gT$) and the *ultrasoft* ($\mu \sim g^2T$) magnetic fluctuations we get:

$$\langle A^2 \rangle_{gT} \sim gT^2 \, , \qquad \qquad \langle A^2 \rangle_{g^2T} \sim g^2T^2 \quad . \tag{2.144}$$

The ultrasoft electric fluctuations ($k \sim g^2T \ll m_D$) are instead suppressed by the Debye mass:

$$\langle A^2 \rangle_{g^2T} \approx T \int^{g^2T} \frac{d^3k}{k^2 + m_D^2} \sim g^4T^2 \quad . \tag{2.145}$$

We can now discuss the coupling of the different modes (hard, soft, ultrasoft) with the *thermal gauge field fluctuations* at the different scales (T, gT, g^2T). For this purpose it is convenient to translate the coupling into momentum space according to:

$$D_\mu = \partial_\mu - ig\bar{A}_\mu \quad \Rightarrow \quad -ik - ig\bar{A}_{\bar{\mu}} \quad , \tag{2.146}$$

where $\bar{\mu}$ is the scale of the gauge field fluctuation.

We begin by considering the coupling between a hard mode (a particle of the plasma) with a hard gauge field fluctuation. We have:

$$-ik - ig\bar{A}_T \sim -iT - igT \quad . \tag{2.147}$$

Thus the interaction among the hard modes can be treated perturbatively and, at the lowest order, ignored. Interactions of the hard modes with softer fluctuations of the gauge field are further suppressed by higher powers of g.

For what concerns the soft modes we see that they are still perturbative, i.e. their self-interaction can be at first ignored since:

$$-ik - ig\bar{A}_{gT} \sim -igT - ig(gT^2)^{1/2} \sim -igT - ig^{3/2}T \quad . \tag{2.148}$$

Even more negligible is the interaction of soft degrees of freedom with the ultrasoft fluctuation.
On the other hand in treating the coupling of the soft modes with the hard thermal fluctuations we need some kind of resummation, since the two terms in the covariant derivative are of the same order:

$$-ik - ig\bar{A}_T \sim -igT - igT \quad . \tag{2.149}$$

In the ultrasoft sector we have to distinguish between electric and magnetic fluctuations. Since $\bar{A}^{el}_{g^2T} \sim g^2T$, while $\bar{A}^{magn}_{g^2T} \sim gT$ it follows that the self-interaction among ultrasoft magnetic modes can't be treated perturbatively, being:

$$k - ig\bar{A}^{magn}_{g^2T} \sim g^2T - ig^2T \quad . \tag{2.150}$$

The above considerations support the philosophy of the HTL approximation which aims at dressing the propagation in the plasma of *soft modes*, keeping into account their interactions with the *hard degrees of freedom*.

2.4 Self-consistent thermodynamics in QFT at finite temperature

In this section we address the question of evaluating thermodynamical quantities (such as the entropy, the pressure, the baryon density...) for a quantum field theory at finite temperature in a self-consistent framework.
The section is organized as follows. We first introduce, following [17, 23, 26], the concept of Φ-derivable approximation. Then we apply the developed

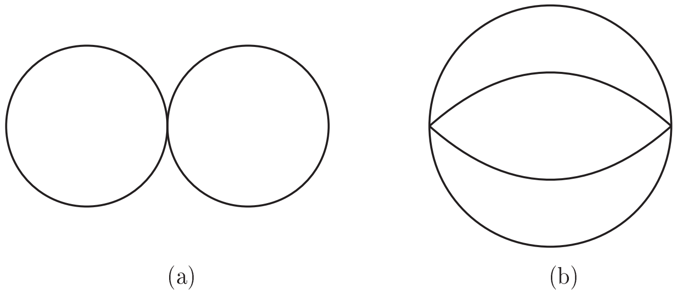

Figure 2.16: The first few skeleton diagrams from the expansion of the thermodynamical potential. The lines are fully dressed propagators.

mathematical tools to the study of the thermodynamics of a scalar field: this provides us a toy model to test further approximations we need in the more involved case of a gauge theory. Finally we move to the case of the QCD plasma, for which a fully self-consistent solution can't be obtained. Thus we will start from the HTL approximation and we will display how the results obtained in such a scheme can be improved.

2.4.1 Φ-derivable approximation

We introduce the basic features of the study of the thermodynamics of a QFT within the framework of a Φ-derivable approximation. For the sake of simplicity we start from the case of a scalar field.
The thermodynamical potential, which is defined as

$$\beta\Omega = -\log(Z) \quad , \tag{2.151}$$

(Z being the gran-canonical partition function), can be written as the following functional of the *fully dressed* propagator D:

$$\beta\Omega[D] = \frac{1}{2}\mathrm{Tr}\log(D^{-1}) - \frac{1}{2}\mathrm{Tr}\Pi D \,+\, \Phi[D] \quad . \tag{2.152}$$

In the above the trace is performed in coordinate space with the following prescription:

$$\mathrm{Tr}X \equiv \int_0^\beta d\tau\, d^3x\, X(\tau,\boldsymbol{x};\tau^+,\boldsymbol{x}) \quad . \tag{2.153}$$

One can express more conveniently eq. (2.153) in Fourier space as given below:

$$
\begin{aligned}
\mathrm{Tr}X &= \int_0^\beta d\tau\, d^3x\, \frac{1}{\beta} \sum_{n=-\infty}^{+\infty} \int \frac{d^3k}{(2\pi)^3}\, e^{i\omega_n\eta}\, X(i\omega_n, \boldsymbol{k}) \\
&= \beta\, V \int [dK]\, e^{i\omega_n\eta} X(K) \quad , \qquad (2.154)
\end{aligned}
$$

where $K = (i\omega_n, \boldsymbol{k})$ and we have adopted the compact notation introduced in eq. (2.74). The factor $\exp(i\omega_n\eta)$, coming from the τ^+ prescription of Eq. (2.153), is important in performing the summation over the Matsubara frequencies.

The link between the dressed propagator and the self energy is given by the Dyson equation:

$$
D^{-1} = D_0^{-1} + \Pi \quad . \qquad (2.155)
$$

Notice that, because of our choice of the plus sign in front of Π, in the evaluation of the self-energy through the Feynman rules, we have to assign to all the diagrams an overall minus sign.

For what concerns the term $\Phi[D]$ in eq. (2.152) it is given by the sum of all the *2-particle-irreducible skeleton* diagrams coming from the expansion of Ω (with the proper combinatorial factors) in which, differently from what happens in the pure perturbative scheme, all the internal lines are fully dressed propagators D instead of bare ones D_0. We report the first few of them, for a ϕ^4 interaction, in fig. (2.16).

The thermodynamical potential Ω (considered as a functional of D) satisfies the following important stationary property: its functional derivative with respect to the dressed propagator D, *taken at fixed* D_0, vanishes. We have:

$$
\left(\frac{\delta\Omega[D]}{\delta D}\right)_{D_0} = 0 \quad . \qquad (2.156)
$$

Once we apply such a property to eq. (2.152) we find that the self-energy Π can be expressed in term of the functional derivative of Φ:

$$
\left(\frac{\delta\Phi}{\delta D}\right)_{D_0} = \frac{1}{2}\Pi \quad . \qquad (2.157)
$$

In fact, applying the stationary condition to the r.h.s. of eq. (2.152), the second term gives origin to two contributions, but the one coming from the variation of Π simplifies with the first term in the r.h.s.. Hence we are left with,

$$
0 = -\frac{1}{2}\mathrm{Tr}\Pi\, \delta D + \delta\Phi \quad , \qquad (2.158)
$$

where:

$$\delta\Phi = \mathrm{Tr}\left(\frac{\delta\Phi}{\delta D}\right)\cdot\delta D \quad . \tag{2.159}$$

Since the variation δD is completely arbitrary we are left with eq. (2.157). A self-consistent, Φ-derivable, approximation consists then in selecting a certain set of skeleton diagrams for $\Phi[D]$. Cutting one (dressed) propagation line, as expressed by eq. (2.157), in all possible ways one gets the corresponding approximation for the self-consistent self-energy.

Let us now perform, in eq. (2.152), the sum over the (bosonic) Matsubara frequencies with a standard contour integration (of course we are taking the trace in Fourier space). We get:

$$\Omega/V = \int \frac{d^4k}{(2\pi)^4} n(\omega)\left(\mathrm{Im}\log(-\omega^2+k^2+\Pi) - \mathrm{Im}\Pi D\right) + T\Phi[D]/V \ , \tag{2.160}$$

where $n(\omega) = 1/(e^{\beta\omega}-1)$ and the integration over ω, in case of ambiguity, has to be considered as the principal value of the integral, in order to avoid the pole at $\omega_n = 0$ [17]. Thus one is left with the evaluation of discontinuities of propagators and self-energies, which can be easily related to well defined physical processes. In our notation $\mathrm{Im}f(\omega) = \mathrm{Im}f(\omega + i\eta)$. The following spectral representation turns out to be useful:

$$D(\omega, k) = -\int_{-\infty}^{+\infty} \frac{dk_0}{2\pi}\frac{\rho(k_0,k)}{\omega - k_0} \quad , \tag{2.161}$$

thus we have, keeping ω real,

$$\mathrm{Im}D(\omega,k) \equiv \mathrm{Im}D(\omega + i\eta, k) = \frac{\rho(\omega,k)}{2} \quad . \tag{2.162}$$

Let us now address the calculation of the entropy density, which is given by:

$$S = -\frac{\partial(\Omega/V)}{\partial T} \quad . \tag{2.163}$$

Here one can appreciate the power of the Φ-derivable approach. In fact the dependence of the thermodynamical potential on the temperature comes from the statistical factor in eq. (2.160), but also from the self-energy Π and the spectral function ρ (which can describe, for example, a scalar particle endowed with a thermal mass arising from the interaction with the bath). Nevertheless, because of the stationary property (2.156), in the evaluation of the entropy density, one has only to take the derivative of the statistical factor $n(\omega)$. It is then convenient to write the entropy density in the following way:

$$\begin{aligned} S &= -\int \frac{d^4k}{(2\pi)^4} \frac{\partial n(\omega)}{\partial T} \mathrm{Im}\log D^{-1}(\omega, k) \\ &\quad + \int \frac{d^4k}{(2\pi)^4} \frac{\partial n(\omega)}{\partial T} \mathrm{Im}\Pi(\omega, k)\, \mathrm{Re}D(\omega, k) + S' \ , \end{aligned} \tag{2.164}$$

where:

$$S' = -\left(\frac{\partial(T\Phi)}{\partial T}\right)_D + \int \frac{d^4k}{(2\pi)^4} \frac{\partial n(\omega)}{\partial T} \mathrm{Re}\Pi(\omega, k)\, \mathrm{Im}D(\omega, k) \ . \tag{2.165}$$

In the following we will display that the first two term in eq. (2.164) can be related to the entropy of a system of independent quasiparticles. On the contrary S' gives the contribution to the entropy due to a residual interaction among the quasiparticles.
Leaving apart for the moment S', we see that eq. (2.164) makes the entropy a privileged quantity to study. First of all the derivative of the statistical factor makes the integrand vanish exponentially for $\omega \to \pm\infty$ and thus our formula has no U.V. divergences. Secondly eq. (2.164) is invariant for field redefinitions $D \to Z\, D$ and $\Pi \to Z^{-1}\, \Pi$ (with Z real).

Let us now try to express eq. (2.164) in a more suggestive way (for what concerns the physical processes involved). Since:

$$\log D^{-1} = \log\left(-\omega^2 + k^2 + \mathrm{Re}\Pi\right) + \log\left(1 + i\frac{\mathrm{Im}\Pi}{-\omega^2 + k^2 + \mathrm{Re}\Pi}\right) \ , \tag{2.166}$$

and recalling the $\omega + i\eta$ prescription, we get:

$$\mathrm{Im}\log D^{-1}(\omega, k) = -\pi\epsilon(\omega)\theta(-\mathrm{Re}D^{-1}) + \arctan\left(\frac{\mathrm{Im}\Pi(\omega + i\eta, k)}{\mathrm{Re}D^{-1}}\right) \ . \tag{2.167}$$

Neglecting S' (which indeed in some approximations vanishes) the entropy density can be written as the sum of two contribution, one related to the quasi-particle poles and one related to their damping.
The pole contribution comes from the first term in the r.h.s. of eq. (2.167) and reads:

$$\begin{aligned} S_{\mathrm{pole}} &= \int \frac{d^4k}{(2\pi)^4} \frac{\partial n(\omega)}{\partial T} \pi\epsilon(\omega)\theta(-\mathrm{Re}D^{-1}) \\ &= \int \frac{d^3k}{(2\pi)^3} \left\{(1 + n_k)\log(1 + n_k) - n_k \log n_k\right\} \ . \end{aligned} \tag{2.168}$$

In going from the first to the second line we have integrated by parts and we have set $n_k = n(\epsilon_k)$, where ϵ_k is the solution of the equation

$$\mathrm{Re}D^{-1}(\omega = \epsilon_k, k) = 0 \quad . \tag{2.169}$$

The contribution stemming from the continuum part of the spectral function, associated with the damping of the quasi-particles, is given by:

$$S_{\mathrm{damp}} = \int \frac{d^4k}{(2\pi)^4} \frac{\partial n(\omega)}{\partial T} \left\{ \mathrm{Im}\Pi\, \mathrm{Re}D - \arctan\left(\frac{\mathrm{Im}\Pi}{\mathrm{Re}D^{-1}} \right) \right\} \quad , \tag{2.170}$$

where the $\omega + i\eta$ prescription is meant. As one can see, if $\mathrm{Im}\Pi = 0$, such a contribution vanishes.

2.4.2 Thermodynamics of a scalar field

We now consider, as a toy model to test the results which can be obtained in such a framework, a massless scalar field with an interaction lagrangian:

$$\mathcal{L}_{\mathrm{int}} = -\frac{\lambda_0}{4!}\phi^4 \quad . \tag{2.171}$$

In the expansion of the thermodynamical potential $\Omega[D]$ we limit ourselves to the two-loop diagram in Fig. (2.16), all the (internal) lines being fully dressed propagators.
First of all we wish to demonstrate that, by considering such an approximation for $\Phi[D]$, we have $S' = 0$. Thus, in this case, the residual interaction among the quasiparticles vanishes. For what concerns the first term in eq. (2.165) we have:

$$\begin{aligned} -T\Phi &= -\frac{\lambda_0}{8}\left[\int [dK] D(i\omega_n, k)\right]^2 = -\frac{\lambda_0}{8}\left[-\frac{1}{\beta}\sum_{n=-\infty}^{+\infty}\int \frac{d^4k}{(2\pi)^4}\frac{\rho(k_0,k)}{i\omega_n - k_0}\right]^2 \\ &= -\frac{\lambda_0}{8}\int \frac{d^4k\, d^4k'}{(2\pi)^8}\rho(k_0,k)\rho(k_0',k')\, n(k_0)n(k_0') \, . \end{aligned} \tag{2.172}$$

The self-consistent self-energy (obtained from our approximation for $\Phi[D]$) is purely real an can be evaluated straightforwardly. We get:

$$\begin{aligned} \mathrm{Re}\Pi &= \frac{\lambda_0}{2}\left[\int [dK] D(i\omega_n, k)\right] = -\frac{\lambda_0}{2}\left[\frac{1}{\beta}\sum_{n=-\infty}^{+\infty}\int \frac{d^4k}{(2\pi)^4}\frac{\rho(k_0,k)}{i\omega_n - k_0}\right] \\ &= \frac{\lambda_0}{2}\int \frac{d^4k}{(2\pi)^4}\rho(k_0,k)\, n(k_0) \, . \end{aligned} \tag{2.173}$$

Inserting Eqs. (2.172) and (2.173) into Eq. (2.165) and remembering that in Eq. (2.172) one has to derive just the statistical factors, it is immediately proved that in this case $S' = 0$.

In our model the self-consistent self-energy turns out to be momentum independent. Thus we can write $\Pi = m^2$ and its only effect is to give the scalar particle a thermal mass. The spectral function associated to the full self-consistent propagator is then given by:

$$\rho(k_0, k) = 2\pi\epsilon(k_0)\delta(k_0^2 - k^2 - m^2). \tag{2.174}$$

Let us define the quantity:

$$I(m) \equiv \frac{1}{2}\int [dK] D(i\omega_n, k) = \frac{1}{2}\int [dK] \frac{1}{\omega_n^2 + k^2 + m^2} \quad . \tag{2.175}$$

Hence we have, from eq. (2.172):

$$T\Phi = \frac{\lambda_0}{2} I^2(m) \quad . \tag{2.176}$$

Inserting the above result into Eq. (2.152), remembering that $\Pi = m^2$, and performing the sum over the Matsubara frequencies we get:

$$-P = \frac{\Omega}{V} = \frac{1}{2}\int \frac{d^3k}{(2\pi)^3}\epsilon_k + \frac{1}{\beta}\int \frac{d^3k}{(2\pi)^3} \log(1 - e^{-\beta\epsilon_k}) - m^2 I(m) + \frac{\lambda_0}{2} I^2(m) \, . \tag{2.177}$$

Of course the above expression is ill defined, since both the first term in the r.h.s and $I(m)$ are affected by U.V. divergences which require renormalization.
For this purpose we start by applying the stationary property to the thermodynamical potential: its derivative with respect to m must vanish. Once we sum over the bosonic frequencies in eq. (2.175), we get

$$I(m) = I_0(m) + I_T(m) = \frac{1}{4}\int \frac{d^3k}{(2\pi)^3}\frac{1}{\epsilon_k} + \frac{1}{2}\int \frac{d^3k}{(2\pi)^3}\frac{n(\epsilon_k)}{\epsilon_k} \tag{2.178}$$

and, setting to zero the derivative of the r.h.s. of eq. (2.177) we are left with the following "gap equation":

$$m^2 = \lambda_0 \, I(m) \quad , \tag{2.179}$$

which still requires renormalization. Here λ_0 is the bare parameter appearing in the lagrangian. Note that in eq. (2.178) we managed to split $I(m)$ in

a divergent part $I_0(m)$, which does not depend on temperature, and in a temperature dependent part $I_T(m)$ which is U.V. finite.
We deal with U.V. divergences working in dimensional regularization. Thus we define the integrals over the spatial momenta in $d = 3 - \epsilon$ dimensions. Being μ the scale introduced by dimensional regularization, we define the dimensionless coupling $\hat{\lambda}_0$ as:

$$\lambda_0 = \mu^\epsilon \hat{\lambda}_0 \quad . \tag{2.180}$$

Thus the gap equation becomes:

$$\frac{1}{\hat{\lambda}_0} m^2 = \mu^\epsilon I(m) \quad . \tag{2.181}$$

In the above we can isolate a $1/\epsilon$ pole coming from $I_0(m)$. We have:

$$\mu^\epsilon I(m) = -\frac{m^2}{32\pi^2}\left(\frac{2}{\epsilon} + \log\frac{\bar{\mu}^2}{m^2} + 1\right) + I_T(m) + O(\epsilon) \quad , \tag{2.182}$$

where $\bar{\mu}^2 = 4\pi e^{-\gamma}\mu^2$.
In order to get a finite result for the mass, solution of the gap equation (2.181), we introduce the renormalized coupling λ, which is defined by the equation:

$$\frac{1}{\lambda} = \frac{1}{\lambda_0 \mu^{-\epsilon}} + \frac{1}{16\pi^2\epsilon} = \frac{1}{\hat{\lambda}_0} + \frac{1}{16\pi^2\epsilon} \quad . \tag{2.183}$$

From the above, it follows immediately that, as one changes the scale μ keeping λ_0 fixed, the renormalized coupling λ evolves according to the renormalization group equation:

$$\frac{d\lambda}{d\log\bar{\mu}} = \frac{\lambda^2}{16\pi^2} \quad . \tag{2.184}$$

In the r.h.s. of the above equation we have just one third of the usual β-function for the ϕ^4 theory. This is due to the fact that we imposed a different renormalization condition. While, usually, one demands to get a finite value for the scattering amplitude $i\mathcal{M}(p_1, p_2 \to p_3, p_4)$, here we asked for a finite solution of the gap equation.
The renormalization of the coupling constant previously introduced is sufficient to get a finite expression for the gap equation. In fact we get:

$$m^2 = \frac{\lambda}{2}\int \frac{d^3k}{(2\pi)^3}\frac{n(\epsilon_k)}{\epsilon_k} + \frac{\lambda m^2}{32\pi^2}\left(\log\frac{m^2}{\bar{\mu}^2} - 1\right). \tag{2.185}$$

Notice that eq. (2.184) makes eq. (2.185) independent on the choice of the scale $\bar{\mu}$.
Since the self-energy is purely real, the entropy density gets contribution only from the pole part, coming from the discontinuity of the logarithm of the inverse propagator, whose cut lies on the real axis from $-\infty$ to $-\epsilon_k$ and from $+\epsilon_k$ to $+\infty$. We have:

$$\mathrm{Im}\log(-\omega^2+\epsilon_k^2) = -\pi\epsilon(\omega)\theta(\omega^2-\epsilon_k^2) \quad , \tag{2.186}$$

where $\epsilon_k^2 = k^2+m^2$, with m solution of the gap equation (2.185). Thus the entropy density reads:

$$S = \int \frac{d^3k}{(2\pi)^3}\left\{(1+n_k)\log(1+n_k) \; - n_k\log n_k\right\} \ . \tag{2.187}$$

Notice that this is exactly the result we would get by evaluating the entropy density for a system of non-interacting bosons with mass m.
For what concerns the pressure this does not occur. Indeed by inserting the results obtained in Eqs. (2.179-2.185) into Eq. (2.177) we get the finite result,

$$P = -T\int \frac{d^3k}{(2\pi)^3}\log(1-e^{-\beta\epsilon_k}) + \frac{m^2}{2}I_T(m) + \frac{m^4}{128\pi^2} \ , \tag{2.188}$$

which does not coincide with the pressure of an ideal gas of boson with mass m. Thus we see that the entropy has a more transparent interpretation in terms of independent quasiparticles.

Even if in this case the gap equation can be solved exactly (though only numerically) we would like to outline a recipe allowing to assess the contribution to it (and to the entropy as well) arising from the different momentum scales.
Let us start from Eq. (2.185), in which we neglect the second term in the right hand side and define $\lambda \equiv 24g^2$. One may then think of solving Eq. (2.185) iteratively, starting from $m=0$. The leading order result is given by:

$$\hat{m}^2 = 24g^2 I_T(0) = g^2T^2 \quad . \tag{2.189}$$

This is the HTL result since the loop integral (with a massless propagator) is saturated by momenta of order T. The next-to-leading order result is obtained by dressing the soft propagator with the thermal mass (2.189) and reads:

$$\begin{aligned}\delta m^2 &= 12g^2\int\frac{d^3k}{(2\pi)^3}\left(\frac{n(\epsilon_k)}{\epsilon_k}-\frac{n_k}{k}\right) \\ &\simeq 12g^2T\int\frac{d^3k}{(2\pi)^3}\left(\frac{1}{k^2+\hat{m}^2}-\frac{1}{k^2}\right) = -\frac{3g^2}{\pi}\hat{m}T \ ,\end{aligned} \tag{2.190}$$

As we can see the correction to the thermal mass turns out to be negative. Thus, for large values of the coupling g,

$$m_{\rm NLO}^2 = \hat{m}^2 + \delta m^2 \tag{2.191}$$

may become negative, leading to an unphysical result. Two different approaches to get rid of this problem might be tested.
The first one consists in considering the first Pade' approssimant to Eq. (2.191), namely:

$$m^2 = \frac{\hat{m}^2}{1 - \frac{\delta m^2}{\hat{m}^2}} \quad . \tag{2.192}$$

The second approach consists in making, within δm^2, the replacement $\hat{m} \to m$, obtaining:

$$m^2 = \hat{m}^2 - \frac{3g^2}{\pi} m T \quad . \tag{2.193}$$

In the following we will refer to such a choice as Next to Leading Approximation (NLA).

Of course, once we give up solving Eq. (2.185) exactly, the approximate results for the thermal mass, the entropy and the other thermodynamical quantities acquire a dependence on the renormalization scale $\bar{\mu}$. Since the only physical scale entering in the problem is the temperature, we expect that assuming $\bar{\mu} \propto T$ should be a good choice, although the coefficient multiplying T appears quite arbitrary. From eq. (2.184) we get that the relation between the renormalized coupling g^2 at the scale $\bar{\mu}'$ and the same quantity at the scale $\bar{\mu}$ is given by:

$$g^2(\bar{\mu}') = \frac{g^2(\bar{\mu})}{1 + \frac{3g^2(\bar{\mu})}{2\pi^2} \log \frac{\bar{\mu}}{\bar{\mu}'}} \quad . \tag{2.194}$$

We give below in Fig. (2.17) the plot of the thermal mass solution of the gap equation (2.185) as a function of the value of the coupling g at the scale $\bar{\mu} = 2\pi T$ (corresponding to the spacing between the Matsubara frequencies) and, in Fig. (2.18), the corresponding behaviour of the entropy density arising from inserting such a solution into eq. (2.187). We also compare the "exact result" with the ones obtained within the Pade' and the NLA approximations, for which we also display the effects of changing the scale $\bar{\mu}$.

2.4.3 QCD thermodynamics

In the Secs. (2.4.1) and (2.4.2) we presented in detail a many-body framework, referred to in the literature as Φ-derivable approximation, allowing to

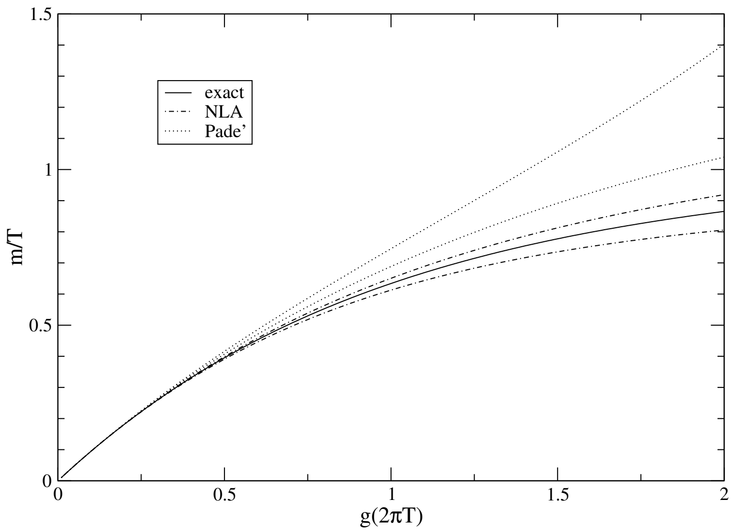

Figure 2.17: The behaviour of the thermal mass solution of the gap equation as a function of $g(\bar{\mu} = 2\pi T)$. The NLA and Pade' approximations are also shown. Within the bands the renormalization scale changes (moving up-wards) from $\bar{\mu} = \pi T$ to $\bar{\mu} = 4\pi T$.

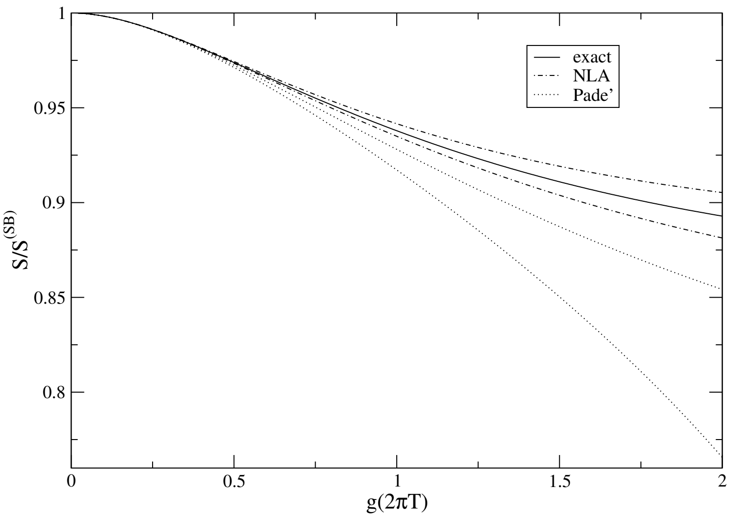

Figure 2.18: The ratio of the entropy coming from eq. (2.187) with respect to the Stephan-Boltzmann result as a function of $g(\bar{\mu} = 2\pi T)$. For the NLA and Pade' approximations, within the bands the renormalization scale changes (moving down-wards) from $\bar{\mu} = \pi T$ to $\bar{\mu} = 4\pi T$.

treat the thermodynamics of a QFT in a self-consistent way. In particular we displayed the results obtained in such a scheme for the case of a scalar field theory.

Here we wish to briefly sketch how the above techniques can be applied to the study of the thermodynamics of a gauge theory like QCD. Such an issue was investigated in detail in Refs. [23, 24, 25, 26].

Such a subject is important in itself since, from a theoretical point of view, the approach we are going to present allows to nicely reproduce the lattice data for the thermodynamics of the QGP; in particular it describes the very slow approach to the Stephan-Boltzmann (ideal gas) limit.

Secondly it represents a beautiful example of application of the HTL approximation and of the problems one meets when one considers observables which get contribution both from the soft modes (described by HTL) and from the hard ones (which require a more careful analysis). Since in Chap. (3), in dealing with the meson spectral functions, we are going to face a similar problem, it will be of help to keep in mind how this issue was addressed in the study of the QGP thermodynamics.

For the sake of simplicity here we only present the case of a pure SU(3) theory.

The entropy of a pure SU(3) plasma gets contribution both from the transverse gluons and from the longitudinal ones. Its expression generalizes the one found in Eq. (2.164) for a scalar field theory and reads (neglecting the residual interaction among the quasiparticles):

$$S_T = -2N_g \int \frac{d^4k}{(2\pi)^4} \frac{\partial n(\omega)}{\partial T} \left\{ \mathrm{Im}\, \log(-\omega^2 + k^2 + \Pi_T) - \mathrm{Im}\,\Pi_T\, \mathrm{Re}\, D_T \right\} \tag{2.195a}$$

$$S_L = -N_g \int \frac{d^4k}{(2\pi)^4} \frac{\partial n(\omega)}{\partial T} \left\{ \mathrm{Im}\, \log(k^2 + \Pi_L) + \mathrm{Im}\,\Pi_L\, \mathrm{Re}\, D_L \right\} , \tag{2.195b}$$

where $N_g = N^2 - 1$ is the number of gluons, the factor 2 in the transverse sector stems from the sum over the two transverse polarizations, $n(\omega)$ is a Bose distribution, $\Pi_{T/L}$ and $D_{T/L}$ are the self-consistent gluon self-energies and propagators.

In the case of a gauge theory like SU(3) constraints due to gauge invariance do not allow to obtain a fully self-consistent solution. This is due to the fact that, in the Φ-derivable approach, in which one selects a certain class of diagrams for the thermodynamical potential where all the lines represent fully dressed propagators, the vertex corrections are not treated on the same

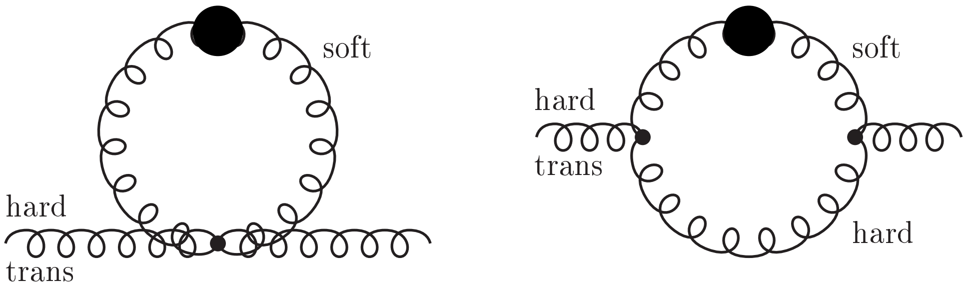

Figure 2.19: The diagrams dressing the propagator of a hard transverse gluon. The dotted lines are soft gluons (both transverse and longitudinal) described by HTL resummed propagators.

footing as the self-energy ones.

On the other hand we showed that the HTL framework allows to get a gauge invariant approximation for the gluon self-energy. A possible way of proceeding consists then in giving up expressing the entropy in terms of the fully self-consistent gluon propagators D_T and D_L. One can instead insert into Eqs. (2.195a) and (2.195b) the HTL results for the self-energies and the resummed propagators.

Indeed the HTL approximations gives a good description of the soft (long wave-length) modes, while Eqs. (2.195a) and (2.195b) require an integration over all the scale of momenta (soft and hard). A possible strategy to overcome this difficulty consists in setting an intermediate cutoff Λ in the integration over the spatial momenta, separating the soft sector (corresponding to long wave-length collective excitation) from the hard one.

In the integration over the soft modes ($k < \Lambda$) HTL self-energies and resummed propagators are employed.

For what concerns the hard sector we already discussed how the longitudinal gluon mode tends to disappear from the spectrum (its residue in the propagator vanishes for large enough spatial momentum), hence we don't expect a sizable contribution in Eq. (2.195b) from the region $k > \Lambda$.
On the other hand hard transverse gluons contributes significantly to Eq. (2.195a) and require a proper treatment. Their interaction with the thermal bath is described by the diagrams in Fig. (2.19), where for the soft modes HTL resummed propagators are employed. In analogy with what done in the case of a scalar field, the effects of the interaction can be accounted for in an effective way through a correction of the HTL result for the asymptotic mass

of the transverse gluon. Such an approximation is referred to in the literature as Next to Leading Approximation (NLA). Hence in this scheme only Eq. (2.195a) gets contribution from the integration over the region $k > \Lambda$. The latter can be easily evaluated in terms of the propagator of a gluon endowed with the asymptotic thermal mass m_∞^{NLA}.

The results obtained in the two approximations (HTL and NLA) are displayed in Fig. (2.4.3) and compared with the lattice data. As it can be seen the slow approach to the ideal gas limit is nicely reproduced.

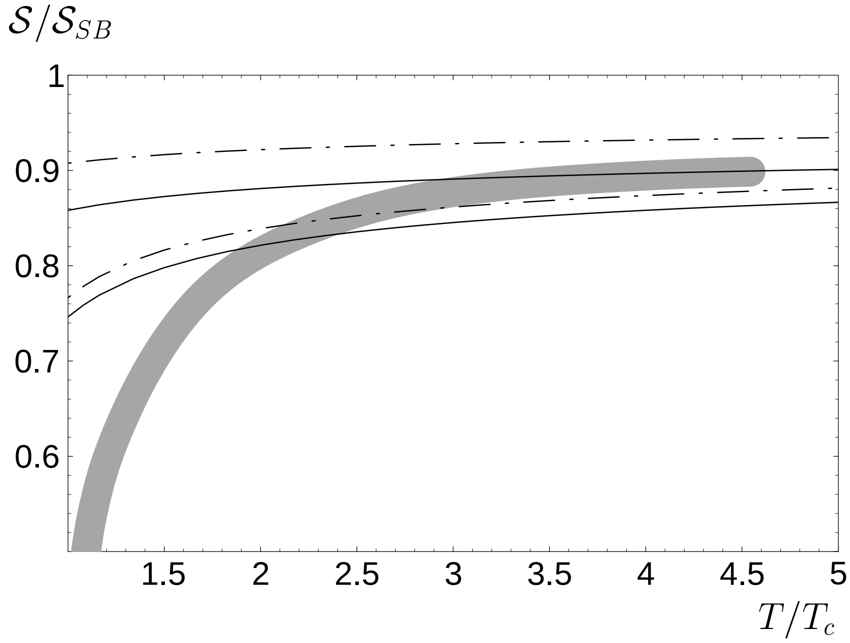

Figure 2.20: The entropy of the SU(3) gauge theory normalized to the Stephan-Boltzmann result [26]. Continuous line: HTL result. Dashed-dotted line: NLA result. The bands correspond to the theoretical uncertainty due to the choice of the scale $\mu \sim T$ at which the running coupling is evaluated and (for the NLA case) of the cutoff Λ separating soft and hard momenta. The grey band represents the lattice data.

Chapter 3

Light mesons in the QGP: spectral functions and temporal correlations

3.1 Introduction

The meson spectral functions in the different channels (scalar, pseudoscalar, vector, pseudovector) in the deconfined phase of QCD have been explored with various techniques, in particular with the *Hard Thermal Loop* (HTL) approximation [67, 16, 19, 50].
In this paper we focus most of our attention on the pseudoscalar channel where we compute the spectral function in a scheme improving upon the HTL approximation. The degrees of freedom we deal with are light quarks (massless for the sake of simplicity) and gluons and our results refer to the case of zero chemical potential (i.e. zero baryon density), a condition which is expected to be realized in the heavy ion experiments at RHIC and even better in the future experiments at LHC. The calculations are performed in the imaginary time formalism, taking at the end a proper analytical continuation to real frequencies when required.
To introduce the subject of our investigation we first shortly revisit the free case, where one computes the 2-point free meson correlation function and its spectral density through the convolution of two free *thermal* quark propagators. Then we evaluate, for illustration in the pseudoscalar case only, the spectral function in the HTL approximation (namely using HTL resummed propagators for the fermionic lines in the loop), thus checking the results lately obtained by Karsh et al. [19, 50].
Actually, for its phenomenological importance, much attention has been

payed in the literature [67, 16, 19, 50, 21, 22] to the vector channel. Indeed the vector spectral function is the basic ingredient to evaluate the dilepton production rate from the plasma [67], possibly of experimental relevance. However in the vector case it turns out that, in addition to the quark propagator, the quark-photon vertex should also be dressed in the HTL approximation, at variance with the pseudoscalar case where the vertex correction vanishes. We shall later shortly discuss this item.

One may worry that at the temperatures reached in heavy ion experiments the QCD coupling g is not so small (in fact $g \sim 1$) and this could cause problems to approximation schemes, like the HTL, based on the separation of different momentum scales (i.e. $g^2T,\ gT,\ T$)[1] which strictly holds in the weak coupling regime. Nevertheless the HTL approximation (especially in its "improved" versions) is able to reproduce quite well the lattice data for the thermodynamics of the QGP phase for temperatures $T \geq 2.5T_c$ as reported for example in [23]. Hence we expect such an approximation to provide reliable results for other observables as well, in the same range of temperatures.

Indeed the kinematical approximations which allow an analytical calculation of the quark self-energy, the basic ingredient of the HTL resummed propagator (see the previous section), are justified only if the components of the external quark four-momentum are soft, i.e. $k \sim gT$. Hence we improve upon the HTL calculation of the meson correlation function by using a prescription which allows for a better treatment of the hard fermionic modes. In this approximation, which was introduced in the analysis of the thermodynamics of the QGP [24, 25, 26] and is referred to as the Next to Leading Approximation (NLA), effects arising from the hard quark modes are taken into account in an effective way through a correction to the asymptotic quark thermal mass. Actually we propose a variant of the NLA which allows for a smoother transition between the two regimes of soft and hard momenta.

Finally, as a general remark, we observe that, within the present approximation scheme, as long as we confine ourselves to the study of the meson spectral functions (i.e. the *imaginary part* of a polarization propagator) we do not need to face any problem related to renormalization.

Our analysis develops as follows.
In Sec. 3.2 we recall the definitions of the basic quantities we address: the meson current operator, the meson spectral function and the meson corre-

[1]At each scale different aspects of the QGP physics disclose themselves.

lator along the (imaginary) temporal direction. In Sec. 3.3 we display the results one obtains in the free case. In Sec. 3.4, after recalling the expression of the HTL quark spectral function, we use HTL resummed quark propagators to obtain the meson correlation function: this accounts for important effects coming from the interaction of the quarks with the thermal bath. Our calculations confirm the results previously obtained by Karsch et al. [19, 50]. In Sec. 3.5 we examine the NLA scheme. Finally, in Sec. 3.6, we display the numerical predictions for the pseudo-scalar meson spectral function and for the temporal correlator $G(\tau)$ within the two approximation schemes (HTL and NLA) and compare them with the free case.

3.2 Thermal meson correlation function

Adopting the same notation as in Ref. [50] we consider the following current operator, carrying the quantum numbers of a meson in the flavour-singlet channel (there is no matrix which mixes the flavours):

$$J_M(-i\tau, \boldsymbol{x}) = \bar{q}(-i\tau, \boldsymbol{x})\Gamma_M q(-i\tau, \boldsymbol{x}) \ , \tag{3.1}$$

where $\Gamma_M = 1, \gamma^5, \gamma^\mu, \gamma^\mu\gamma^5$ for the scalar, pseudoscalar, vector and pseudovector channels, respectively. We next define the fluctuation operator $\widetilde{J}_M$ as

$$\widetilde{J}_M(-i\tau, \boldsymbol{x}) = J_M(-i\tau, \boldsymbol{x}) - \langle J_M(-i\tau, \boldsymbol{x})\rangle \ , \tag{3.2}$$

the average being taken on the statistical ensemble.
The chief quantity we address is the *thermal meson 2 point correlation function*:

$$\begin{aligned} G_M(-i\tau, \boldsymbol{x}) &= \langle \widetilde{J}_M(-i\tau, \boldsymbol{x})\widetilde{J}_M^\dagger(0, \boldsymbol{0})\rangle \\ &= \langle J_M(-i\tau, \boldsymbol{x})J_M^\dagger(0, \boldsymbol{0})\rangle - \langle J_M(-i\tau, \boldsymbol{x})\rangle\langle J_M^\dagger(0, \boldsymbol{0})\rangle \\ &= \frac{1}{\beta}\sum_{n=-\infty}^{+\infty}\int \frac{d^3p}{(2\pi)^3} e^{-i\omega_n\tau} e^{i\boldsymbol{p}\cdot\boldsymbol{x}} \chi_M(i\omega_n, \boldsymbol{p}) \ , \end{aligned} \tag{3.3}$$

with $\tau \in [0, \beta = 1/T]$ and $\omega_n = 2n\pi T$ $(n = 0, \pm 1, \pm 2 \dots)$.
It is convenient to adopt the following spectral representation for the meson propagator in momentum space:

$$\chi_M(i\omega_n, \boldsymbol{p}) = -\int_{-\infty}^{+\infty} d\omega \frac{\sigma_M(\omega, \boldsymbol{p})}{i\omega_n - \omega} \quad \Rightarrow \quad \sigma_M(\omega, \boldsymbol{p}) = \frac{1}{\pi}\mathrm{Im}\, \chi_M(\omega + i\eta, \boldsymbol{p}). \tag{3.4}$$

Hence it is possible to express the thermal meson propagator in a mixed representation through the *spectral function* σ_M. Indeed starting from the definition:

$$
\begin{aligned}
G_M(-i\tau, \boldsymbol{p}) &= \frac{1}{\beta} \sum_{n=-\infty}^{+\infty} e^{-i\omega_n \tau} \chi_M(i\omega_n, \boldsymbol{p}) \\
&= -\frac{1}{\beta} \sum_{n=-\infty}^{+\infty} e^{-i\omega_n \tau} \int_{-\infty}^{+\infty} d\omega \frac{\sigma_M(\omega, \boldsymbol{p})}{i\omega_n - \omega} ,
\end{aligned}
$$

and performing the sum over the Matsubara frequencies with a standard contour integration in the complex ω plane [16, 13], one obtains [50]:

$$
G_M(-i\tau, \boldsymbol{p}) = \int_0^{+\infty} d\omega \; \sigma_M(\omega, \boldsymbol{p}) \frac{\cosh(\omega(\tau - \beta/2))}{\sinh(\omega\beta/2)} . \tag{3.5}
$$

In the following, confining ourselves to light mesons (namely the pions if one considers the pseudoscalar flavour triplet channel), we will explore in various approximation schemes the behaviour of the meson spectral function. Indeed the survival of a meson as a bound state in the deconfined phase of QCD should be signaled by a delta like structure of the spectral function. We will see that this is not the case (at least according to the approaches adopted in this paper, which keep into account only the interaction of the fermionic modes with the thermal bath). On the other hand, for what concerns *heavier mesons*, recent lattice results [27, 28, 29], obtained in quenched QCD, do display very pronounced peaks for the charmonium spectral functions in the pseudoscalar and vector channels, which survive till $T \sim 2.25T_c$. Actually, as recently pointed out by Shuryak [30, 31], the existence of a whole sequence of loosely bound states above T_c (not necessarily colour-singlet states) would entail large cross sections among the constituents of the plasma; this in turn would justify the adoption of hydrodynamical models for the *fireball* arising from the ultra-relativistic heavy-ion collisions; it would also explain certain collective phenomena, such as the elliptic flow, observed at SPS and more recently at RHIC. The QGP, at least for T just above T_c, as previously discussed, seems to behave more like a liquid with a very small viscosity rather than like a gas of quasiparticles.

In the light of these results, which indicate the survival of mesonic resonances in the QGP phase, the existence of bound states in the broken-symmetry phase of the three-dimensional Ising model [32, 33] gains considerable interest. We remind the reader that, on the lattice, the 3d Ising model is related through a duality transformation to the Z_2 gauge model [34], the center of the group $SU(2)$.

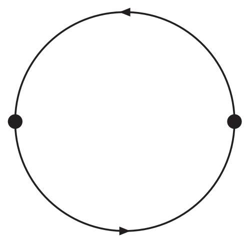

Figure 3.1: Diagram illustrating the free meson correlation function. The propagation lines are free thermal quark propagators. The two interaction vertices correspond to Γ matrices.

3.3 Free spectral functions

We start by revisiting the computation of the free meson spectral functions for the different channels. We use the short-hand notation $(\tau, \boldsymbol{x})$ for $(t = -i\tau, \boldsymbol{x})$. In order to display more transparently how one gets the final result we write explicitly the spinor indices. We have to compute the expression

$$\begin{aligned}\langle J_M(\tau,\boldsymbol{x})J_M^\dagger(0,\mathbf{0})\rangle &= \langle \bar{q}(\tau,\boldsymbol{x})\Gamma_M q(\tau,\boldsymbol{x})(\bar{q}(0,\mathbf{0})\Gamma_M q(0,\mathbf{0}))^\dagger\rangle \\ &= \langle \bar{q}_\alpha(\tau,\boldsymbol{x})q_\beta(\tau,\boldsymbol{x})\bar{q}_\lambda(0,\mathbf{0})q_\mu(0,\mathbf{0})\rangle \times \\ &\quad \times(\Gamma_M)_{\alpha\beta}(\gamma^0\Gamma_M^\dagger\gamma^0)_{\lambda\mu} \qquad (3.6)\end{aligned}$$

diagrammatically displayed, after subtracting the disconnected contribution, in Fig. (3.1).
Since the field operators inside the average over the ensemble are already *time-ordered* (being $\tau > 0$) we apply Wick's theorem. From the customary definitions

$$\begin{aligned}\langle T_\tau\left[q_\beta(\tau,\boldsymbol{x})\bar{q}_\lambda(0,\mathbf{0})\right]\rangle &= S^F_{\beta\lambda}(\tau,\boldsymbol{x}) \qquad (3.7)\\ \langle T_\tau\left[\bar{q}_\alpha(\tau,\boldsymbol{x})q_\mu(0,\mathbf{0})\right]\rangle &= -S^F_{\mu\alpha}(-\tau,-\boldsymbol{x}) \\ &= S^F_{\mu\alpha}(\beta-\tau,-\boldsymbol{x})\ , \qquad (3.8)\end{aligned}$$

S^F being the quark propagator, it follows that:

$$\langle \widetilde{J}_M(\tau,\boldsymbol{x})\widetilde{J}_M^\dagger(0,\mathbf{0})\rangle = \mathrm{Tr}(\Gamma_M S_F(\tau,\boldsymbol{x})\gamma^0\Gamma_M^\dagger\gamma^0 S_F(\beta-\tau,-\boldsymbol{x}))\ . \qquad (3.9)$$

Hence in Fourier space the mesonic 2 point correlation function reads [50]:

$$\chi_M(i\omega_l,\boldsymbol{p}) = -2N_c\frac{1}{\beta}\sum_{n=-\infty}^{+\infty}\int\frac{d^3k}{(2\pi)^3}\mathrm{Tr}[\Gamma_M S_F(i\omega_n,\boldsymbol{k})\gamma^0\Gamma_M^\dagger\gamma^0 S_F(i\omega_n-i\omega_l,\boldsymbol{k}-\boldsymbol{p})], \qquad (3.10)$$

where the mesonic frequency is $\omega_l = 2l\pi T$, while in the quark propagators $\omega_n = (2n+1)\pi T$, l and n assuming any integer value. The overall factor $2N_c$ (N_c being the number of colours) comes from the trace over the light flavours and colours.
If one considers the flavour triplet channel the overall flavour factor $N_f = 2$ has to be replaced by

$$\mathrm{Tr}\left[\tau^a \tau^b\right] = 2\delta^{ab} , \tag{3.11}$$

where τ^a and τ^b are Pauli matrices acting in the flavour space. The same prescription allows one to translate the results obtained in the following for the interacting case to the non-singlet channel.

We can now write down explicitly the free meson propagator in the different channels getting:

$$\chi^{\mathrm{s}}(i\omega_l, \boldsymbol{p}) = -2N_c \frac{1}{\beta} \sum_{n=-\infty}^{+\infty} \int \frac{d^3k}{(2\pi)^3} \mathrm{Tr}[S_F(i\omega_n, \boldsymbol{k}) S_F(i\omega_n - i\omega_l, \boldsymbol{k} - \boldsymbol{p})] \tag{3.12}$$

$$\chi^{\mathrm{ps}}(i\omega_l, \boldsymbol{p}) = 2N_c \frac{1}{\beta} \sum_{n=-\infty}^{+\infty} \int \frac{d^3k}{(2\pi)^3} \mathrm{Tr}[\gamma^5 S_F(i\omega_n, \boldsymbol{k}) \gamma^5 S_F(i\omega_n - i\omega_l, \boldsymbol{k} - \boldsymbol{p})] \tag{3.13}$$

$$\chi^{\mathrm{v}}(i\omega_l, \boldsymbol{p}) = -2N_c \frac{1}{\beta} \sum_{n=-\infty}^{+\infty} \int \frac{d^3k}{(2\pi)^3} \mathrm{Tr}[\gamma^\mu S_F(i\omega_n, \boldsymbol{k}) \gamma_\mu S_F(i\omega_n - i\omega_l, \boldsymbol{k} - \boldsymbol{p})] \tag{3.14}$$

$$\chi^{\mathrm{pv}}(i\omega_l, \boldsymbol{p}) = 2N_c \frac{1}{\beta} \sum_{n=-\infty}^{+\infty} \int \frac{d^3k}{(2\pi)^3} \mathrm{Tr}[\gamma^\mu \gamma^5 S_F(i\omega_n, \boldsymbol{k}) \gamma^5 \gamma_\mu S_F(i\omega_n - i\omega_l, \boldsymbol{k} - \boldsymbol{p})] , \tag{3.15}$$

where in the vector (see also Ref. [50]) and pseudovector channels the Dirac matrices have been contracted with the Minkowskian metric tensor $g_{\mu\nu}$. Note that in the massless, non interacting case, since $\{S_F, \gamma^5\} = 0$, $\chi^{\mathrm{s}} = \chi^{\mathrm{ps}}$ and $\chi^{\mathrm{v}} = \chi^{\mathrm{pv}}$.
Next we evaluate the imaginary part of the above quantities, thus obtaining the free meson spectral function. We sketch the calculation in the vector case and just quote the results for the other channels. To simplify the problem we confine ourselves to the $\boldsymbol{p} = 0$ limit. Yet, even in this limit, we can grasp important aspects of the plasma physics once the interaction of the quarks with the thermal bath is switched on. Indeed $\sigma(\omega, 0)$ (the zero momentum projection of the spectral function) is the quantity which is studied on the lattice in order to determine whether a meson can survive as a bound state

also in the deconfined phase of QCD [27]. Furthermore, as previously mentioned, $\sigma^{\mathrm{v}}(\omega, 0)$ is directly related to the back-to-back dilepton production rate [67].
Introducing the four-vectors $A = (i\omega_n, \boldsymbol{k})$ and $B = (i\omega_n - i\omega_l, \boldsymbol{k})$ one can easily perform the trace in Eq. (3.14) obtaining:

$$\mathrm{Tr}[\gamma^\mu(\not{A} + m)\gamma_\mu(\not{B} + m)] = -8(A \cdot B) + 16m^2 \,, \tag{3.16}$$

m being the bare quark mass. Thus what is left out to compute is the following sum over the Matsubara frequencies

$$\frac{1}{\beta}\sum_n \frac{8(\omega_n^2 + E_k^2) - 8\omega_n\omega_l + 8m^2}{(\omega_n^2 + E_k^2)[(\omega_n - \omega_l)^2 + E_k^2]} \,, \tag{3.17}$$

which can be easily done with standard techniques [16].Then, after performing a proper analytical continuation letting $i\omega_l \to \omega + i\eta^+$ (ω being real), one takes the imaginary part of the obtained result. Note that the term in round brackets in the numerator of Eq. (3.17) leads to a purely real result (which, incidentally, would require to be renormalized) and hence does not contribute to the meson propagator. We thus recover the well-known result for the free vector spectral function (for $\omega > 0$):

$$\begin{aligned}\sigma^{\mathrm{v}}(\omega, \mathbf{0}) &= -2N_c \int \frac{d^3k}{(2\pi)^3}(1 - \tilde{n}(\omega/2))\delta(\omega - 2E_k) \cdot 2 \cdot \left(\frac{m^2}{E_k^2} + \frac{\omega}{E_k}\right) \\ &= \frac{N_c}{4\pi^2}\theta(\omega - 2m)\sqrt{1 - \left(\frac{2m}{\omega}\right)^2}\,\omega^2 \tanh(\omega/4T)\left(-2 - \left(\frac{2m}{\omega}\right)^2\right) \,.\end{aligned} \tag{3.18}$$

In the above one recognizes the typical threshold behaviour, the square root stemming from the integration over the phase space.
Globally the results for the different channels can be summarized in the compact expression:

$$\sigma_M^{\mathrm{free}}(\omega, \mathbf{0}) = \frac{N_c}{4\pi^2}\theta(\omega - 2m)\sqrt{1 - \left(\frac{2m}{\omega}\right)^2}\,\omega^2 \tanh(\omega/4T)\left(a + b\left(\frac{2m}{\omega}\right)^2\right) \,, \tag{3.19}$$

where the coefficient (a, b) turn out to be given respectively by (1,-1), (1,0), (-2,-1), (-2,3) in the scalar, pseudoscalar, vector and pseudovector channel[2].

[2] These coefficients do not coincide with the ones of Refs. [19, 50], due to our choice of working with ordinary Dirac matrices satisfying the anti-commutation relation $\{\gamma^\mu, \gamma^\nu\} = 2g^{\mu\nu}$, $g^{\mu\nu}$ being the Minkowskian metric tensor.

3.4 Spectral functions in HTL approximation

In this section we evaluate the meson spectral function in HTL approximation for the pseudoscalar and vector channel. In both cases this amounts to dressing the quark propagator with the self-energy of Fig. 2.6, keeping only the term proportional to g^2T^2, as discussed in detail, for example, in [16]. In performing this task it is useful to express the fermionic propagator thus obtained through its spectral function (see the previous chapter). The latter, in HTL, turns out to read [67, 16]:

$$\rho_\pm(\omega,k) = \frac{\omega^2-k^2}{2m_q^2}[\delta(\omega-\omega_\pm)+\delta(\omega+\omega_\mp)] + \beta_\pm(\omega,k)\theta(k^2-\omega^2)\ , \quad (3.20)$$

with

$$\beta_\pm(\omega,k) = -\frac{m_q^2}{2}\frac{\pm\omega-k}{\left[k(-\omega\pm k)+m_q^2\left(\pm 1-\frac{\pm\omega-k}{2k}\ln\frac{k+\omega}{k-\omega}\right)\right]^2+\left[\frac{\pi}{2}m_q^2\frac{\pm\omega-k}{k}\right]^2}\ , \quad (3.21)$$

where the two dispersion relations $\omega_\pm(k)$ are shown in Fig. (2.7), while the behaviour of $\beta_\pm(\omega,k)$ is plotted in Fig. (2.8). In the above $m_q = gT/\sqrt{6}$ is the so-called *thermal gap mass* of the quark, clearly appearing in Fig. (2.7) at $k=0$. The HTL quark spectral functions in Eq. (3.20) consist of two pieces: a pole term, arising from the zeros of the real part of the denominators of ${}^\star\Delta_\pm$ in Eq. (2.93), and a continuum term, corresponding to the Landau damping of a quark propagating in the bath. In the time-like domain $\omega > k$ the dispersion relation $\omega_+(k)$ solves the equation ${}^\star\Delta_+^{-1}(\omega_+(k),k) = 0$ and corresponds to the propagation of a quasi-particle with chirality and helicity eigenvalues of the same sign. On the other hand $\omega_-(k)$ satisfies the equation ${}^\star\Delta_-^{-1}(\omega_-(k),k) = 0$ and describes the propagation of an excitation, referred to as *plasmino*, with negative helicity over chirality ratio. Note that both these excitations are undamped at this level of approximation, since the logarithm in ${}^\star\Delta_\pm$ doesn't develop any imaginary part in the time-like domain. On the contrary, for space-like momenta $\omega < k$, the quark spectral function receives contribution from the imaginary part stemming from the logarithm contained in Eq. (2.94): this gives rise to the term $\beta_\pm$ in Eq. (3.20).
We now address the meson spectral functions in two specific cases.

3.4.1 Pseudoscalar channel

The pseudoscalar vertex receives no HTL correction as shown in [35]. Hence in the pseudoscalar channel, following Ref. [50], one has simply to replace,

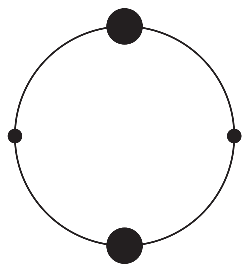

Figure 3.2: Diagram giving the pseudoscalar meson 2-point function in the HTL approximation. The interaction vertices are γ^5 matrices, while the dressed lines are HTL resummed propagators. No vertex correction is required within this scheme.

in Eq.(3.13), the free thermal quark propagators with HTL resummed ones (which we shall denote with a star), obtaining:

$$\chi^{\rm ps}(i\omega_l,\boldsymbol{p}) = 2N_c\frac{1}{\beta}\sum_{n=-\infty}^{+\infty}\int\frac{d^3k}{(2\pi)^3}\mathrm{Tr}[\gamma^5\,{}^\star S(i\omega_n,\boldsymbol{k})\gamma^5\,{}^\star S(i\omega_n - i\omega_l,\boldsymbol{k}-\boldsymbol{p})]\ . \tag{3.22}$$

Setting $\boldsymbol{q} = \boldsymbol{k} - \boldsymbol{p}$ and making use of the spectral representation (2.97) of the quark propagator one gets:

$$\chi^{\rm ps}(i\omega_l,\boldsymbol{p}) = 2N_c\frac{1}{\beta}\sum_{n=-\infty}^{+\infty}\int\frac{d^3k}{(2\pi)^3}\int_{-\infty}^{+\infty}d\omega_1\int_{-\infty}^{+\infty}d\omega_2\frac{1}{i\omega_n-\omega_1}\frac{1}{i\omega_n-i\omega_l-\omega_2}\times$$
$$\times\ \mathrm{Tr}[\gamma^5\rho_{\rm HTL}(\omega_1,\boldsymbol{k})\gamma^5\rho_{\rm HTL}(\omega_2,\boldsymbol{q})]\ . \tag{3.23}$$

Summing over the Matsubara frequencies with a standard contour integration, performing the usual analytical continuation $i\omega_l \to \omega + i\eta^+$ and taking the imaginary part of the result thus obtained one gets:

$$\sigma^{\rm ps}(\omega,\boldsymbol{p}) = -2N_c\int\frac{d^3k}{(2\pi)^3}(e^{\beta\omega}-1)\int_{-\infty}^{+\infty}d\omega_1\int_{-\infty}^{+\infty}d\omega_2\tilde{n}(\omega_1)\tilde{n}(\omega_2)\times$$
$$\times\ \delta(\omega-\omega_1-\omega_2)\cdot\mathrm{Tr}[\gamma^5\rho_{\rm HTL}(\omega_1,\boldsymbol{k})\gamma^5\rho_{\rm HTL}(-\omega_2,\boldsymbol{q})]\ . \tag{3.24}$$

Now, inserting Eq. (2.98) into Eq. (3.24) and since

$$\mathrm{Tr}\left[\gamma^5\frac{\gamma^0\mp\boldsymbol{\gamma}\cdot\hat{\boldsymbol{k}}}{2}\gamma^5\frac{\gamma^0\mp\boldsymbol{\gamma}\cdot\hat{\boldsymbol{q}}}{2}\right] = -(1-\hat{\boldsymbol{k}}\cdot\hat{\boldsymbol{q}}), \tag{3.25a}$$

$$\mathrm{Tr}\left[\gamma^5\frac{\gamma^0\mp\boldsymbol{\gamma}\cdot\hat{\boldsymbol{k}}}{2}\gamma^5\frac{\gamma^0\pm\boldsymbol{\gamma}\cdot\hat{\boldsymbol{q}}}{2}\right] = -(1+\hat{\boldsymbol{k}}\cdot\hat{\boldsymbol{q}})\ , \tag{3.25b}$$

one gets [50]:

$$\sigma^{\rm ps}(\omega,\boldsymbol{p})=2N_c\int\frac{d^3k}{(2\pi)^3}(e^{\beta\omega}-1)\int_{-\infty}^{+\infty}d\omega_1\int_{-\infty}^{+\infty}d\omega_2\tilde{n}(\omega_1)\tilde{n}(\omega_2)\delta(\omega-\omega_1-\omega_2)\times$$
$$\times\Big\{(1+\hat{\boldsymbol{k}}\cdot\hat{\boldsymbol{q}})[\rho_+(\omega_1,k)\rho_+(\omega_2,q)+\rho_-(\omega_1,k)\rho_-(\omega_2,q)]+$$
$$+(1-\hat{\boldsymbol{k}}\cdot\hat{\boldsymbol{q}})[\rho_+(\omega_1,k)\rho_-(\omega_2,q)+\rho_-(\omega_1,k)\rho_+(\omega_2,q)]\Big\}\ . \quad (3.26)$$

where the identity $\rho_+(-\omega,k)=\rho_-(\omega,k)$ has been used.
In the case $\boldsymbol{p}=0$ the above formula reduces to:

$$\begin{aligned}\sigma^{\rm ps}(\omega,\boldsymbol{0}) &= \frac{2N_c}{\pi^2}(e^{\beta\omega}-1)\int_0^{+\infty}dk\,k^2\int_{-\infty}^{+\infty}d\omega_1\int_{-\infty}^{+\infty}d\omega_2\tilde{n}(\omega_1)\tilde{n}(\omega_2)\\ &\quad\delta(\omega-\omega_1-\omega_2)[\rho_+(\omega_1,k)\rho_+(\omega_2,k)+\rho_-(\omega_1,k)\rho_-(\omega_2,k)]\ .\end{aligned} \quad (3.27)$$

Inserting then into Eq. (3.27) the explicit expression for $\rho_\pm$ given in Eq. (3.20), one finds, as first pointed out in Ref. [67], that the meson spectral function consists of the sum of three terms: pole-pole (pp), pole-cut (pc) and cut-cut (cc). These different contributions will be discussed in Sec. 3.6.

3.4.2 Vector channel

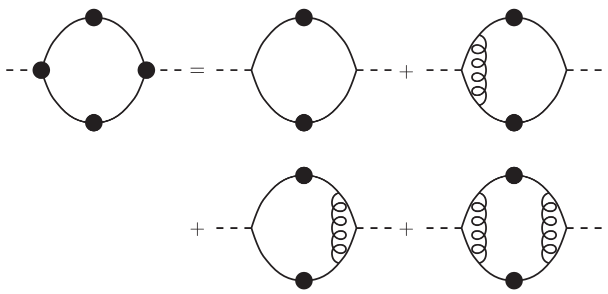

Figure 3.3: The diagrams contributing to the vector meson spectral function in the HTL approximation. Dressed lines and vertices denote HTL resummed propagators and HTL effective quark-photon vertices respectively. The momentum flowing in the loops dressing the vertices is hard. The external dashed lines denote a photon (or a probe with the same quantum-numbers).

The vector meson spectral function in the deconfined phase, being related to the thermal dilepton production rate from the plasma, is clearly of importance for the QGP phenomenology. When computed in the HTL approximation it should provide a reliable estimate for the soft dilepton production rate. For the sake of completeness we quote here the HTL vector spectral function previously obtained in [67, 16, 19, 50], whose meaning in term of Feynman diagrams is illustrated in Fig. (3.3). Its expression is considerably more cumbersome than the pseudoscalar one reading [16, 19, 50, 67]

$$
\begin{aligned}
\sigma^{\mathrm{V}}(\omega,\mathbf{0}) &= \frac{4N_c}{\pi^2}(e^{\beta\omega}-1)\int_0^{+\infty} dk\, k^2 \int_{-\infty}^{+\infty} d\omega_1 \int_{-\infty}^{+\infty} d\omega_2 \tilde{n}(\omega_1)\tilde{n}(\omega_2)\delta(\omega-\omega_1-\omega_2) \\
&\times \left\{ 4\left(1-\frac{\omega_1^2-\omega_2^2}{2k\omega}\right)^2 \rho_+(\omega_1,k)\rho_-(\omega_2,k) + \left(1+\frac{\omega_1^2+\omega_2^2-2k^2-2m_q^2}{2k\omega}\right)^2 \right. \\
&\times \rho_+(\omega_1,k)\rho_+(\omega_2,k) + \left(1-\frac{\omega_1^2+\omega_2^2-2k^2-2m_q^2}{2k\omega}\right)^2 \rho_-(\omega_1,k)\rho_-(\omega_2,k) \\
&\left. +\Theta(k^2-\omega_1^2)\frac{m_q^2}{4k\omega^2}(1-\frac{\omega_1^2}{k^2})\left[(1+\frac{\omega_1}{k})\rho_+(\omega_2,k)+(1-\frac{\omega_1}{k})\rho_-(\omega_2,k)\right]\right\} ;
\end{aligned}
\tag{3.28}
$$

it is derived by dressing, in Eq. (3.14), both the propagation lines (replacing the free thermal quark propagators with HTL resummed ones) and the bare vertices. For the latter the following effective HTL vertex for the coupling of a quark with a vector probe is adopted:

$$
{}^{\star}\Gamma_\mu(P_1,P_2) = \gamma_\mu + m_q^2 \int \frac{d\Omega_k}{4\pi} \frac{\hat{\not{K}}\,\hat{K}_\mu}{\left[(P_1\cdot\hat{K})(P_2\cdot\hat{K})\right]} , \tag{3.29}
$$

where $\hat{K}=(1,\hat{\boldsymbol{k}})$, $P_1=(i\omega_{n_1},\boldsymbol{p_1})$ is the four-momentum of the incoming quark, while $P_2=(i\omega_{n_2},\boldsymbol{p_2})$ refers to the outgoing one. Again we note that, because our γ^μ matrices satisfy the usual Dirac algebra (with the Minkowskian metric tensor $g^{\mu\nu}$), we get a different sign in front of the vertex correction with respect to what quoted in Ref. [16].

At this point a careful analysis of the momenta over which one performs the integration is appropriate. In fact, according to the original proposal by Braaten and Pisarski [36] for constructing an effective theory for the soft modes in the QGP, one has to replace every soft fermionic line (i.e. with $K\sim gT$) with an HTL resummed propagator, while the hard propagation lines should be left undressed. This is because, for $K\sim gT$, also the self-energy $\Sigma_{\mathrm{HTL}}(K)\sim gT$: hence all the diagrams with repeated self-energy insertions in the fermionic lines give contributions of the same order, i.e.

$$\frac{-1}{\not{K}} \cdot (-\Sigma) \frac{-1}{\not{K}} \cdot (-\Sigma) \frac{-1}{K} \cdots \sim \frac{-1}{\not{K}} \sim \frac{1}{gT} \, .$$

In addition, if all the lines entering into a vertex are soft one has to replace it with the HTL one given by Eq. (3.29), otherwise the vertex should be left untouched. On the other hand a hard fermion propagator (i.e. with $K \sim T$) can be expanded perturbatively, since the kinetic term dominates over the interaction, and in first approximation one can keep its non-interacting expression. Hence the integration over k in Eq. (3.28) really should cover only the soft regime of momenta, while in the integration over the hard momenta domain one should use the bare quantities.

Actually the vector meson spectral function in the deconfined phase and the associated thermal dilepton rate have been recently evaluated on the lattice [37, 38, 39]. It turns out that their behaviour at low energies is very different from the HTL result given by Eq. (3.28). Specifically, whereas the HTL spectral function develops an infrared divergence for $\omega \to 0$ (stemming from the cut-cut contribution) [67], the lattice result drops to zero below $\omega/T \simeq 3$, suggesting a threshold effect due to a thermal mass acquired by the quarks. In this connection we remind the reader that the spectral function of a meson is not measured directly on the lattice, but has to be obtained by inverting Eq. (3.5). A procedure referred to as Maximum Entropy Method [27, 28, 29, 37, 38, 39] is usually employed to accomplish this task.

Finally, for what concern the experimental results, in a heavy ion collision dilepton pairs are produced also in processes different from the annihilation of $q\bar{q}$ quasi-particles in the plasma phase[3]. To get an estimate for the production rate which can be eventually compared with the experiment, one has to account also for other sources [21]: in particular the (non-thermal) contribution due to Drell-Yan processes, the dileptons coming from the hadronic phase and the decay of vector mesons.

In the following we shall concentrate on the pseudoscalar channel only, aiming at an improved treatment of the latter.

[3]Actually, even in the deconfined phase as we will discuss in detail for the pseudoscalar case, the HTL meson spectral function gets contributions from non-trivial many-body processes.

(a) (b)

Figure 3.4: Next to Leading corrections to a hard quark propagator, arising from the interaction with a soft transverse (a) and longitudinal (b) gluon: for these HTL resummed propagators are used. Thus the two diagrams receive contributions from all orders in perturbation theory.

3.5 Beyond HTL

In this section we attempt to improve upon the quark spectral functions appearing in the loop of Fig. (3.2). For this purpose we observe again that, in making the convolution of the two fermionic propagators, one has to integrate over *all the scale of momenta* (hard and soft). Now, while the HTL approximation is supposed to dress correctly the propagation of the *soft modes*, this is not so for what concerns the *hard modes*. Thus, by replacing naively the free thermal quark propagators in Eq. (3.10) with HTL resummed ones, one treats incorrectly the contribution to the integral arising from hard momenta. This is analogous to what happens when one tries to evaluate thermodynamical quantities for the QGP, like the entropy and the baryon density, in a pure HTL approximation. As pointed out in Ref. [23], in HTL one gets the right contribution of order g^2 to such quantities, but *only* part of the g^3 term (actually this one is strictly a non-perturbative contribution, being non analytical in $\alpha_s = g^2/4\pi$), namely the contribution arising from the soft modes alone.

Now we shortly examine how the Next to Leading contributions, amounting to properly dress the propagation of the hard degrees of freedom in a QGP, are kept into account in a self-consistent calculation of quantities like the entropy, the baryon density and the quark-number susceptibilities [23, 24, 26].
These observables receive a non-analytical contribution of order g^3 both from the soft modes and from the proper dressing of the hard propagators. To get the latter one has to evaluate the correction $\delta\Sigma_\pm(\omega = \pm k)$[4] to the

[4]Note that only the light-cone projection of the hard quark self-energy enters into the

self energy of a normal quark mode (with hard momentum). Such a contribution corresponds to the two diagrams displayed in Fig. 3.4 where the hard quark interacts with a *soft* gluon, longitudinal and transverse, respectively, whose *resummed* propagators are the HTL ones (being the gluons soft such an approximation is fully justified). Note that this is a non-perturbative procedure, the two diagrams in Fig. 3.4 getting contributions from all orders of perturbation theory.

Actually the correction $\delta\Sigma_{\pm}(\omega = \pm k)$ is a far from trivial function of the momentum and generally it can be dealt with only numerically. Nevertheless its contribution of order g^3 to the entropy and the baryon density can be analytically evaluated. Indeed in [23, 24, 26] the authors replace this momentum-dependent self-energy correction with a constant shift of the asymptotic quark mass in order to reproduce the right coefficients of the terms of order g^3 coming from the hard sector for the entropy and the baryon density[5].

This mass correction turns out to be negative, reading [23, 24, 26]:

$$\delta m_\infty^2 = -\frac{1}{2\pi}\, g^2\, C_f\, T\, \hat{m}_D \;, \tag{3.30}$$

where (in the case of zero chemical potential) the Debye screening mass in the HTL approximation is:

$$\hat{m}_D = \sqrt{\frac{N_c}{3} + \frac{N_f}{6}}\, gT \;; \tag{3.31}$$

in the above N_f the number of flavours and $C_f = 4/3$ the *quadratic Casimir operator* for the fundamental representation of $SU(3)$.

It is worth stressing that at the experimentally accessible temperatures (i.e. a few times T_c) $g \geq 1$, hence the (negative) correction (3.30) becomes of the same order of magnitude of the HTL asymptotic mass $\hat{m}_\infty$ which reads

$$\hat{m}_\infty^2 = 2m_q^2 = \frac{g^2 T^2}{3} \;, \tag{3.32}$$

thus possibly leading to a tachyonic singularity.

This problem was addressed in Ref. [23] where two possible solutions where

thermodynamical calculations. The same is true for the hard transverse gluon as well. Since on the light-cone the HTL self-energies coincide with the full one-loop calculation, the entropy and the baryon density might be privileged quantities to study within the HTL approximation.

[5]Analogously the correction $\delta\Pi_T(\omega = \pm k)$ to the self-energy of a hard momentum transverse gluon is absorbed in a shift of its asymptotic mass.

proposed. The first amounts to replace the expression $m_\infty^2 = \hat{m}_\infty^2 + \delta m_\infty^2$ with its first Pade' approximant, namely

$$m_\infty^2 = \hat{m}_\infty^2 + \delta m_\infty^2 \quad \longrightarrow \quad m_\infty^2 = \frac{\hat{m}_\infty^2}{1 - \dfrac{\delta m_\infty^2}{\hat{m}_\infty^2}} \; . \tag{3.33}$$

The other starts with the correct equation for the Next to Leading quark asymptotic mass m_∞, namely

$$m_\infty^2 = \hat{m}_\infty^2 - \frac{1}{2\pi}\, g^2\, C_f \sqrt{N_c + \frac{N_f}{2}}\, T\, \hat{m}_\infty \; , \tag{3.34}$$

and replaces $\hat{m}_\infty \to m_\infty$ in the term linear in $\hat{m}_\infty$, thus obtaining the "self-consistent like" equation:

$$m_\infty^2 = \hat{m}_\infty^2 - \frac{1}{2\pi}\, g^2\, C_f \sqrt{N_c + \frac{N_f}{2}}\, T\, m_\infty \; , \tag{3.35}$$

whose positive root provides the asymptotic mass for the hard quark. In the following, in accord with the literature [23], we shall refer to such an approach as the Next to Leading Approximation (NLA).
To replace in the term linear in $\hat{m}_\infty$ the HTL mass with its "self-consistent" value may appear somewhat arbitrary. Yet the effects of such a procedure were tested in a scalar toy model [23], where one can solve the gap equation exactly (although numerically), and the discrepancy between the exact result and the above discussed procedure turned out to be $\sim 1\%$ even for large values of the coupling ($g \sim 2$), at least as far as the entropy is concerned.
The NLA asymptotic mass m_∞ applies to the hard quark modes. Since the soft modes are correctly described by the HTL approximation, the strategy followed in Refs. [23, 24, 26] was to single them out by introducing a cutoff Λ at an intermediate scale of momenta. A good choice for the latter appears to be:

$$\Lambda = \sqrt{2\pi T \hat{m}_D} \quad , \tag{3.36}$$

which represents the geometric average of the spacing between the Matsubara frequencies (hard scale) and the Debye screening mass in HTL (soft scale). Later we will investigate the sensitivity of the results to the value of this cutoff.
Now, in accord with the above discussion, in the integration over the spatial momenta in the formulas for the entropy and the baryon density one is allowed to keep the HTL expression of the integrand for $k < \Lambda$ (k being the modulus of the three-momentum). Hence the entropy will receive

contributions from the quasi-particle poles (normal quark mode, plasmino, transverse and longitudinal gluons) and from the Landau damping as well. For $k > \Lambda$ instead one takes into account only the propagation of the *physical modes* (normal quarks and transverse gluons), which are now dressed by the asymptotic masses obtained in NLA, neglecting the damping contribution. A comparisons of the results obtained in such a framework with the ones coming from lattice calculations are reported in Refs. [23, 24, 26] and the agreement appears satisfactory.

A similar strategy is here applied to the evaluation of mesonic correlation functions. In particular we explore in detail how an improved approximation at the level of the quark propagator is reflected on the (zero momentum) meson spectral function (in the pseudo-scalar channel) $\sigma(\omega, \boldsymbol{p} = \boldsymbol{0})$ and thus on the temporal correlation function $G(\tau, \boldsymbol{p} = \boldsymbol{0})$ obtained through Eq. (3.5). Before addressing the issue of improving the HTL results, let us discuss the basic features of the HTL quark spectral function that we want to keep in the new scheme.
The structure of the HTL quark propagator given in Eq. (2.92) guarantees that:

$$\{{}^\star S, \gamma^5\} = 0 \; , \tag{3.37}$$

${}^\star S$ being the HTL resummed quark propagator. This expresses the fact that, in spite of the appearance in the spectrum of a *gap mass* m_q and of an *asymptotic mass* $\hat{m}_\infty$ for the normal quark mode, both temperature dependent, nevertheless the chirality of a quark propagating in the thermal bath is conserved.
One would like Eq. (3.37) to hold even when a better description for the hard fermionic modes is given. Thus, in analogy with Eqs. (2.97) and (2.98), the following spectral representation for the NLA quark propagator is assumed to hold:

$$S^{\mathrm{NLA}}(i\omega_n, \boldsymbol{k}) = -\int_{-\infty}^{+\infty} d\omega \frac{\rho^{\mathrm{NLA}}(\omega, \boldsymbol{k})}{i\omega_n - \omega} \; , \tag{3.38}$$

where

$$\rho^{\mathrm{NLA}}(\omega, \boldsymbol{k}) = \frac{\gamma^0 - \boldsymbol{\gamma} \cdot \hat{\boldsymbol{k}}}{2} \rho_+^{\mathrm{NLA}}(\omega, k) \; + \; \frac{\gamma^0 + \boldsymbol{\gamma} \cdot \hat{\boldsymbol{k}}}{2} \rho_-^{\mathrm{NLA}}(\omega, k) \; . \tag{3.39}$$

The functions $\rho_\pm^{\mathrm{NLA}}$ are discussed below.
Now the HTL quark spectral functions $\rho_\pm$ obey the following *sum rule* [16]

$$\int_{-\infty}^{+\infty} d\omega \, \rho_\pm(\omega, k) = 1 \; , \tag{3.40}$$

which can be cast in the form

$$Z_+(k) + Z_-(k) + \int_{-k}^{+k} d\omega\, \rho_\pm(\omega, k) = 1 \;, \tag{3.41}$$

where the functions

$$Z_\pm(k) = \frac{\omega_\pm^2(k) - k^2}{2m_q^2} \tag{3.42}$$

are the residues of the quasi-particle excitations.
Since Eq. (3.40) is derived directly from the equal-time anticommutation relation:

$$\{\psi_\alpha(t, \boldsymbol{x}), \psi_\beta^\dagger(t, \boldsymbol{x'})\} = \delta_{\alpha\beta}\delta(\boldsymbol{x} - \boldsymbol{x'}) \tag{3.43}$$

one would like it to hold for the NLA quark spectral function as well.
It is of interest to discuss how the saturation of the sum rule (3.40) is implemented in the HTL approximation. To this aim we recall the asymptotic behaviour of the HTL fermionic dispersion relations for $k \gg m_q$ which is found to be

$$\omega_+(k) \simeq \sqrt{k^2 + \hat{m}_\infty^2} \;, \qquad \omega_-(k) \simeq k + 2k \,\exp\left(-\frac{2k^2 + m_q^2}{m_q^2}\right) \;, \tag{3.44}$$

where the HTL quark asymptotic mass has been defined in Eq. (3.32). Concerning the residues one gets, always for $k \gg m_q$,

$$Z_+(k) \simeq 1 + \frac{m_q^2}{2k^2}\left(1 - \ln\frac{2k^2}{m_q^2}\right) \;, \quad Z_-(k) \simeq \frac{2k^2}{m_q^2}\,\exp\left(-\frac{2k^2 + m_q^2}{m_q^2}\right) \;. \tag{3.45}$$

From the above it follows that:

$$\lim_{k\to\infty} Z_+(k) = 1 \quad \text{and} \quad \lim_{k\to\infty} Z_-(k) = 0 \;. \tag{3.46}$$

Hence, for $k \gg m_q$ (admittedly a situation where the HTL approximation is no longer realistic) the normal quark mode tends to saturate the sum rule (3.41) and its dispersion relation approaches the one of a free particle of mass $\hat{m}_\infty$.

In line with the above arguments we propose an improved expression for the quark spectral function which satisfies the following constraints:

- for small momenta it reduces to the HTL one;
- for large momenta it yields a spectrum dominated by an undamped excitation whose dispersion relation approaches $\epsilon_k^{\rm NLA} = \sqrt{k^2 + m_\infty^2}$, m_∞ being the solution of Eq. (3.35);

- it obeys the sum rule (3.40);
- the associated quark propagator anti-commutes with γ^5.

A prescription should also be given to allow a transition from the soft to the hard momenta regime. In this connection, keeping for the intermediate cutoff Λ the value given in Eq. (3.36), a natural choice might appear the following one:

$$\rho_\pm^{\rm NLA}(\omega,k)=\theta(\Lambda-k)\rho_\pm(\omega,k)+\theta(k-\Lambda)\delta(\omega\mp\epsilon_k^{\rm NLA})\ , \tag{3.47}$$

where $\rho_\pm$ are the HTL quark spectral functions, while $\epsilon_k^{\rm NLA}=\sqrt{k^2+m_\infty^2}$, being m_∞ the NLA quark asymptotic mass.
Actually, since $\omega_+(\Lambda)>\epsilon_k^{\rm NLA}(k=\Lambda)$, a narrow interval of values of ω (i.e. $2\epsilon^{\rm NLA}(\Lambda)<\omega<2\omega_+(\Lambda)$) exists in which the meson spectral function would get contribution both from the normal quark mode $\omega_+(k)$, namely

$$\frac{2N_c}{\pi^2}(e^{\beta\omega}-1)\int_0^\Lambda dk\,k^2\,\tilde n^2(\omega_+(k))Z_+^2(k)\delta(\omega-2\omega_+(k))\ , \tag{3.48}$$

and from the asymptotic quark dispersion relation $\epsilon_k^{\rm NLA}$, namely

$$\frac{2N_c}{\pi^2}(e^{\beta\omega}-1)\int_\Lambda^\infty dk\,k^2\,\tilde n^2(\epsilon_k^{\rm NLA})\delta(\omega-2\epsilon_k^{\rm NLA})\ . \tag{3.49}$$

Hence, due to this overcounting of the same physical mode, the meson spectral function would display an unphysical bump for $2\epsilon^{\rm NLA}(\Lambda)<\omega<2\omega_+(\Lambda)$, $\sigma(\omega)$ being discontinuous at the border of the interval.
In order to cure this problem (at least partially, as we will see in the following) and to interpolate smoothly between the soft and hard regimes we introduce two additional momenta Λ_1 and Λ_2 defined as follows:

$$\omega_+(\Lambda_1)=\sqrt{\Lambda^2+m_\infty^2} \tag{3.50a}$$

$$\omega_+(\Lambda)=\sqrt{\Lambda_2^2+m_\infty^2}\ . \tag{3.50b}$$

Hence the following guess on the spectral functions $\rho_\pm^{\rm NLA}(\omega,k)$ entering into Eq. (3.39), namely

$$\rho_\pm^{\rm NLA}(\omega,k)=\begin{cases}\rho_\pm(\omega,k) & \text{if } k<\Lambda_1\\ \cos^2(\alpha(k))\rho_\pm(\omega,k)+\sin^2(\alpha(k))\delta(\omega\mp\epsilon_k^{\rm NLA}) & \text{if } \Lambda_1<k<\Lambda_2\\ \delta(\omega\mp\epsilon_k^{\rm NLA}) & \text{if } k>\Lambda_2\end{cases} \tag{3.51}$$

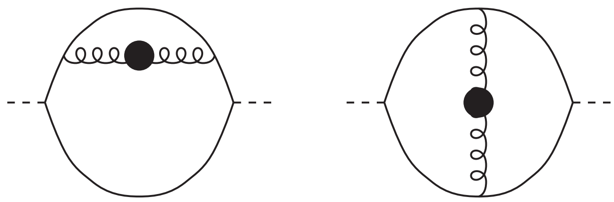

Figure 3.5: Higher order diagrams contributing to the pseudoscalar meson spectral function. All the fermionic lines are hard. The dressed wavy lines are HTL resummed gluon propagators. The effect of diagram (a) (together with the corresponding one with the self energy insertion in the other fermionic line) are taken into account in an effective way through the introduction of the NLA quark effective mass. The effects of diagram (b), which in principle might give a contribution of the same order of (a), are not accounted for in our NLA scheme.

with

$$\alpha(k) = \frac{\pi}{2} \cdot \frac{k - \Lambda_1}{\Lambda_2 - \Lambda_1} \, , \tag{3.52}$$

appears suitable.
Replacing then the HTL quark spectral functions entering into Eq. (3.27) with the above given Ansatz, one gets the following NLA expression for the pseudo-scalar meson spectral function (for $\omega > 0$):

$$\begin{aligned}\sigma^{\mathrm{ps}}_{\mathrm{NLA}}(\omega, \mathbf{0}) = \frac{2N_c}{\pi^2}(e^{\beta\omega} - 1)\int_0^{+\infty} dk\, k^2 \int_{-\infty}^{+\infty} d\omega_1 \int_{-\infty}^{+\infty} d\omega_2 \tilde{n}(\omega_1)\tilde{n}(\omega_2) \\ \delta(\omega - \omega_1 - \omega_2)[\rho_+^{\mathrm{NLA}}(\omega_1, k)\rho_+^{\mathrm{NLA}}(\omega_2, k) + \rho_-^{\mathrm{NLA}}(\omega_1, k)\rho_-^{\mathrm{NLA}}(\omega_2, k)] \, .\end{aligned} \tag{3.53}$$

In conformity with Eq. (3.5), one can next obtain the associated zero momentum temporal correlator $G^{\mathrm{ps}}_{\mathrm{NLA}}(\tau, \mathbf{0})$ whose behaviour will be later shown for different values of the temperature.

Before presenting our numerical results we stress that our approach is just an effective way of accounting for the contribution to the meson correlation function arising from the hard fermionic modes, for which the HTL approximation no longer holds. Specifically we embody, in analogy with entropy calculations of Refs. [23, 24, 25, 26], the effects of diagram (a) in Fig. (3.5) into the NLA quark asymptotic mass, which turns out to be lower than the HTL one. On the other hand we neglect the corrections arising from diagram (b) which in principle could be equally important.

3.6 Numerical results

In this section we first assess the weight of the different contributions (pole-pole, pole-cut and cut-cut) to the HTL pseudoscalar spectral function

$$\sigma^{\rm ps}_{\rm HTL}(\omega,\mathbf{0}) = \sigma^{\rm pp}(\omega,\mathbf{0}) + \sigma^{\rm pc}(\omega,\mathbf{0}) + \sigma^{\rm cc}(\omega,\mathbf{0}) \ . \tag{3.54}$$

Next we explore the modifications of the HTL results stemming from the more proper NLA treatment of the hard modes.
For the sake of consistency, we start from the explicit expression for the three terms involved in $\sigma^{\rm ps}_{\rm HTL}(\omega,\mathbf{0})$. These have already been deduced in Ref. [50]. For zero spatial momentum the pole-pole term, which selects the quasi-particle peaks in both quark spectral functions in Eq. (3.27), is given by:

$$\begin{aligned}\sigma^{\rm pp}(\omega) = \frac{N_c}{2\pi^2}\frac{e^{\beta\omega}-1}{m_q^4}\Bigg[&\tilde{n}^2(\omega_+(k_1))(\omega_+^2(k_1)-k_1^2)^2\frac{k_1^2}{2|\omega'_+(k_1)|}+\\ +2\sum_{k_2}\tilde{n}(\omega_+(k_2))[1-\tilde{n}(\omega_-(k_2))](\omega_+^2(k_2)-k_2^2)&(\omega_-^2(k_2)-k_2^2)\frac{k_2^2}{|\omega'_+(k_2)-\omega'_-(k_2)|}+\\ &+\sum_{k_3}\tilde{n}^2(\omega_-(k_3))(\omega_-^2(k_3)-k_3^2)^2\frac{k_3^2}{2|\omega'_-(k_3)|}\Bigg] \ .\end{aligned} \tag{3.55}$$

In the above k_1 is the unique solution of the equation $\omega - 2\omega_+(k_1) = 0$, whereas two are the values of k_2 fulfilling $\omega - \omega_+(k_2) + \omega_-(k_2) = 0$ and, likewise, two values of k_3 satisfy $\omega - 2\omega_-(k_3) = 0$.
In order to identify the different contributions to the pole-pole term with well defined physical processes let us introduce the notation q_+ ($\bar{q}_+$) for the normal (anti-) quark mode, q_- ($\bar{q}_-$) for the (anti-) plasmino mode and M for the pseudo-scalar meson.
Thus the first term in Eq. (3.55) corresponds to the annihilation of a normal quark anti-quark pair into a meson at rest

$$q_+ \ + \ \bar{q}_+ \longrightarrow M \ ,$$

which clearly turns out to be proportional to the mean occupation number of normal (anti-) quarks states, hence the factor $\tilde{n}^2(\omega_+(k_1))$. Due to energy conservation the density of states turns out to be proportional to $|d(2\omega_+)/dk|^{-1}$.
On the other hand the second term is related to the decay of a normal quark mode into a plasmino mode with the same momentum and a meson at rest, namely

$$q_+ \longrightarrow q_- + M \ .$$

Therefore in this term one of the statistical factor accounts for the mean occupation number of normal quarks states (hence the Fermi distribution $\tilde{n}(\omega_+(k_2))$), while the other one expresses the fact that the final plasmino has to occupy empty states (hence the Pauli-blocking factor $1 - \tilde{n}(\omega_-(k_2))$). In this case the density of states is proportional to $|d(\omega_+ - \omega_-)/dk|^{-1}$.
Finally the third term describes the annihilation of a plasmino anti-plasmino pair into a meson

$$q_- \; + \; \bar{q}_- \longrightarrow M \; ,$$

whence the statistical $\tilde{n}^2(\omega_-(k_3))$ and the density of states $|d(2\omega_-)/dk|^{-1}$ factors.
It is important to realize that, owing to the minimum in the plasmino dispersion relation, two values of ω exist for which the denominators in Eq. (3.55) $|\omega'_+(k_2) - \omega'_-(k_2)|$ and $|\omega'_-(k_3)|$ vanish, thus yielding singularities in the meson spectral function . These are the so-called Van Hove singularities, essentially reflecting a divergence in the density of states. One finds (numerically) that they occur at $\omega \approx 0.47 m_q$ and at $\omega \approx 1.86 m_q$. The impact of these singularities on the meson spectral function is dramatic for soft values of ω. Here indeed the HTL meson spectral function turns out to be orders of magnitude larger than the free one, as it can be seen in Fig. (3.6).
Turning to the pole-cut contribution (for positive energies) it is found to be:

$$\begin{aligned} \sigma^{\rm pc}(\omega) = & \frac{2N_c}{\pi^2}\frac{e^{\beta\omega}-1}{m_q^2}\int_0^\infty dk\, k^2 \; \cdot \\ & \cdot \left[\theta(k^2-(\omega-\omega_+)^2)\tilde{n}(\omega-\omega_+)\tilde{n}(\omega_+)\beta_+(\omega-\omega_+,k)(\omega_+^2-k^2)\right. \\ & \left.+\theta(k^2-(\omega-\omega_-)^2)\tilde{n}(\omega-\omega_-)\tilde{n}(\omega_-)\beta_-(\omega-\omega_-,k)(\omega_-^2-k^2)\right] \; . \end{aligned} \tag{3.56}$$

Finally the cut-cut contribution is given by:

$$\begin{aligned} \sigma^{\rm cc}(\omega) = & \frac{2N_c}{\pi^2}(e^{\beta\omega}-1)\int_0^\infty dk\, k^2 \int_{-k}^{+k} dx\, \tilde{n}(x)\tilde{n}(\omega-x)\theta(k^2-(\omega-x)^2) \cdot \\ & \cdot \left[\beta_+(x,k)\beta_+(\omega-x,k) + \beta_-(x,k)\beta_-(\omega-x,k)\right] \; . \end{aligned} \tag{3.57}$$

The three above quoted contributions to the meson spectral function in the pseudoscalar channel in a pure HTL approximation are plotted in Fig. 3.6: they numerically coincide with the results previously obtained by Karsch et al. [50].

The question we now raise is whether the behaviour of the meson spectral function at soft energies, displayed in Fig. 3.6, is qualitatively modified once

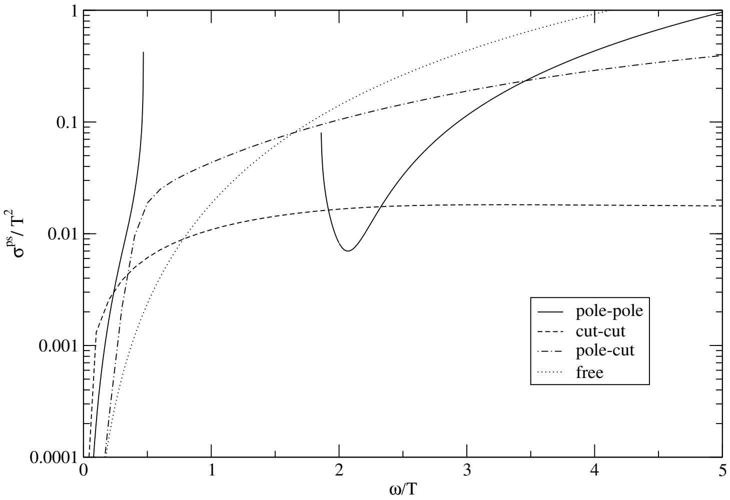

Figure 3.6: The various contributions (pole-pole, pole-cut and cut-cut) to the dimensionless spectral function of a pseudoscalar meson σ^{ps}/T^2 at zero spatial momentum as a function of $x = \omega/T$. Here the quark propagators have been evaluated in the HTL approximation both for hard and soft momenta. In order to test the present results versus the ones obtained in Ref. [50], *here* the plot is given for a value of T such that $g(T) = \sqrt{6}$, entailing $m_q = T$. In the pole-pole contribution one recognizes the occurrence of the Van Hove singularities at $x = 0.47$ and at $x = 1.856$. Also plotted is the free spectral function.

a better description of the hard fermionic modes is adopted.
Since the divergence in the density of states, which gives rise to the Van Hove singularities in the pole-pole term, stems from the stationary points of the curves given by the equations

$$\omega = 2\omega_-(k) \tag{3.58a}$$

and

$$\omega = \omega_+(k) - \omega_-(k)\ , \tag{3.58b}$$

to answer the above question one should check whether the choice of the intermediate cutoff Λ separating the soft modes from the hard ones yields $\Lambda > \tilde{k}_i$, where $\tilde{k}_i$ are the stationary points of the curves (3.58a) and (3.58b). In such a case indeed the Van Hove singularities will still be present in the spectral function. Therefore we report below the numerical values of $\Lambda_1, \Lambda, \Lambda_2$ (normalized to the quark thermal mass m_q) for two different choices of the intermediate cutoff Λ, for $T = 2T_c$ and $T = 4T_c$. We also report the corresponding value of the gauge coupling g obtained through the QCD β-function as discussed below.

$T = 2T_c$ (g=1.785)	Λ_1/m_q	Λ/m_q	Λ_2/m_q
$\Lambda = \sqrt{\pi T \hat{m}_d}$	3.312	3.492	3.665
$\Lambda = \sqrt{2\pi T \hat{m}_d}$	4.806	4.939	5.069

$T = 4T_c$ (g=1.548)	Λ_1/m_q	Λ/m_q	Λ_2/m_q
$\Lambda = \sqrt{\pi T \hat{m}_d}$	3.593	3.750	3.902
$\Lambda = \sqrt{2\pi T \hat{m}_d}$	5.188	5.303	5.417

From the comparison with the curves in Figs. 2.7 and 3.7 which, being normalized to the quark thermal mass m_q, hold for every value of the temperature, one realizes that the stationary points leading to the Van Hove singularities *always* occur in the soft domain $k < \Lambda_1$. Hence we conclude that, *qualitatively*, the behaviour of the HTL meson spectral function does not change once a better treatment of the hard fermionic modes is kept into account. The quantitative changes are examined below.

Accordingly, we next present the results obtained in the Next to Leading Approximation (NLA), which has been briefly discussed in the previous section and which allows a better treatment of the contribution of the hard quark modes in the meson spectral function.

Before addressing the discussion of the numerical results a few words, regarding how the running of α_s is related to the temperature, are in order.

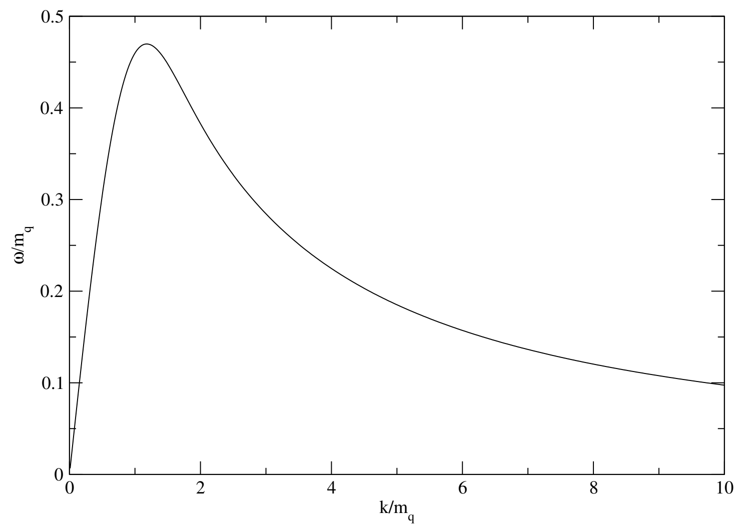

Figure 3.7: The behaviour of the difference between the two fermionic dispersion relations $\tilde{\omega}_+(x) - \tilde{\omega}_-(x)$. The dimensionless variables $\tilde{\omega} = \omega/m_q$ and $x = k/m_q$ are used. The maximum of the curve occurs at $x = 1.179$ and corresponds to a value of $\tilde{\omega} = 0.4698$.

The running of the QCD coupling g with the renormalization scale $\bar{\mu}$ (introduced in the dimensional regularization scheme) is here obtained through the two-loop β-function with $N_f = 2$, in accord with [23]. The modified Minimal Subtraction ($\overline{\text{MS}}$) renormalization scheme is employed. Dealing with massless quarks, the only physical scale entering into the problem is the temperature. Hence the evaluation of the coupling g at the scale $\bar{\mu} = 2\pi T$, which corresponds to the spacing between the Matsubara frequencies, appears to be a reasonable choice. For further details see [23] and references therein.

In Fig. 3.8 we display the ratio of the Pade' and NLA asymptotic mass with respect to its HTL value. The two curves represent the solution of Eqs. (3.33) and (3.35). It appears clearly that the interaction of the hard quark modes with soft longitudinal and transverse gluons (for which one uses HTL resummed propagators) lowers the value of the asymptotic quark mass and that the two approximation schemes lead to similar results.
In Fig. 3.9 the behaviour of the ratio Λ/T as a function of the temperature is given. In case of absence of running of the coupling g with the temperature the ratio should stay constant.

In Fig. 3.10 we plot the pseudoscalar meson spectral function obtained in

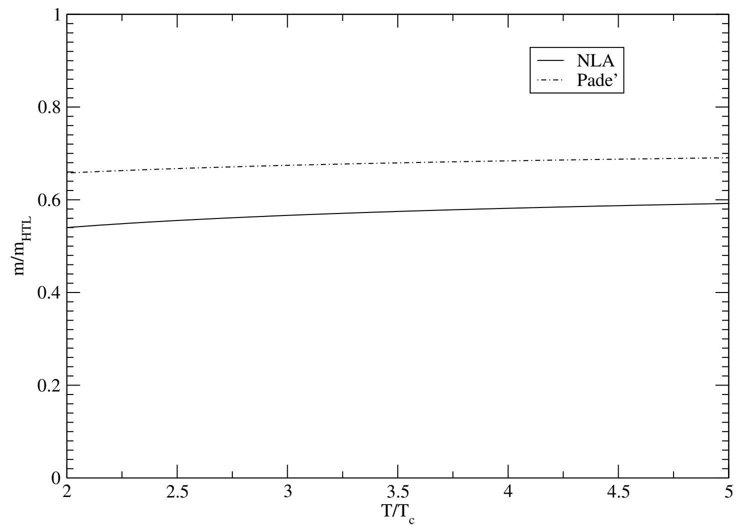

Figure 3.8: Ratio of the asymptotic quark mass over its HTL value as a function of T/T_c: here the (negative) correction δm_∞^2 has been included in two different ways: with the first Pade' approximant (dot-dashed line) and in the "self-consistent like" way (continuous line).

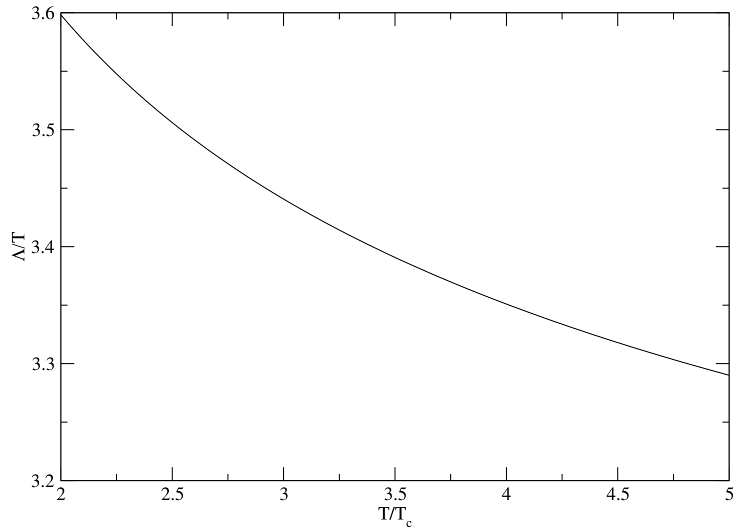

Figure 3.9: Temperature behaviour of the intermediate cutoff $\Lambda = \sqrt{2\pi T \hat{m}_D}$ separating soft and hard momenta. Dimensionless units Λ/T and T/T_c are adopted. The decreasing of the ratio Λ/T reflects the running of the strong coupling constant.

the NLA scheme with two different choices of the cut-off parameter Λ. This is compared with the pure HTL result, with the curve obtained assigning to the quarks a mass $m_\infty^{\rm NLA}$ and with the non interacting case. Notice that the curves NLA1 and NLA2 display a peak which has no physical meaning, but this is an artifact of our approximation for the quark spectral function. In fact a narrow energy interval exists where the meson spectral function gets contribution both from the normal HTL quark mode and from the NLA asymptotic dispersion relation. On the other hand, as discussed in the previous section, without the prescription (3.51) the spectral function would display an even worse unphysical behaviour. Although our findings for this intermediate scale of frequencies cannot be trusted, nevertheless for the soft and hard regimes they are reliable.
In Fig. 3.10 the kernel entering into the definition of the meson temporal correlation function (see formula (3.5)), namely

$$K(\tau,\omega)=\cosh(\omega(\tau-\beta/2))/\sinh(\omega\beta/2)\ , \tag{3.59}$$

is also plotted for $\tau=\beta/2$. One infers from the behaviour of $K(\tau=\beta/2,\omega)$ that, for this value of τ, the contribution from the soft sector to the integral in Eq. (3.5) is significant.

Finally in Figs. 3.12 and 3.13 we show, for two different values of the temperature, the zero-momentum temporal correlator $G(t=-i\tau,\boldsymbol{p}=\boldsymbol{0})$ in the two different approximations schemes discussed in this paper: HTL and NLA. We also show the curve obtained dressing the quark modes with the NLA asymptotic mass and setting to zero the plasmino and the damping contribution to the quark spectral function.
As expected from the general theory, the curves are symmetric for $\tau\to\beta-\tau$. The correlation function diverges for $\tau\to 0$ (β) independently from the approximation scheme employed and even in the non-interacting case. Hence the meaningful quantity to study in order to assess the impact of the interaction with the thermal bath on the meson correlation function is the ratio $G(\tau)/G^{\rm free}(\tau)$ given in panel B in Figs. 3.12 and 3.13. Note that for $\tau\to 0(\beta)$ one recovers the free result.
For τ sufficiently small (or close to β) the NLA curves stay above the HTL result. This may be understood on the following basis. As τ gets smaller, the contribution to $G(\tau)$ coming from large frequencies grows, as one can see from Eq. (3.5). But for large values of ω the meson spectral function (both in HTL and in NLA) is dominated by the normal quark modes, in which $m_\infty^{\rm (NLA)}<\hat{m}_\infty^{\rm (HTL)}$.
On the contrary, for τ close to $\beta/2$, where the contribution from soft frequencies becomes more important, the HTL result stays significantly above the

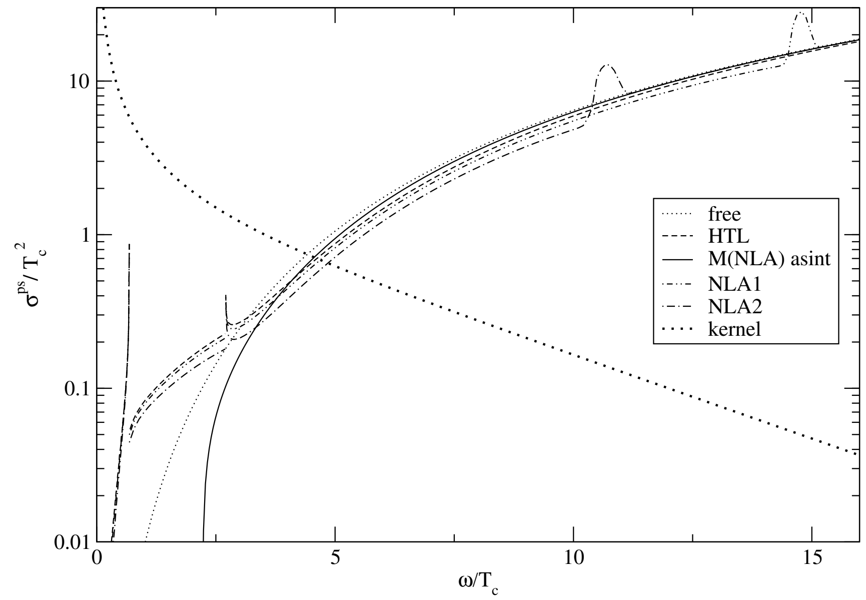

Figure 3.10: Behaviour of the zero momentum pseudoscalar spectral function σ^{ps}/T_c^2 versus ω/T_c in different approximations: free result, HTL, NLA and quarks endowed with a thermal mass $m_{\rm NLA}$. NLA1 corresponds to the choice $\Lambda = \sqrt{2\pi T \hat{m}_D}$, NLA2 to $\Lambda = \sqrt{\pi T \hat{m}_D}$. The plot refers to $T = 2T_c$.

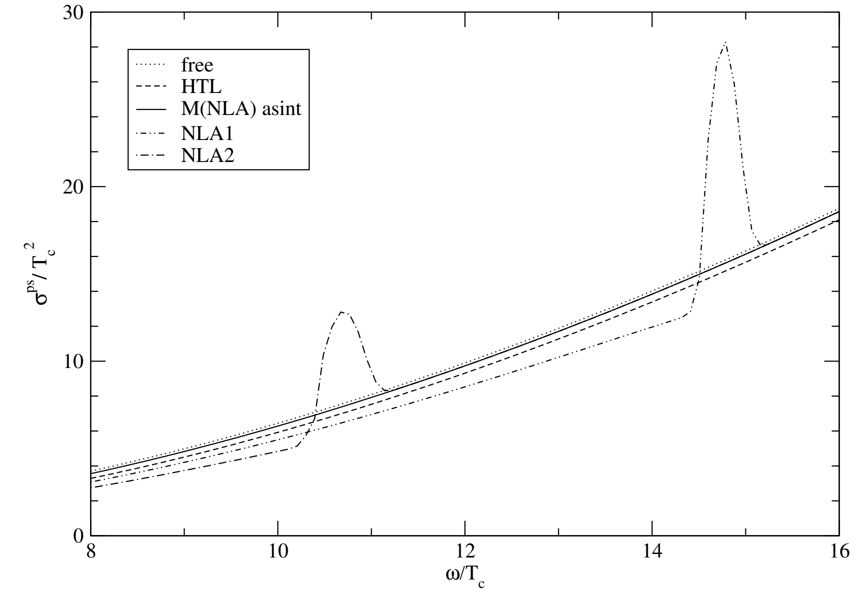

Figure 3.11: The same quantity as in Fig. (3.10) in two different energy domains.

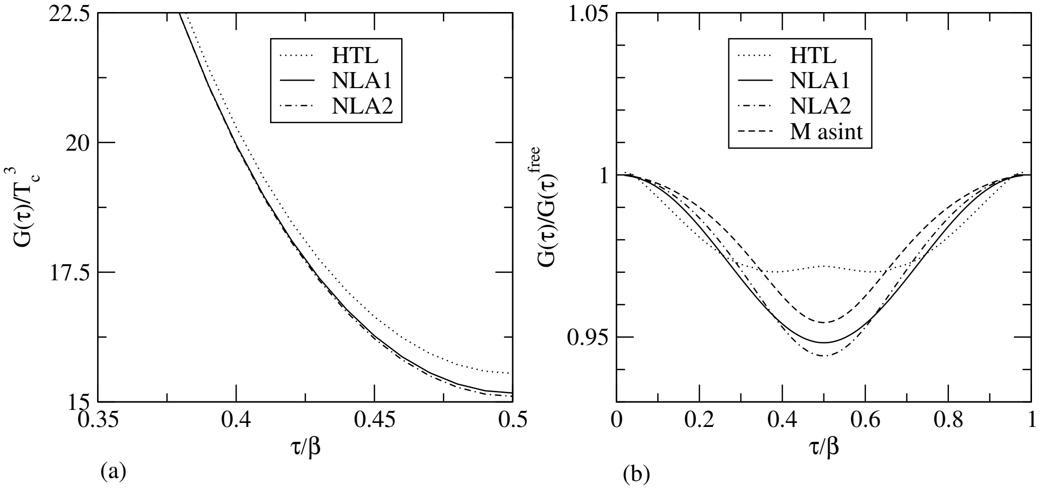

Figure 3.12: (a): Behaviour of $G(\tau)/T_c^3$ vs τ/β. (b): Behaviour of $G(\tau)/G^{\rm free}(\tau)$ vs τ/β. NLA1 corresponds to $\Lambda = \sqrt{2\pi T \hat{m}_D}$, NLA2 corresponds to $\Lambda = \sqrt{\pi T \hat{m}_D}$. In panel (b) we also display the result obtained in the case of quarks endowed with a thermal mass $m = m_{\rm NLA}$. The curves are given for $T = 2T_c$.

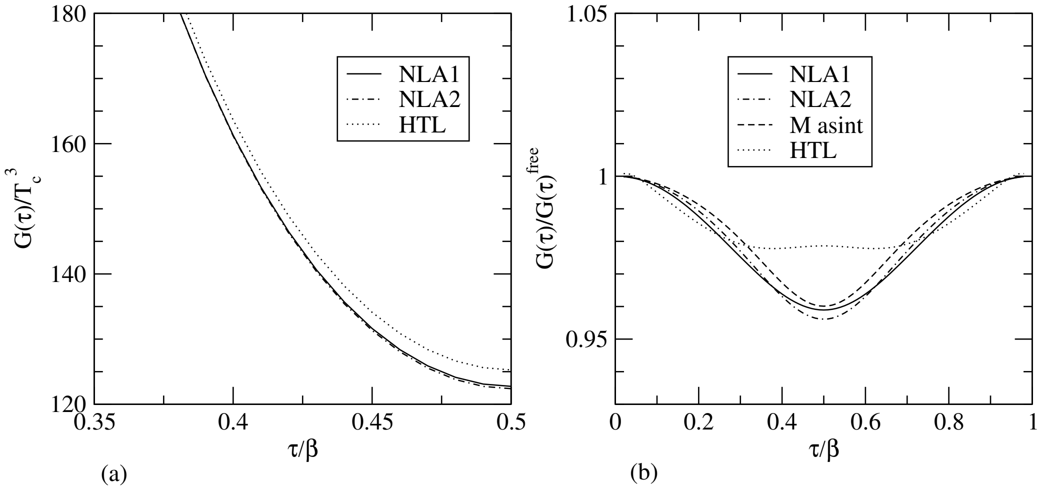

Figure 3.13: The same as in Fig. 3.12, but for $T = 4T_c$.

NLA curves.
It is also evident that the NLA curve are not much sensitive to the choice of the cutoff Λ and that, as one moves to larger values of the temperature, one approaches (slowly) the free result.
In any case, in the whole range $0 < \tau < \beta$, is $G(\tau) < G^{\mathrm{free}}(\tau)$. This outcome appears to agree with the results for the correlation function along the z-axis obtained in [40]. Here, on the basis of a dimensionally reduced effective lagrangian, a positive correction (of the order of 5%) was found to occur for the meson screening mass.

3.7 Conclusions

In this chapter of the thesis we have explored the predictions of the NLA framework on the thermal meson correlation functions in the deconfined phase of QCD, thus extending past work of Blaizot et al. who successfully investigated, employing the NLA scheme, the thermodynamical properties of the QGP. Notably their results turned out to be well supported by lattice calculations, even in a regime of temperatures where g is not small ($g \sim 1$ or larger), in which the separation of different momentum scales (i.e. g^2T, gT, T) might appear questionable. Hence we felt justified to employ here the same scheme to deal with other observables, like the meson correlation functions.
Actually what we have proposed is a variant of the NLA scheme, smoothly matching the soft and hard momenta regimes.
With a more careful treatment of the contribution to the meson correlation function arising from the hard quark modes we have still found that the NLA does not change dramatically the HTL results which turns out to be quite robust. In particular the peculiar behaviour of the meson spectral function for soft energies (Van-Hove singularities) remains (almost) unaltered.
The detection of the V.H. singularities in the meson spectral functions, being related to the minimum in the plasmino dispersion relation, would be a clear signal of deconfinement. Indeed the doubling of the fermionic dispersion relation for non-vanishing three-momentum is not strictly related to the HTL approximation, whose validity, for values of the temperature just above T_c, is questionable. Actually, as discussed in [41, 42], it is possible to show, in a totally non perturbative framework, that in the high temperature chirally symmetric phase of QCD the fermion propagator *does always display* two distinct dispersion relations, one of which developing a minimum.
Unfortunately the possibility of getting an experimental evidence of these singularities, for instance from the dilepton production rate for what con-

cerns the vector channel, is dim, owing to the fact that during the expansion of the fireball their position moves toward lower energies as the temperature decreases (experiments provide time-integrated yields). Furthermore there are other sources of dileptons which may cover the signal.
At present, lattice calculations of (zero momentum) meson spectral functions (of light quarks) $\sigma_M(\omega)$ do not show any evidence of sharp resonances in the soft energy domain which could be related to the V.H. singularities [37, 38, 39]. This occurrence may depend on the fact that what one actually measures on the lattice is the temporal correlator $G_M(\tau)$ on a finite set of euclidean times. Hence, to get $\sigma_M(\omega)$ from the lattice requires to invert Eq. (3.5) and the left hand side of this equation is known only on a finite set of values of τ. To perform this inversion, the Maximum Entropy Method has been recently adopted [27, 28, 29, 37, 38, 39], which in any case requires some *a priori* information both on $G_M(\tau)$ and on $\sigma_M(\omega)$. As a consequence it is not possible at present to assure that the spectral function reconstructed in this way is unique and that the existence of very sharp resonances like the V.H. singularities can be brought to evidence with this method.
Also of interest is to point out that the V.H. singularities, associated to the vanishing of the group velocity of a propagating wave, also occur in other contests in many-body physics. For example in a non relativistic ferromagnetic system at $T = 0$ undergoing a spontaneous symmetry breaking (*Quantum Phase Transition*), the dispersion relation of the Goldstone mode (magnon) displays a maximum, at which the group velocity is zero [43].
A promising route to the study of mesonic correlations in the deconfined phase of QCD is offered by the possibility of applying the same strategy developed in this paper to the evaluation of meson screening masses (i.e. considering the propagation along a spatial direction) and comparing the results with those obtained in different approaches (for instance on the lattice or with effective lagrangians). Indeed, due to the larger number of sites along the spatial directions with respect to the (euclidean) temporal one, lattice calculations should provide more reliable results for this kind of observables.
Concerning the shortcoming of the framework employed in this chapter, it should be pointed out that we took into account corrections to the free meson correlation functions arising merely from dressing the fermionic propagators, due to their interactions with the medium (i.e. the gluons of the thermal bath). On the other hand, if, within the HTL scheme, one is allowed to leave the pseudoscalar vertex untouched (since the HTL correction to the pseudoscalar vertex vanishes), this is no longer true when one tries to go beyond the HTL approximation. While we have not accounted for this fact in our analysis, it certainly represents an item worth to be addressed.
Equally important appears to be the study of the chiral and of the quark

number susceptibilities in a scheme improving upon the HTL results obtained in Refs. [44, 45].

Finally we stress that we don't expect the framework employed in this paper to give reliable results for temperature values lower than $2.5 \div 3T_c$. For the range of T just above T_c other schemes [30, 31], predicting the presence of bound states also in the deconfined phase, appear more realistic.

Chapter 4

Heavy quark bound states above T_c

4.1 Motivations

As already discussed in the Introduction the anomalous suppression of the J/ψ production in heavy ion collisions, which has been experimentally observed [4, 5] in the depletion of the dilepton multiplicity in the region of invariant mass corresponding to the J/ψ meson, was proposed long time ago as a possibly unambiguous signal of the onset of deconfinement [10]. Indeed in Ref. [10] it is argued that charmonium states can only be produced in the first instants after the nucleus-nucleus collision, before the formation of a thermalized QGP. Then, in their path through the deconfined medium, the original $c\bar{c}$ bound states tend to melt, since the binding (colour) Coulomb potential is screened by the large number of colour charges. This, in turn, produces an anomalous (with respect to normal nuclear absorption) drop in the J/ψ yields.

In this picture it is implicitly assumed that, once the charmonium dissociates, the heavy quarks hadronize by combining with light quarks only (recombination leading to a secondary J/ψ production is neglected). This assumption is certainly justified at the SPS conditions, due to the very small number of $c\bar{c}$ pairs produced per collision ($N_{c\bar{c}} \sim 0.2$ in a central collision), but at RHIC ($N_{c\bar{c}} \sim 10$) and LHC ($N_{c\bar{c}} \sim 200$) energies it is no longer warranted [46].

Moreover in a hadronic collisions only about 60% of the observed J/ψ's are directly produced, the remaining stemming from the decays of excited charmonium states (notably the χ_c and the ψ'). Since each $c\bar{c}$ bound state dissociates at a different temperature, a model of *sequential suppression* was developed, with the aim of reproducing the J/ψ suppression pattern as a function of the energy density reached in the heavy ion collision (the highest temperatures and energy densities being reached in the most central collisions) [47, 48, 49, 50, 51]. SPS experimental data for Pb-Pb collisions at different centralities seem indeed to support the dissociation pattern predicted by this model [4, 5].

Alternative mechanisms for the J/ψ production, like the Statistical Coalescence Model (SCM), have also been proposed [52]. In the SCM one assumes again that all the $c\bar{c}$ pairs are produced in hard processes at the initial stage of the collision. Any heavy quark bound state, if present, is assumed to melt in the QGP phase and the number of $c\bar{c}$ pairs in the fireball is considered fixed. At the chemical freeze-out open and hidden charmed hadrons are then produced with multiplicity *ratios*[1] fixed by their masses, according to the laws of statistical mechanics. Hence, in such a scheme, the measured J/ψ multiplicity is not related to the presence of charmonium bound states in the plasma phase, but to the statistical hadronization of the initially produced $c(\bar{c})$ (anti-)quarks. This may lead, at LHC energies, to a completely different picture characterized by an enhanced charmonium production even if all the $c\bar{c}$ bound states dissociate during the plasma phase.

In any case the hypothesis that all the primary produced J/ψ's melt during the QGP lifetime is hardly realized at SPS conditions. Hence models have been developed [53, 54] attempting to account both for the initial state production, eventually subject to in-medium dissociation, and for the thermal production at the hadronization.

Concerning the heavy quarkonia in the QGP phase, recent lattice data [27, 28, 29] in quenched approximation (hence neglecting effects arising from virtual processes involving dynamical fermions), which display narrow peaks for the charmonium spectral functions in the pseudoscalar and vector channels (even up to $T \sim 2T_c$), seem to point to the existence of heavy quark bound states up to temperatures above T_c[2]. Clearly these results, if confirmed, would entail striking experimental consequences.

We have already discussed the fact that the meson spectral functions cannot be measured directly on the lattice. From the numerical simulations one gets the current-current correlation function along the (imaginary) temporal direction on a finite number of points. Such a correlator corresponds to the convolution of the meson spectral function with a thermal kernel. The spectral function can then be obtained only indirectly. With this aim

[1] Due to the low rate of inelastic reactions full chemical equilibrium cannot be reached by charmed hadrons: their total multiplicity measured at SPS stays well above the thermal value.

[2] Actually, in Ref. [28] the analysis has been done for $s\bar{s}$ mesons.

in Refs. [27, 28, 29] a procedure called Maximum Entropy Method (MEM) has been adopted. Clearly, an independent test of the results obtained with MEM appears desirable: this indeed is the scope I pursue in this part of the Thesis.

For this purpose, we first extract from the lattice data a heavy quark potential accounting for thermal effects and then we solve the Schrödinger equation for the charmonium (and bottomonium). As shown in Refs. [55, 56, 57, 58, 59], from the Polyakov loop correlation function it is possible to extract the free energy (in the different color channels) of a heavy quark-antiquark pair placed at a distance r in a thermal bath of gluons and light dynamical fermions. Once a good parameterization of the color singlet free energy is obtained, the entropy and internal energy contributions can be disentangled. Since the quarks acting as static sources of the color field are considered infinitely heavy, the internal energy coincides with the potential. The latter is then inserted into the Schrödinger equation, from which the binding energy of the different stable states — if there are any — and their evolution with the temperature are obtained.

Indeed a clear distinction between the $Q\overline{Q}$ free and potential energies is necessary in order to get a reliable estimate of the quarkonium dissociation temperature T_d in the different spin-parity channels.

In Refs. [48, 49, 60, 61], where the colour singlet *free energy* was directly inserted into the Schrödinger equation, the dissociation temperatures $T_d = 1.10T_c$ [49] and $T_d = 0.99T_c$ [60] were found for the J/ψ, all the other charmonium states melting well below T_c.

On the other hand, in Ref. [62], where a parameterization of the lattice color singlet *potential* (in the quenched approximation) was used, the temperature T_d for the *spontaneous dissociation* of the J/ψ was estimated to occur at about $2T_c$, a value even larger than the one obtained from the spectral analysis performed in Refs. [27, 28, 29]. Also results for different charmonium and bottomonium states have been reported in Ref. [62]. The case $N_f = 2$ was addressed in Ref. [63], where the J/ψ meson was found to be bound till $T \sim 2.7T_c$.

Actually, even if the potential supports the existence of bound states, other physical processes may lead to the dissociation of the quarkonium. First, if the $Q\overline{Q}$ binding energy is lower than the temperature — and assuming that the quarkonia have reached the thermal equilibrium with the plasma — a certain fraction of their total number will be thermally excited to resonant states according to a Bose-Einstein distribution: such a process is referred to as *thermal dissociation* [60, 62]. Furthermore, the collisions with the gluons and the light quarks of the plasma may lead to the *collisional dissociation* of the quarkonium. In this connection, the reaction $g + J/\psi \to c + \overline{c}$

was studied in detail in Ref. [62]. Hence, in spite of the presence of a bound state solution of the Schrödinger equation till $T \sim 2T_c$, the J/ψ turned out to be really stable only up to temperatures lower than $2T_c$ [62]. Clearly the two processes above mentioned are not encoded in the Polyakov loop correlation function, where the heavy quarks act as unthermalized static sources of the color field; rather they have to be accounted for *a posteriori*.

Of course, if the process $g + J/\psi \to c + \overline{c}$ can lead to the dissociation of the charmonium, the same reaction can also occur in the opposite direction. Hence a consistent calculation of J/ψ multiplicity implies the solution of a kinetic rate equation integrated over the lifetime of the QGP phase in which both processes (dissociation and recombination) enter [62, 64]. To carry out this detailed balance calculation the knowledge of the J/ψ binding energy and wave function in the thermal bath turns out to be an important input. This is of relevance because, as mentioned above, the usual assumption in considering the J/ψ suppression as a signature of deconfinement is that its production can only occur in the very initial stage of the collision. Actually, if at SPS the role played by recombination is numerically negligible, this is no longer true at RHIC as pointed out in Ref. [64].

In any case here we limit ourselves to check the existence of bound state solutions of the Schrödinger equation. A quantitative study of the dissociation and recombination processes is left for future work.

Here we take advantage of all the available lattice data, obtained not only in quenched QCD ($N_f = 0$), but also including two and, more recently, three light flavors. We are then in a position to study also the flavor dependence of the dissociation process, a perspective not yet achieved by the parallel studies of the spectral functions, which are, as already mentioned, only available in quenched QCD.

4.2 Polyakov loop correlation functions and heavy quark free energies

In this section, for the sake of consistency, we first summarize briefly the arguments given in Ref. [55] relating the free energy of a heavy quark-antiquark ($Q\overline{Q}$) pair to the Polyakov loop correlation function. Then, closely following Refs. [56, 58, 59], we display how the above quantities can be measured on the lattice.
Adopting the short-hand notation $\psi(t = -i\tau) = \psi(\tau)$ (with $0 < \tau < \beta$ real) one introduces the operators

$$\psi_a(\boldsymbol{r}, \tau) \quad \text{and} \quad \psi_a^\dagger(\boldsymbol{r}, \tau) \ , \tag{4.1}$$

destroying (creating) a heavy quark Q with color a at the point $(\vec{r},\tau)$. The operators

$$\psi^c_a(\boldsymbol{r},\tau) \quad \text{and} \quad \psi^{\dagger\,c}_a(\boldsymbol{r},\tau) \tag{4.2}$$

play the same role for the antiquark $\overline{Q}$. We stress that Q and $\overline{Q}$ are to be viewed as static (infinitely heavy) sources for the color field.
The heavy quark field obeys the standard equal-time anticommutation rule

$$\left\{\psi_a(\boldsymbol{r}_i,\tau),\psi^\dagger_b(\boldsymbol{r}_j,\tau)\right\} = \delta_{ij}\delta_{ab} \tag{4.3}$$

and the same relation holds for its charge conjugate.
The field ψ at the time $t=-i\beta$ is related to its value at the time $t=0$ by the equation:

$$\psi_i(\boldsymbol{r},\beta) = \mathrm{P}\exp\left(ig\int_0^\beta d\tau\, t^a\cdot A^a_0(\boldsymbol{r},\tau)\right)_{ij}\psi_j(\boldsymbol{r},0) = W_{ij}(\boldsymbol{r})\psi_j(\boldsymbol{r},0)\ , \tag{4.4}$$

where P stands for a *path-ordered* exponential (the theory being non abelian), t^a are the N^2-1 generators of the group $SU(N)$ in the fundamental representation, the indices $i,j=1,\dots N$ label the color of the quark field and the (untraced) Polyakov line $W(\boldsymbol{r})$ has been introduced, according to the definition:

$$W(\boldsymbol{r}) = \mathrm{P}\exp\left(ig\int_0^\beta d\tau\, t^a\cdot A^a_0(\boldsymbol{r},\tau)\right)\ . \tag{4.5}$$

On the other hand, the antiquark field transforms according to the antifundamental representation of the gauge group $SU(N)$. Hence:

$$\psi^c_i(\boldsymbol{r},\beta) = \mathrm{P}\exp\left(ig\int_0^\beta d\tau\, \overline{t}^a\cdot A^a_0(\boldsymbol{r},\tau)\right)_{ij}\psi^c_j(\boldsymbol{r},0) = \overline{W}_{ij}(\boldsymbol{r})\psi^c_j(\boldsymbol{r},0)\ . \tag{4.6}$$

Since $\overline{t}^a=-(t^a)^\star=-\tilde{t}^a$ (the tilde denoting transposition) the relation

$$\overline{W}(\boldsymbol{r}) = \widetilde{W}^\dagger(\boldsymbol{r}) \tag{4.7}$$

holds. The Polyakov loop is then introduced according to the definition:

$$L(\boldsymbol{r}) \equiv \frac{1}{N}\mathrm{Tr}\,\mathrm{P}\exp\left(ig\int_0^\beta d\tau\, t^a\cdot A^a_0(\boldsymbol{r},\tau)\right) = \frac{1}{N}\mathrm{Tr}\,W(\boldsymbol{r})\ . \tag{4.8}$$

It has been known for a long time that the free energy of a heavy $Q\overline{Q}$ pair can be related to the Polyakov loop correlation function. In order to see how this comes about we recall that the free energy of a system described by a

$SU(N)$ gauge theory with a heavy static quark (antiquark) placed at $\boldsymbol{x}$ ($\boldsymbol{y}$) is given by

$$
\begin{aligned}
e^{-\beta F_{Q\overline{Q}}(\boldsymbol{x};\boldsymbol{y})} &= \frac{1}{N^2}\sum_s \langle s|e^{-\beta H}|s\rangle \\
&= \frac{1}{N^2}\sum_{s'}\sum_{a,b}\langle s'|\psi_a(\boldsymbol{x},0)\psi_b^c(\boldsymbol{y},0)e^{-\beta H}\psi_a^\dagger(\boldsymbol{x},0)\psi_b^{\dagger c}(\boldsymbol{y},0)|s'\rangle \ ,
\end{aligned}
\tag{4.9}
$$

where the factor $1/N^2$ stems from the average over the colors, while s and s' denotes states with and without heavy quark sources respectively. Since $e^{-\beta H}$ is just the operator performing imaginary temporal translations by applying Eqs. (4.4)-(4.6) one obtains:

$$
\begin{aligned}
e^{-\beta F_{Q\overline{Q}}(\boldsymbol{x};\boldsymbol{y})} &= \frac{1}{N^2}\sum_{s'}\langle s'|e^{-\beta H}\psi_a(\boldsymbol{x},\beta)\psi_a^\dagger(\boldsymbol{x},0)\psi_b^c(\boldsymbol{y},\beta)\psi_b^{\dagger c}(\boldsymbol{y},0)|s'\rangle \\
&= \frac{1}{N^2}\sum_{s'}\langle s'|e^{-\beta H}W_{al}(\boldsymbol{x})\psi_l(\boldsymbol{x})\psi_a^\dagger(\boldsymbol{x})\overline{W}_{bm}(\boldsymbol{y})\psi_m^c(\boldsymbol{y})\psi_b^{\dagger c}(\boldsymbol{y})|s'\rangle \ ,
\end{aligned}
\tag{4.10}
$$

where now all the fields are evaluated at $\tau = 0$. Applying then the anticommutation rule (4.3) and since the states $|s'\rangle$ contain no heavy quark (antiquark) one gets:

$$
\begin{aligned}
e^{-\beta F_{Q\overline{Q}}(\boldsymbol{x};\boldsymbol{y})} &= \sum_{s'}\langle s'|e^{-\beta H}\frac{1}{N}\mathrm{Tr}W(\boldsymbol{x})\frac{1}{N}\mathrm{Tr}W^\dagger(\boldsymbol{y})|s'\rangle \\
&= \mathrm{Tr}\left[e^{-\beta H}L(\boldsymbol{x})L^\dagger(\boldsymbol{y})\right] \ ,
\end{aligned}
\tag{4.11}
$$

where the definition (4.8) has been used. On the other hand for a thermal bath at the inverse temperature $\beta = 1/T$ with no static quark (antiquark) sources the free energy is:

$$
e^{-\beta F_{00}} = \mathrm{Tr}\left[e^{-\beta H}\right] \ . \tag{4.12}
$$

Hence, in the frame of a $SU(N)$ theory, the change in the free energy due to the additional heavy static $Q\overline{Q}$ pair (with the quark in $\boldsymbol{x}$ and the antiquark in $\boldsymbol{y}$) turns out to be:

$$
e^{-\beta\Delta F_{Q\overline{Q}}(\boldsymbol{x};\boldsymbol{y})} = \frac{\mathrm{Tr}\left[e^{-\beta H}L(\boldsymbol{x})L^\dagger(\boldsymbol{y})\right]}{\mathrm{Tr}[e^{-\beta H}]} = \langle L(\boldsymbol{x})L^\dagger(\boldsymbol{y})\rangle \ , \tag{4.13}
$$

the thermal average of an operator O being

$$\langle O\rangle = \frac{\mathrm{Tr}\left[e^{-\beta H}O\right]}{\mathrm{Tr}\left[e^{-\beta H}\right]} \ . \qquad (4.14)$$

Eq. (4.9) clearly shows that the above described procedure provides the *color averaged* free energy of a $Q\overline{Q}$ pair, which is given by the thermal average over the possible color channels according to the well known decomposition

$$\overline{N} \otimes N = 1 \oplus (N^2 - 1) \ , \qquad (4.15)$$

yielding (for the case $N = 3$)

$$e^{-\beta F_{Q\overline{Q}}(r,T)} = \frac{1}{9}e^{-\beta F_1(r,T)} + \frac{8}{9}e^{-\beta F_8(r,T)} \ . \qquad (4.16)$$

Here $r = |\boldsymbol{x} - \boldsymbol{y}|$ and F_1 and F_8 are the color singlet and octet free energies respectively.
In order to understand the meaning of data we are going to parametrize in Sec. (4.3) we now discuss how the above introduced observables are defined on the lattice in Refs. [56, 57, 58, 59].
The link variable

$$U_\mu(x) \in SU(N) \qquad (\mu = 0 \ldots 3) \qquad (4.17)$$

connecting the sites x and $x + a\hat{\mu}$ (a being the lattice spacing) is introduced, whose behavior, under gauge transformations, is given by:

$$U_\mu(x) \to V(x + a\hat{\mu})U_\mu(x)V^\dagger(x) \ . \qquad (4.18)$$

The Polyakov line $W(\boldsymbol{x})$, defined in Eq. (4.5), on the lattice is given by the product of the link variables along the temporal direction:

$$W(\boldsymbol{x}) = \prod_{\tau=1}^{N_\tau} U_0(\boldsymbol{x},\tau) \ , \qquad (4.19)$$

where $U_0(\boldsymbol{x},\tau) \in SU(3)$ from now on. Under a *periodic* gauge transformation it transforms in the following way:

$$W(\boldsymbol{x}) \to V(\boldsymbol{x}, N_\tau + 1)W(\boldsymbol{x})V^\dagger(\boldsymbol{x},1) = V(\boldsymbol{x},1)W(\boldsymbol{x})V^\dagger(\boldsymbol{x},1) \ . \qquad (4.20)$$

The free energy of a heavy quark-antiquark pair in a thermal bath of gluons and N_f light dynamical quarks, in the different color channels, is given by:

$$e^{-\beta F_1(r,T)+C(T)} = \frac{1}{3}\mathrm{Tr}\langle W(\boldsymbol{x})W^\dagger(\boldsymbol{0})\rangle \ , \qquad (4.21a)$$

$$e^{-\beta F_8(r,T)+C(T)} = \frac{1}{8}\langle \mathrm{Tr}W(\boldsymbol{x})\mathrm{Tr}W^\dagger(\boldsymbol{0})\rangle - \frac{1}{24}\mathrm{Tr}\langle W(\boldsymbol{x})W^\dagger(\boldsymbol{0})\rangle \ . \qquad (4.21b)$$

In accord with Eq. (4.13), the color averaged free energy is defined as:

$$e^{-\beta F_{Q\overline{Q}}(r,T)+C(T)} = \frac{1}{9}\langle \mathrm{Tr}W(\boldsymbol{x})\mathrm{Tr}W^\dagger(\mathbf{0})\rangle = \langle L(\boldsymbol{x})L^\dagger(\mathbf{0})\rangle \; . \tag{4.22}$$

One can easily verify that the above definitions are consistent with Eq. (4.16). The constant (with respect to the distance) $C(T)$ appearing in the above equations has been fixed in Refs. [56, 57, 58, 59], for each value of the temperature, by matching at the shortest distance available on the lattice the color singlet free energy with the zero temperature heavy quark potential. In fact for distances $r \ll 1/T$ the physics is not affected by the presence of the thermal bath. Such a normalization unambiguously fixes the long distance behaviour of the free energy at the different temperatures. Note that Eqs. (4.21a) and (4.21b) are not invariant under the gauge transformation (4.20). Hence the definition of the color singlet (octet) free energy requires gauge fixing. In Refs. [56, 57, 58, 59] the calculations were performed in the Coulomb gauge. On the contrary, the color averaged free energy defined in Eq. (4.22) is invariant under gauge transformation.

Since one of the standard parameterizations of the color singlet $Q\overline{Q}$ free energy, at least for what concerns its high temperature - large distance behaviour, is given in terms of an electrostatic screening mass (Debye screening) we briefly recall the arguments given in Ref. [66, 67] which would, at a first glance, suggest such interpretation.
A separation of different momentum scales is usually introduced: hard ($\sim 2\pi T$), soft ($\sim gT$, g being the coupling constant) and ultrasoft ($\sim g^2T$). Within the imaginary time formalism of finite temperature QFT, the propagators of fermionic and non-static bosonic modes are rapidly suppressed, at large distances, by a non vanishing value of the Matsubara frequency which is at least equal to πT, corresponding to a hard scale. Hence the long distance behaviour of hot QCD can be described, in first instance, by an effective field theory referred to in the literature as electrostatic QCD (EQCD) [66, 67]. Its action is expressed in terms of a magnetostatic field $A_i(\boldsymbol{x}) = A_i^a(\boldsymbol{x})t^a$ and an electrostatic field $A_0(\boldsymbol{x}) = A_0^a(\boldsymbol{x})t^a$ and reads

$$S_{\mathrm{EQCD}} = \int d^3x \left[\frac{1}{2}\mathrm{Tr}(G_{ij}G_{ij}) + \mathrm{Tr}(D_iA_0D_iA_0) + m_E^2\mathrm{Tr}(A_0A_0) + \delta\mathcal{L}_{EQCD}\right] \; , \tag{4.23}$$

where

$$G_{ij} = \partial_iA_j - \partial_jA_i + ig_3[A_i, A_j] \; , \tag{4.24a}$$
$$D_iA_0 = \partial_iA_0 + ig_3[A_i, A_0] \tag{4.24b}$$

and $\delta\mathcal{L}_{EQCD}$ contains all the other gauge invariant operators of dimension 2 and higher. For dimensional reasons, the fields in the effective theory are related to the original ones according to $A_i = A_i^{(d=4)}/\sqrt{T}$ and $A_0 = A_0^{(d=4)}/\sqrt{T}$. The parameters g_3 and m_E^2 have to be determined in such a way that the results obtained for the long distance static correlators in hot QCD coincide with the ones calculated in the effective theory. At leading order the matching procedure yields [66, 67]:

$$g_3 = g(T)\sqrt{T}\ , \tag{4.25a}$$

$$m_E^2 = \frac{2N_c + N_f}{6} g^2(T)T^2\ . \tag{4.25b}$$

Hence the mass of the electrostatic field in the effective theory coincides, at the leading order, with the Debye screening mass in the HTL approximation[3] (which accounts for the contribution to the screening mass arising from the hard thermal fluctuations).

In EQCD, where all the fields are static, the definition of the Polyakov line $W(\boldsymbol{x})$ greatly simplifies according to the relation

$$W(\boldsymbol{x}) = \mathrm{P}\exp\left(ig\int_0^\beta d\tau A_0^{(d=4)}(\boldsymbol{x},\tau)\right) \longrightarrow \exp\left(ig\sqrt{\beta}A_0(\boldsymbol{x})\right)\ , \tag{4.26}$$

where in the RHS the path ordering can be omitted. The color singlet free energy of a heavy $Q\overline{Q}$ pair in the effective theory then reads, according to Eq. (4.21a):

$$\begin{aligned} e^{-\beta\Delta F_1(r;T)} &= \frac{1}{N}\mathrm{Tr}\langle\exp\left(ig\sqrt{\beta}A_0(\boldsymbol{x})\right)\exp\left(-ig\sqrt{\beta}A_0(\mathbf{0})\right)\rangle \\ &= 1 + \frac{1}{N}\mathrm{Tr}(t^at^b)\beta g^2\langle A_0^a(\boldsymbol{x})A_0^b(\mathbf{0})\rangle + \dots\ , \end{aligned} \tag{4.27}$$

where $\Delta F_1(r;T) = F_1(r;T) - TC(T)$ and the second line is deduced by expanding the exponentials and exploiting the property $\mathrm{Tr}t^a = 0$. *At the tree level of the effective theory* the non interacting electrostatic propagator reads

$$\langle A_0^a(\boldsymbol{x})A_0^b(\mathbf{0})\rangle^{(0)} = \delta^{ab}\frac{e^{-m_E r}}{4\pi r}\ . \tag{4.28}$$

Hence Eq. (4.27) reduces to

$$\begin{aligned} e^{-\beta\Delta F_1(r;T)} &= 1 + \frac{1}{2N}\delta^{ab}\beta g^2\langle A_0^a(\boldsymbol{x})A_0^b(\mathbf{0})\rangle^{(0)} + \dots \\ &= 1 + \frac{N^2-1}{2N}\beta g^2\frac{e^{-m_E r}}{4\pi r} + \dots\ , \end{aligned} \tag{4.29}$$

[3]Indeed the HTL result for the Debye mass coincides with the full one-loop perturbative calculation.

which leads to the following result for the leading order expression of the color singlet free energy

$$\Delta F_1^{(0)}(r,T) = -\frac{N^2-1}{2N} \cdot \frac{g^2}{4\pi} \cdot \frac{e^{-m_E r}}{r} \ , \tag{4.30}$$

where both the coupling and the electrostatic mass depend on the temperature.
Hence, apart from an overall additive constant which depends solely on the temperature, the large distance behaviour of the free energy, in the high temperature and weak coupling regime, reduces to a Coulomb screened (Yukawa-like) form.

4.3 Parameterization of the lattice data

In this section we provide a unified parameterization of the lattice data for the *color singlet $Q\bar{Q}$ free energy* F_1 in the case of quenched [56], 2-flavor [59] and 3-flavor [65] QCD. The lattice findings are shown (in dimensionless units) in Fig. 4.1.

For what concerns the critical temperature we assume the values $T_c = 270$ MeV ($N_f = 0$), $T_c = 202$ MeV ($N_f = 2$) and $T_c = 193$ MeV ($N_f = 3$) given in Ref. [59].

As discussed above the free energy on the lattice is defined up to an additive normalization constant, which has to be fixed using some physical constraint. In Refs. [56, 59, 65] it has been normalized to match, at the shortest available distance for each temperature, the $T = 0$ heavy quark potential. Such a normalization amounts to make the (reasonable) assumption that thermal effects become negligible at very short distances.

In Refs. [56, 59] the zero temperature heavy quark potential has been determined through a best fit procedure of the available $T = 0$ lattice data with a Cornell-like parameterization[4]:

$$\frac{V(r)}{\sqrt{\sigma}} = -\frac{4}{3}\frac{\alpha}{r\sqrt{\sigma}} + \sqrt{\sigma}r, \tag{4.31}$$

σ representing the *string tension*. The values $\alpha = 0.195(1)$ for the case $N_f = 0$ and $\alpha = 0.212(3)$ for the case $N_f = 2$ are given in Ref. [59], where the value $\sqrt{\sigma} = 420$ MeV is employed to translate the lattice results into physical units.

[4]Note that the $1/r$ term accounts for two different physical processes: the perturbative one-gluon-exchange at short distances and the transverse string fluctuations at large distances.

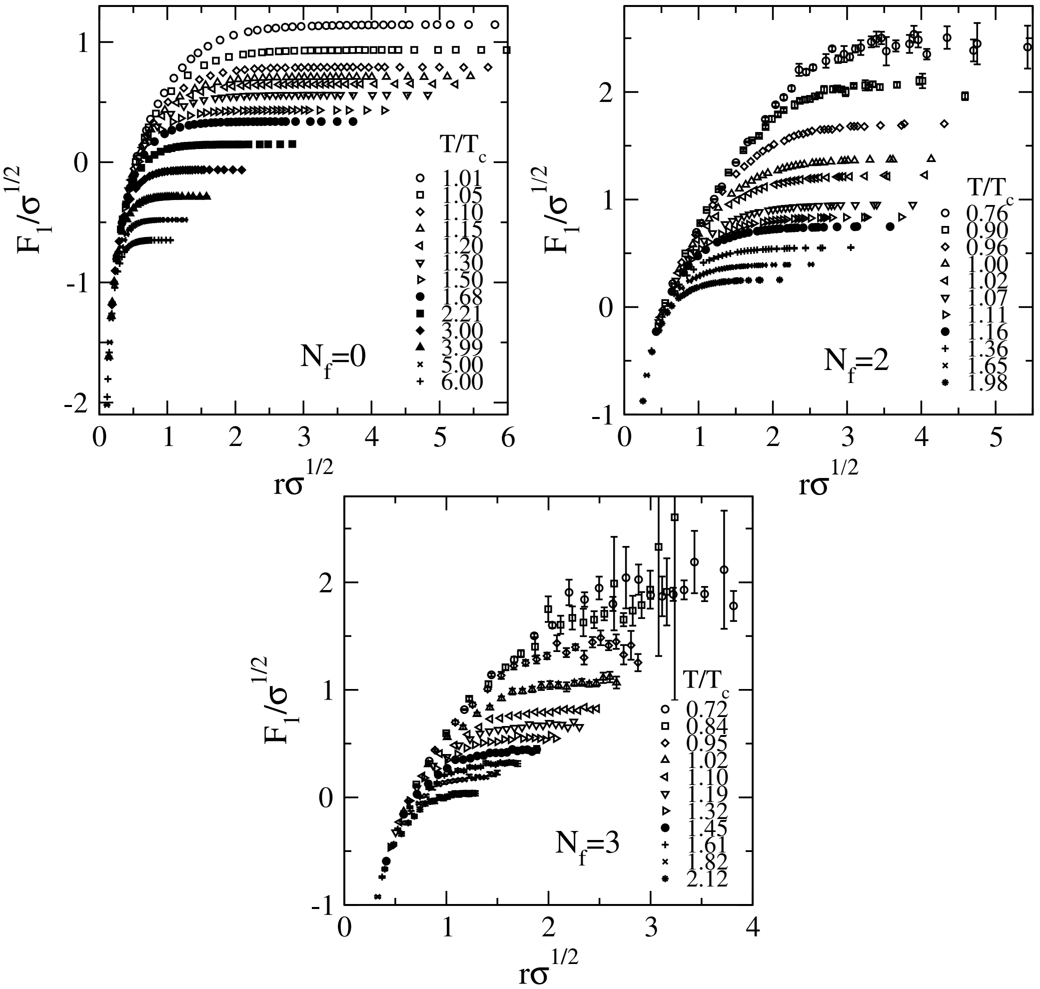

Figure 4.1: A sample of the available data for $F_1(r,T)/\sqrt{\sigma}$ at different values of T/T_c as a function of the separation $r\sqrt{\sigma}$ of the $Q\bar{Q}$ sources. Data are taken from Ref. [56] ($N_f = 0$), Ref. [59] ($N_f = 2$) and Ref. [65] ($N_f = 3$). Dimensionless units are employed, with $\sqrt{\sigma} = 420$ MeV ($N_f = 0$ and $N_f = 2$) and $\sqrt{\sigma} = 460$ MeV ($N_f = 3$).

In Ref. [65] a similar parameterization (Cornell potential plus a $1/r^2$ term to mimic the effects of asymptotic freedom at the shortest distances reachable on the lattice) is employed for the case $N_f = 3$. Note that in that work the free energy is provided directly in physical units: however, for the sake of comparison, we show it in dimensionless units, using for the string tension the value $\sqrt{\sigma} = 460$ MeV extracted from the parameterization of the $T = 0$ potential given in Ref. [65].

In past calculations [48, 49, 60, 61] the free energy has been often identified with the heavy quark potential and inserted directly into the Schrödinger equation. However, a better candidate for a more appropriate finite temperature potential is given by the internal energy of the $Q\bar{Q}$ system, defined by the well known relation

$$F = U - TS, \tag{4.32}$$

where

$$U = -T^2 \frac{\partial(F/T)}{\partial T} \tag{4.33}$$

is the internal energy and

$$S = -\frac{\partial F}{\partial T} \tag{4.34}$$

is the entropy. One can see from the data in Fig. 4.1 that the role played by the entropy is more relevant at large distances.

Getting the internal energy from the free energy involves a derivative of the latter with respect to the temperature: it is thus clear that one needs an accurate parameterization of the temperature dependence of F.

In order to establish a suitable form for this parameterization of the lattice data, we first consider the two limits in which the underlying physics is supposed to be known.

At very short distances ($r \ll 1/T$) thermal effects are negligible and the colour singlet free energy is dominated by the perturbative one-gluon exchange with the typical behaviour:

$$F_1(r,T) \underset{rT\ll 1}{\sim} -\frac{4}{3}\frac{\alpha(r)}{r}, \tag{4.35}$$

the coupling α depending only upon the $Q\bar{Q}$ separation.

On the other hand, for $T \gg T_c$, the large distances ($r \gg 1/T$) behaviour of the free energy is expected to be dominated by the exchange of a resummed electrostatic gluon leading to the expression [66]:

$$F_1(r,T) \underset{rT\gg 1}{\sim} -\frac{4}{3}\frac{\alpha(T)}{r} e^{-m_D(T)r} + F_1(r=\infty,T). \tag{4.36}$$

In this limit, the coupling α is a function of the temperature and $m_D(T)$ is the Debye screening mass arising from the dressing of the electrostatic gluon.

In the two above limits, the running of the coupling is determined by a Renormalization Group Equation (RGE), allowing to express $\alpha = g^2/4\pi$ as a known (at least in the weak coupling regime) function of an energy scale μ. In the short distance limit the relevant energy scale is given by the inverse of the distance ($\mu \sim 1/r$), while for large separations the major role in setting the scale is expected to be played by the temperature ($\mu \sim T$).

Actually, in order to solve the Schrödinger equation for heavy quarkonia, one really needs a parameterization of the free energy covering the whole range of distances. For this purpose, on the basis of Eqs. (4.35) and (4.36) it appears convenient to cast the dependence of F_1 on r and T into the following functional form[5]:

$$F_1(r,T) = -\frac{4}{3}\frac{\alpha(r,T)}{r}e^{-M(T)r} + C(T). \tag{4.37}$$

In order to recover from the above the short and large distance limits given by Eqs. (4.35) and (4.36) one can, e.g., assume α to depend on the following combination of r and T:

$$\alpha(r,T) = \alpha(\mu = c_r/r + c_t T), \tag{4.38}$$

where $\alpha(\mu)$ is obtained by solving the RGE, while c_r and c_t are numerical coefficients to be fixed through a best fit of the data.

If supported by the data, Eq. (4.38) would allow to interpolate between the short distance regime ($r \ll 1/T$), where $\mu \sim 1/r$, and the long distance one ($r \gg 1/T$), where on the contrary $\mu \sim T$.

Now we describe in detail the fitting procedure employed. The data for the colour singlet free energy, taken from Ref. [56] ($N_f = 0$), Ref. [59] ($N_f = 2$) and Ref. [65] ($N_f = 3$), are displayed in Fig. 4.1 in dimensionless units, namely $y = F_1/\sqrt{\sigma}$ and $x = r\sqrt{\sigma}$, for different values of the temperature both below and above T_c. For each value of $T > T_c$ the data have been parameterized with the following (four parameter) fitting function:

$$y = -\frac{4}{3}\frac{\alpha(\tilde{\mu})}{x}e^{-a_3 x} + a_0 \qquad \text{with} \qquad \tilde{\mu} = \frac{a_1}{x} + a_2 \tag{4.39}$$

where for $\alpha(\tilde{\mu})$ we use the RGE result obtained with the two-loop QCD beta-function quoted in Appendix A, the dimensionless variable $\tilde{\mu}$ being identified with the ratio $\mu/\Lambda_{\mathrm{QCD}}$.

The fitting procedure yields a very mild dependence on T for the parameters a_1 and a_2. Actually, on the basis of the above discussion, one would have expected the coefficient a_2 to scale linearly with the temperature, but this finding might just signal that the range of temperatures spanned here is still not in the asymptotic regime $T \gg T_c$. On the other hand, a constant

[5]Note that the mass $M(T)$ appearing in this exponential will not necessarily coincide with the Debye screening mass of Eq. (4.36), the latter being determined by fitting only the large distance data.

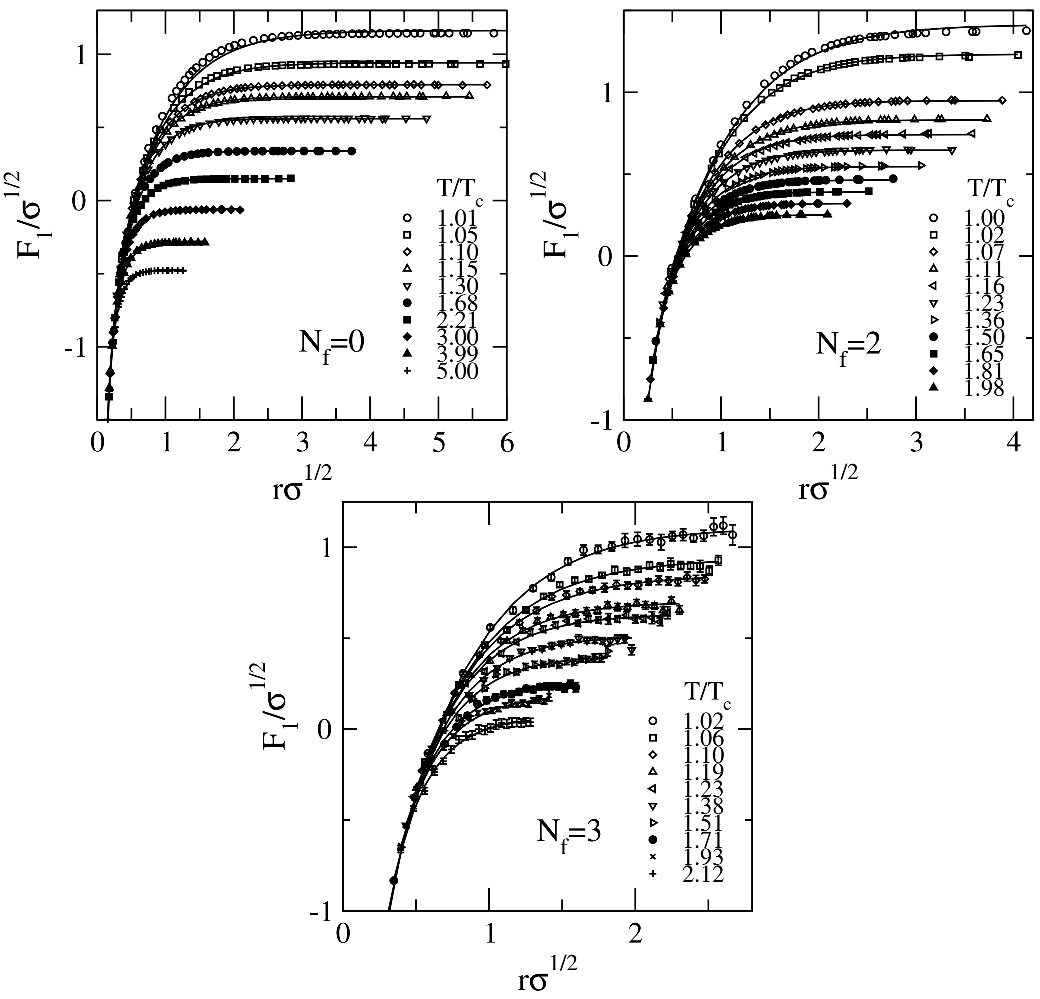

Figure 4.2: The colour singlet free energy resulting from our fitting procedure compared to the lattice data at different temperatures above T_c.

value for a_1 is in agreement with the ansatz of Eq. (4.38). This has suggested the following procedure: a weighted average of the values obtained for a_1 has been performed, yielding $a_1 = 0.2719(2)$ for $N_f = 0$, $a_1 = 0.2687(7)$ for $N_f = 2$ and $a_1 = 0.2354(17)$ for $N_f = 3$. We have then fitted again the data keeping a_1 fixed and using only a_0, a_2 and a_3 as free parameters. This parameterization works well — yielding values of χ^2 per degree of freedom of the order of 1 at all the temperatures — and it is compared to the data in Fig. 4.2.

The finite temperature lattice data are limited to distances $r > 0.1 \div 0.2$ fm. Since the data here examined have been normalized assuming that at

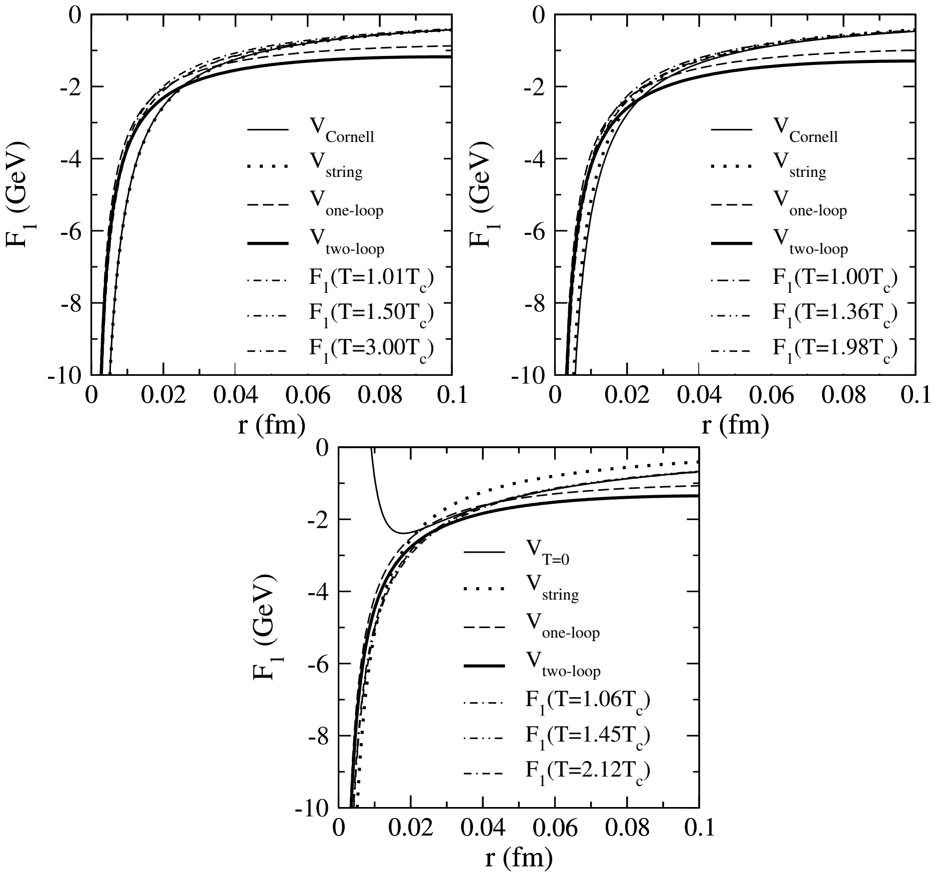

Figure 4.3: The short distance behaviour of the colour singlet free energy resulting from our fits for different values of T/T_c. For each value of N_f three different temperatures among the available ones, covering the range of experimental interest, have been chosen. The dependence on the temperature turns out to be very small at such short distances. We also display for comparison the $T = 0$ potentials given by different schemes: the potentials employed to normalize the data at short distance [59, 65], the potential obtained in the Nambu string model and the one and two-loop short distance perturbative potentials [68, 69, 70].

short distances thermal effects are negligible, one should check that the above parameterization does not introduce any sizable (and spurious) temperature dependence for small values of r, remaining in this region close to the $T = 0$ perturbative potential (we remind that at $T = 0$ free energy and internal energy coincide). In this respect our choice of refitting the data keeping the coefficient a_1 fixed fulfills this requirement.

The behaviour of the parameterization of the free energy for $r < 0.1$ fm is displayed, at three different temperatures, in Fig. 4.3 where one indeed sees that spurious short distance thermal effects appear negligible. It is gratifying (and somewhat surprising) that the curves seem to interpolate smoothly between the $T = 0$ Cornell potential and the short distance perturbative potential. The Cornell curve reported in the figure is the one employed in Ref. [59] to fix the normalization of the free energy at the different temperatures. As already discussed at the beginning of this section it was obtained by fitting zero temperature lattice data which cover distances $r > 0.05$ fm. Of course for shorter distances the Cornell parameterization cannot account for running coupling effects (asymptotic freedom) and the perturbative calculation [68, 69, 70] should provide more reliable results. More details on the one- and two-loop perturbative potential used in Fig. 4.3 are given in Appendix A.

The curves V_{string} reported in Fig. 4.3 refer to the $Q\overline{Q}$ potential

$$V(r) = -\frac{\pi}{12}\frac{1}{r} + \sigma r \tag{4.40}$$

obtained in the Nambu string model, the term $1/r$ arising from the quantum fluctuations of the flux tube in the transverse directions.

As a next step we have provided a parameterization of the T-dependence of a_0, a_2 and a_3, which allows one to analytically perform the derivative of F_1 with respect to the temperature (actually, for the calculation of the $Q\bar{Q}$ binding energies the knowledge of a_0 is unnecessary: this contribution to the potential is shown for completeness). Lacking compelling physical hints to the form of the T-dependence, we have sought for the simplest and smoothest expressions yielding a satisfactory interpolation of the values calculated from the fit to the lattice data (see Appendix B for details). The parameters and their interpolations are displayed in Fig. 4.4.

The value of $a_0(T)$ at each temperature is essentially fixed by the normalization of the data, which has been determined using similar procedures in all the lattice calculations. Notably this parameter, once plotted as a function of T/T_c, turns out to be fairly close for all values of N_f. On the contrary, the remaining two parameters display some quantitative flavor dependence, but within the same qualitative pattern. An exception to this behavior is represented by $a_2(T)$ for $N_f = 3$, although one should note that the three-flavor case is the one where the parameterization (4.39) has the largest uncertainties. Moreover, the variation of $a_2(T)$ with T is actually magnified by the scale of the figure, being generally around 20% for the range of temperatures considered here. As one will see in the following the resulting effective potential is rather robust with respect to these variations.

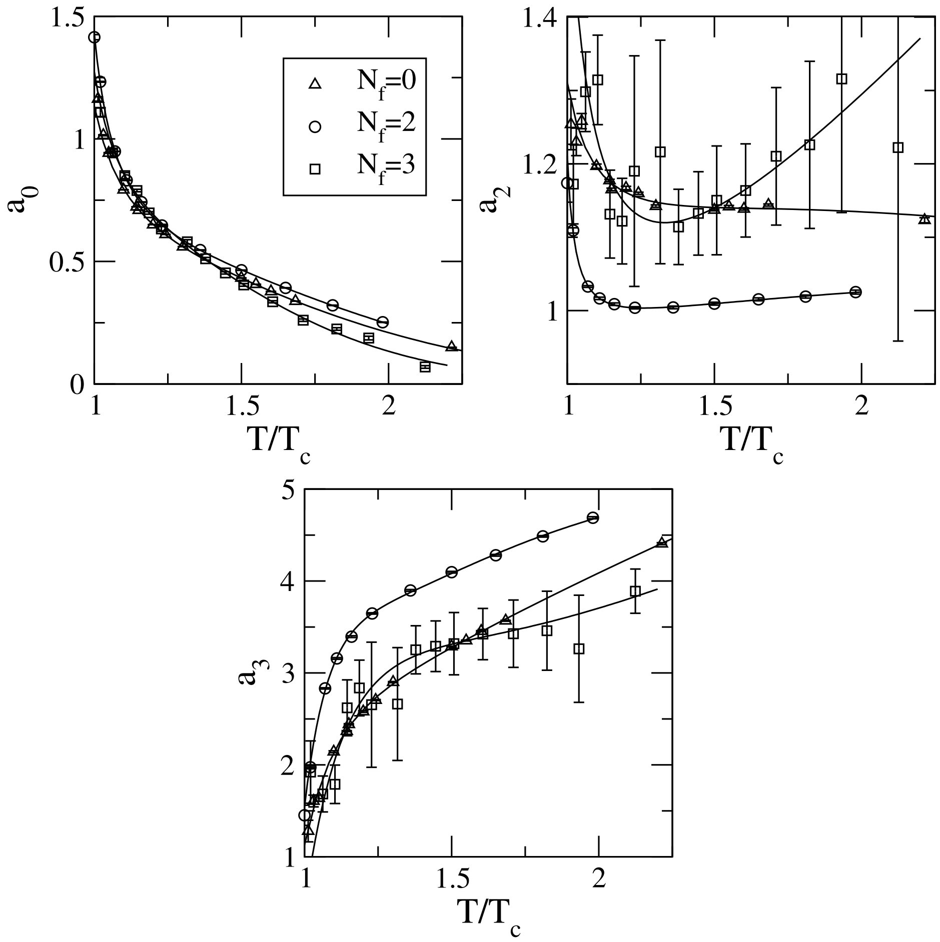

Figure 4.4: Temperature dependence of the parameters a_0, a_2 and a_3 employed in fitting the color singlet free energy with Eq. (4.39). The solid lines are interpolating functions.

Note also that the strongest variation of the parameters with the temperature is confined around values of T very close to T_c. Since extracting the internal energy from F_1 involves a derivative with respect to T, this is the temperature domain where the sensitivity to the details of the parameterization might be high. For this reason we felt it safer to use the resulting potentials at temperatures larger than T_c, say for $T > 1.05T_c$, where they turn out to be stable with respect to changes in the parameterization.

Finally, we recall that the quenched QCD data [56] are actually available also at temperatures much larger than those for the unquenched cases: here we limit our analysis up to about twice the critical temperature, since this is the range where lattice calculations with two and three flavors are available and, moreover, since this is the range of interest for the problem of the J/ψ dissociation. Here we just remark that an analysis of the $N_f = 0$ data at larger temperatures (till $T \sim 5T_c$) with the parameterization of Eq. (4.39) shows that the fitting parameters maintain, also at these high temperatures, the trend displayed in Fig. 4.4.

4.4 $Q\overline{Q}$ bound states in a quark-gluon plasma

The $Q\bar{Q}$ free energy obtained in lattice calculations has been used in the past as an input for the $Q\bar{Q}$ potential energy in the non-relativistic Schrödinger equation [48, 49, 60, 61]. More recently [56, 62, 63] it has been recognized that the $Q\bar{Q}$ potential energy can be more appropriately identified with the $Q\bar{Q}$ internal energy (see Eq. (4.33))[6].

Once the temperature dependence of the color-singlet free energy F_1 has been parameterized, the corresponding color-singlet internal energy U_1 is easily obtained and one can define an effective potential

$$V_1(r,T) = U_1(r,T) - U_1(r \to \infty, T) \tag{4.41}$$

to be used in the Schrödinger equation

$$\left[-\frac{\nabla^2}{2\mu} + V_1(r,T)\right]\psi(\mathbf{r},T) = \varepsilon(T)\psi(\mathbf{r},T), \tag{4.42}$$

where μ is the reduced mass of the $Q\bar{Q}$ system.

In Fig. 4.5 we display, at two different temperatures, the effective $Q\bar{Q}$ potentials that we have obtained by using the parameterizations discussed in the previous section. At high temperature the form of V_1 is the one typical of a screened Coulomb potential, the $N_f = 3$ potential providing a stronger attraction; at temperatures close to T_c the shape of V_1 appears somewhat distorted because of the strong temperature dependence of the coefficients a_2 and a_3 (see Fig. 4.4), the $N_f = 3$ potential being still more attractive. Remarkably, the behaviour of the color singlet potential energies obtained with our procedure appears qualitatively in agreement with the one given in Refs. [57, 71], where the internal energy has been directly calculated on the lattice for $N_f = 0$ and $N_f = 2$, respectively.

[6] Actually, the author of Ref. [62] tries to disentangle, in the total internal energy $U_1(r,T)$, the gluon and the $Q\overline{Q}$ contributions. This leads to a lower value for the J/ψ dissociation temperature with respect to the result $T_d \sim 2T_c$ obtained with the full internal energy.

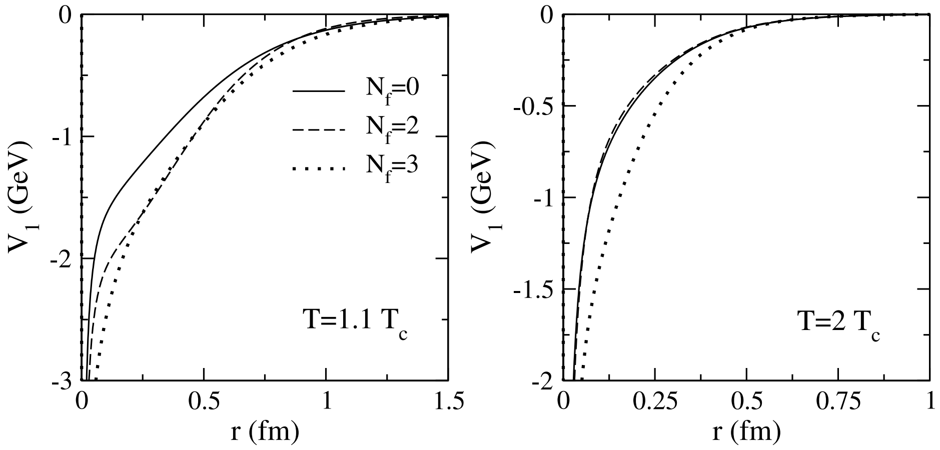

Figure 4.5: The effective $Q\bar{Q}$ potentials extracted from the unquenched and quenched lattice calculations at two different temperatures.

We now employ the effective potential previously derived for the study of the charmonium and bottomonium spectroscopy above the critical temperature.

For what concerns the charmonium states we plot the values of the binding energies (Fig. 4.6) and of the mean square radii (Fig. 4.7) of the different bound state solutions of Eq. (4.42) as functions of T/T_c. For the sake of comparison the results obtained for a different number of dynamical fermions ($N_f = 0, 2, 3$) are plotted in the same panel.

In our analysis we have chosen $m_c = 1.3$ GeV for the charm quark mass; however, we have also studied the sensitivity of our results to variations of m_c in the range given in the Particle Data Group (PDG) listings [72], namely 1.15 GeV$< m_c <$1.35 GeV. For reference, in Fig. 4.7 the arrows point to the $T = 0$ mean square radii obtained in a potential model calculation [73]. Note that potential models at $T = 0$ typically follow a different philosophy: they fix the quark mass and the confining potential parameters to reproduce the mass of the lowest states, whereas here the potential is provided by lattice calculations and the quark mass is the running mass in the $\overline{MS}$ scheme.

The $1P$ and $2S$ states turn out to melt at temperatures $1.1T_c < T_d < 1.15T_c$. On the contrary the J/ψ stays bound up to temperatures $1.7T_c < T_d < 2.3T_c$, the precise limits depending upon N_f. The lower bound ($T_d \sim 1.7T_c$) refers to the quenched case and appears in striking agreement with the limiting value obtained in Ref. [29] through the study of the J/ψ and η_c spectral functions.

Note that the free energy measured on the lattice provides a spin averaged

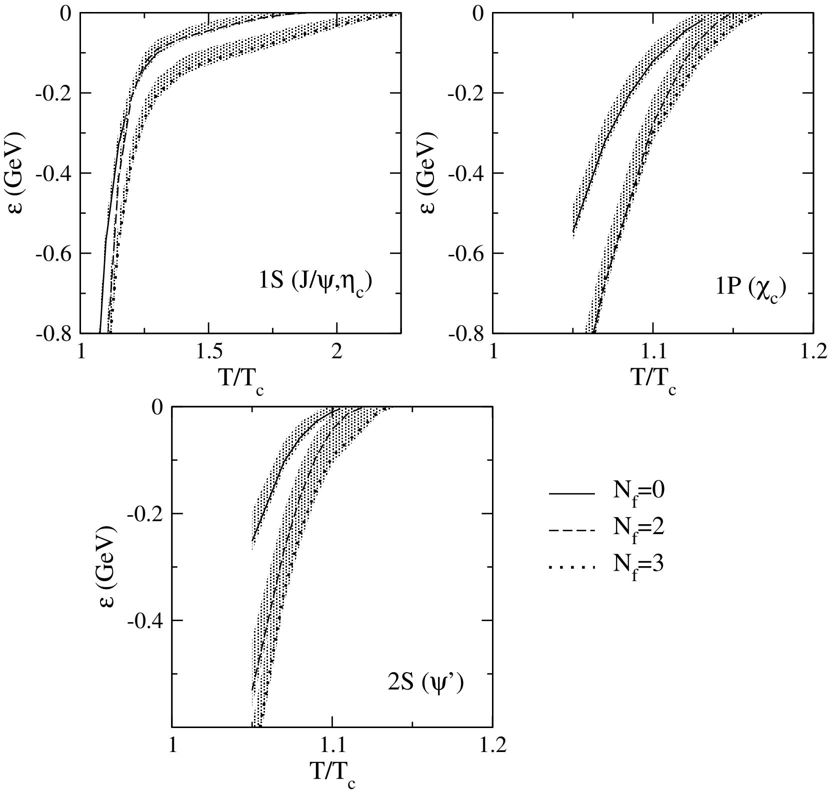

Figure 4.6: Binding energy of charmonium states above the deconfinement temperature. The lines show the results for $m_c = 1.3$ GeV; the grey areas around the lines display the variations for 1.15 GeV< m_c <1.35 GeV.

result of the singlet and triplet channels: hence, in Figs. 4.6 and 4.7 the J/ψ and η_c mesons appear degenerate. This degeneracy is expected to be removed by a short range spin-spin force, whose effect, at $T = 0$, is often treated perturbatively assuming a contact interaction of the type [74]:

$$H_{ss} = \frac{8\pi}{9}\frac{\alpha_s(\mu)}{m_q m_{\bar{q}}}\boldsymbol{\sigma}_q \cdot \boldsymbol{\sigma}_{\bar{q}}\delta(\mathbf{r}). \tag{4.43}$$

Again, the short range nature of this force makes it plausible the assumption that it is not affected by thermal effects and that it can be employed also at finite temperatures. Then, for the J/ψ and η_c energy shifts one gets:

$$\Delta E_{J/\psi} = \frac{8\pi}{9}\frac{\alpha_s(\mu)}{m_c m_{\bar{c}}}|\psi(0,T)|^2 \tag{4.44a}$$

$$\Delta E_{\eta_c} = -\frac{24\pi}{9}\frac{\alpha_s(\mu)}{m_c m_{\bar{c}}}|\psi(0,T)|^2, \tag{4.44b}$$

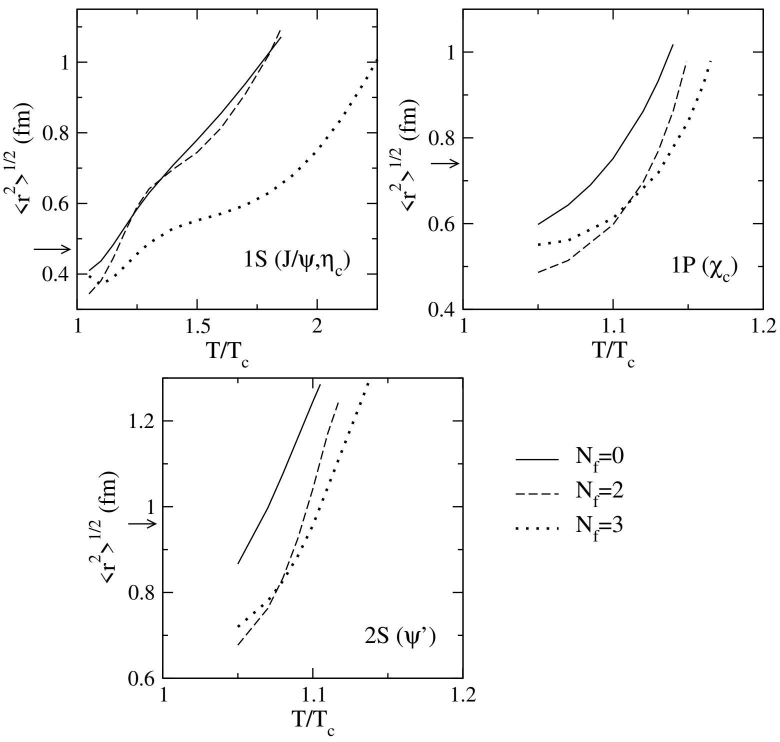

Figure 4.7: Mean square radii of the charmonium states above the deconfinement temperature. The arrows point to the $T = 0$ results of Ref.[73]. The curves stop where the system is no longer bound.

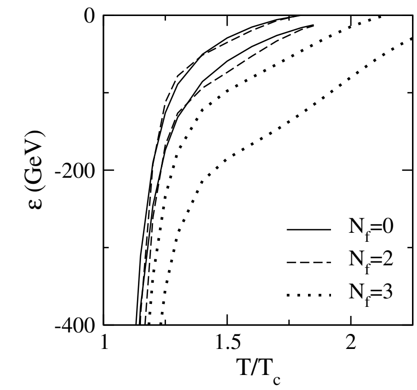

Figure 4.8: Binding energy of the $1S$, $J = 1$ (J/ψ, upper lines) and $1S$, $J = 0$ (η_c, lower lines) states above the deconfinement temperature; $m_c = 1.3$ GeV.

where for $\alpha_s(\mu)$ we have used the two-loop expression of Eq. (A.5), evaluated at $\mu = m_c$. As one can see, the temperature dependence of this term stems entirely from the value of the $c\bar{c}$ wave function at the origin.

We display in Fig. 4.8 the binding energies of the J/ψ and η_c mesons above the deconfinement temperature. The spin-spin contribution gives rise to a mild reduction of the dissociation temperature, without altering the qualitative features of the results. For instance, for $N_f = 2$ at $T = 1.05T_c$ one gets a $J/\psi - \eta_c$ splitting of 145 MeV (the experimental value at $T = 0$ is about 117 MeV), whereas at the J/ψ melting temperature, $T \cong 1.8T_c$, one gets a splitting of 13 MeV (although, strictly speaking, in this case the perturbative expansion is no longer justified).

In Figs. 4.9 and 4.10 we plot the binding energies and the mean square radii of the bottomonium bound states above T_c. We have chosen $m_b =$ 4.3 GeV for the bottom quark mass, but again we have studied the sensitivity to variations of m_b in the range of the PDG listings, 4.1 GeV$< m_b <$4.4 GeV. The arrows in Fig. 4.10 point to the results of $T = 0$ potential model calculations [73]. Of course, for heavier quark masses more states than in the charmonium case survive above the deconfinement temperature.

In Fig. (4.11) we display the behaviour of the mass of the $1S$ charmonium and bottomonium states as a function of the temperature given by the formula:

$$M(T) = 2m_{c(b)} + \epsilon(T) + U_1(r \to \infty, T) \ .$$

We can finally summarize our results for the dissociation temperatures of the different quarkonium states:

	$T_d/T_c\,(N_f = 0)$	$T_d/T_c\,(N_f = 2)$	$T_d/T_c\,(N_f = 3)$
J/Ψ	1.75-1.95	1.78-1.92	2.15-2.35
χ_c	1.13-1.15	1.14-1.15	1.15-1.17
Ψ'	1.10-1.11	1.11-1.12	1.12-1.14
$\Upsilon(1S)$	4.4-4.7	6.4-6.8	4.1-4.3
χ_b	1.55-1.61	1.60-1.65	1.90-1.98
$\Upsilon(2S)$	1.40-1.45	1.38-1.46	1.62-1.72
$\Upsilon(1D)$	1.19-1.20	1.19-1.20	1.23-1.24
χ_b'	1.17-1.18	1.18-1.19	1.20-1.21
$\Upsilon(3S)$	1.14-1.15	1.14-1.15	1.17-1.18

We also quote, for comparison, the results for the charmonium melting temperatures obtained in Ref. [49], where the $Q\overline{Q}$ free energy was directly employed as an effective potential:

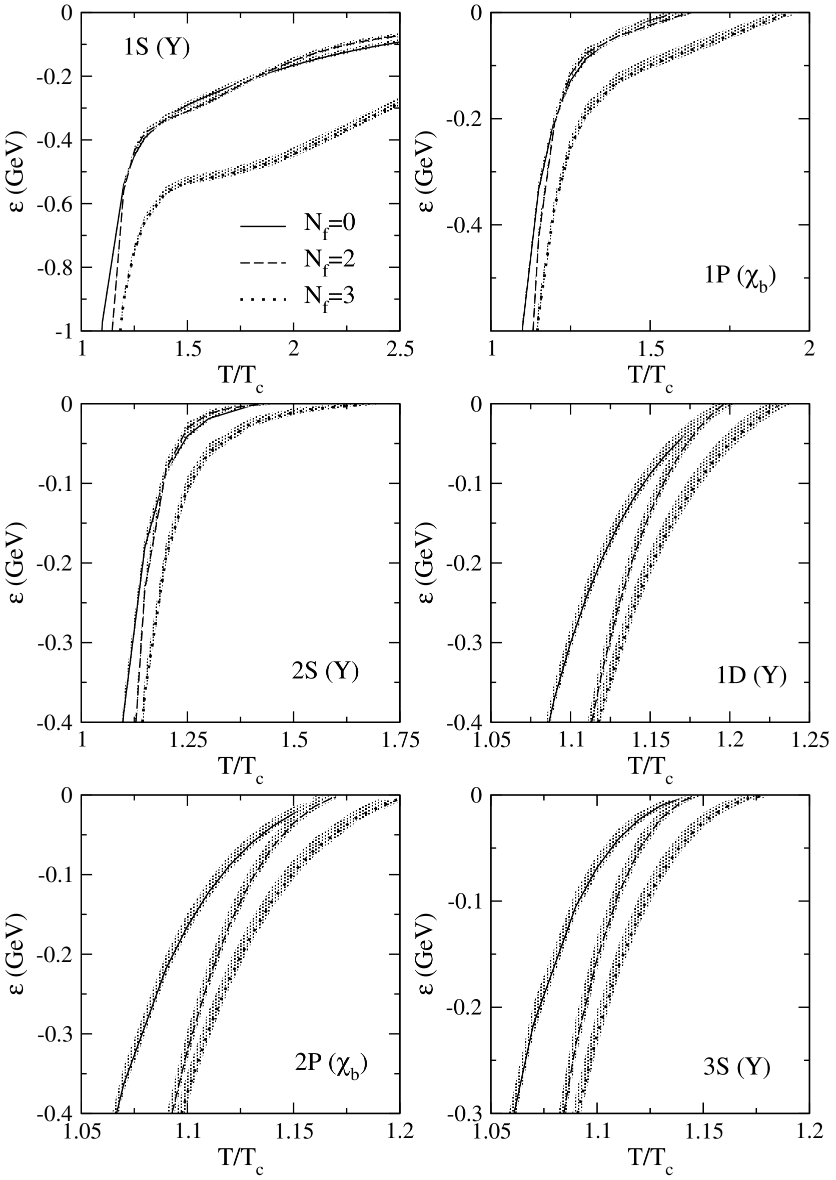

Figure 4.9: Binding energy of the bottomonium states above the deconfinement temperature. The lines show the results for $m_b = 4.3$ GeV; the grey areas around the lines display the variations for 4.1 GeV$< m_b <$4.4 GeV.

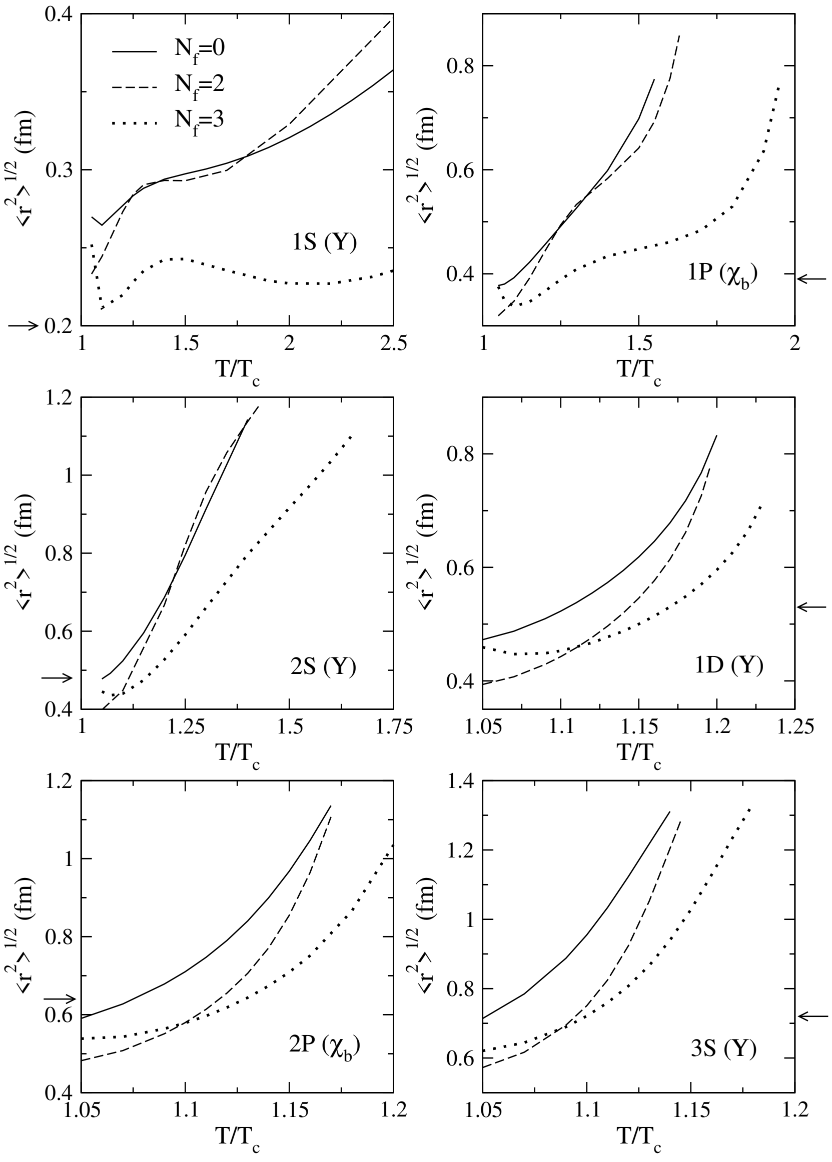

Figure 4.10: Mean square radii of the bottomonium states above the deconfinement temperature. The arrows point to the $T = 0$ results of Ref.[73]. The curves stop where the system is no longer bound.

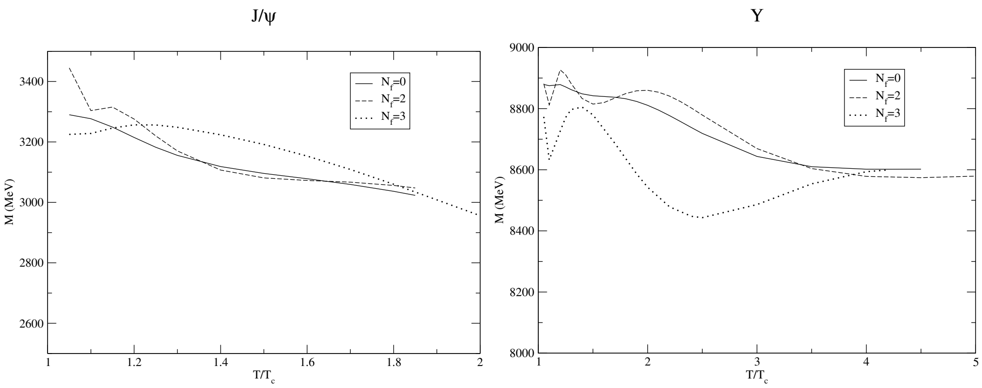

Figure 4.11: The mass of the $1S$ charmonium and bottomonium states (J/Ψ and Υ) as a function of the temperature for different numbers of dynamical fermions.

	J/Ψ	$\chi_c(1P)$	$\Psi'(2S)$
T_d/T_c	1.10	0.74	0.1-0.2

As it can be seen the two approaches lead to completely different suppression patterns, to be tested with the experiment.

Both for the charmonium and for the bottomonium states the binding energy gets smaller and the mean square radius gets larger as the temperature grows. This should reflect into a huge increase of the elastic cross section $\sigma(Q\bar{Q} \to Q\bar{Q})$ at low energy. In fact, for a small relative momentum k of the two particles, when in the partial wave expansion the contribution of the s-wave is dominant, the presence of a $l = 0$ state near zero binding energy leads to a dramatic increase of the cross section as $k \to 0$, according to the formula:

$$\sigma_{l=0} \underset{k\to 0}{\sim} \frac{4\pi}{k^2 + 2\mu|\epsilon|}, \tag{4.45}$$

where μ is reduced mass of the system and ϵ the energy of the state near zero binding, no matter whether it is positive (virtual level) or negative (bound state). If something analogous happened also for the heavy-light states (for which lattice data, however, are not available yet) this would clearly accelerate the thermalization of the heavy quarks.

From Figs. 4.5, 4.6 and 4.9 the effective potential obtained with $N_f = 3$ appears more attractive. Indeed the critical temperature T_c in the three cases $N_f = 0, 2, 3$ assumes different values, hence a naive comparison might not be so meaningful. Furthermore the finite temperature $N_f = 3$ lattice data so far available are affected by larger errors, so that our parameterization presents larger uncertainties with respect to the other two cases.

4.5 Experimental results

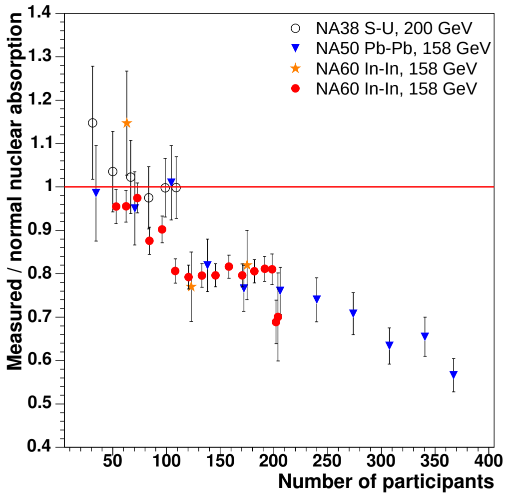

Figure 4.12: The J/Ψ multiplicity (normalized to the expected one in a normal nuclear matter absorption scenario) measured by the NA50 and NA60 collaboration as a function of the number of participants [78].

In order to understand the experimental results for the J/Ψ yields obtained in the high nucleus-nucleus collisions some preliminary considerations on the charmonium production and absorption mechanisms have to be done [75, 76].

The dominant charmonium production mechanism in hadron-hadron collisions is given by gluon fusion to form a $c\bar{c}$ pair. Due to the large value of the charm quark mass such a process occurs almost istantaneously with a formation time of order $\tau_c \approx (2m_c)^{-1} \approx 0.07$fm.

The $c\bar{c}$ pair is in general in a color-octet state. In order to neutralize its color turning into a color-singlet state, it has to emit a gluon. The time required by such a process to occur can be estimated through virtuality arguments and is found to be $\tau_8 \approx 0.3$fm in the $c\bar{c}$ rest frame. Hence in the Lab frame this pair, if produced with sufficiently high momentum, can travel quite a long distance, of order $d_8 \approx \tau_8(P_{\rm Lab}/2m_c)$, $P_{\rm Lab}$ being the $c\bar{c}$ spatial momentum in the Lab frame. If during this time this *pre-resonant state* finds to cross a dense system like nuclear matter, inelastic processes may suppress the formation of any charmonium state (J/Ψ, Ψ', χ_c...) on the same footing. A further amount of time is then required by the singlet state to get its vacuum properties, during which nuclear absorption can occur too.

The above described process is known as (normal nuclear matter) *pre-resonance absorbtion* and represents the typical phenomenon occurring in a proton-nucleus (p-A) collision. It leads to a depletion of the J/Ψ multiplicity in p-A collisions with respect to the p-p case which can be quantified through the introduction of the J/Ψ *survival probability*

$$S_{pA} \equiv \sigma_{pA}/A\sigma_{pp} \;, \tag{4.46}$$

representing the probability that a produced J/Ψ survives nuclear matter absorption.

The above quantity is experimentally measured and the process is described within a Glauber approach which allows to extract the *effective* absorption cross sections of the different charmonium states. The most recent analysis gives [77]:

$$\sigma^{\rm abs}_{J/\Psi} = 4.6 \pm 0.8 \text{mb} \qquad \sigma^{\rm abs}_{\Psi'} = 7.7 \pm 1.1 \text{mb} \;.$$

From these findings it appears that the formation times of the different charmonium states are small enough to allow nuclear matter to distinguish between the more loosely bound Ψ', suffering a stronger absorption, and the deeply bound J/Ψ with a smaller inelastic cross section.

In a high energy nucleus nucleus (A-B) collision, on top of the above process, if a deconfined medium is produced, also suppression due to color-screening in the QGP can occur. Hence , in order to use the J/Ψ suppression as a signature of the onset of deconfinement, one has to be able to disentangle the two suppression mechanisms. This analysis has been done by the NA50 and NA60 collaborations [78] and we shall comment on their findings in the light of our results concerning the melting temperature of the different charmonium states.

In Fig. (4.12) the number of measured J/Ψ has been plotted as a function of the number of participants[7] (nucleons) in the collisions (which can be easily measured through a Zero Degree Calorimeter), normalized to the expected multiplicity in the case of normal nuclear matter absorption as the only source of suppression. A value below 1 signals then QGP absoption.

In Fig. (4.12) one can see that, for small numbers of participants normal nuclear matter absorption is sufficient to explain the observed J/Ψ suppression. For larger numbers of participants the ratio sharply drops signaling the

[7]Clearly, larger numbers of participants correspond to higher energy densities.

onset of *anomalous suppression.* In any case one can see that, even for the largest values of $N_{\rm part}$ reached in Pb-Pb collisions, still about 60% of the expected (in the case of no QGP absorption) J/Ψ are detected. This appears compatible with a scenario, supported by our findings, in which the anomalous J/Ψ suppression arises only from the melting of excited charmonium states (Ψ' and χ_c) which, in a normal hadron-hadron collision, contribute about 40% of the observed yields.

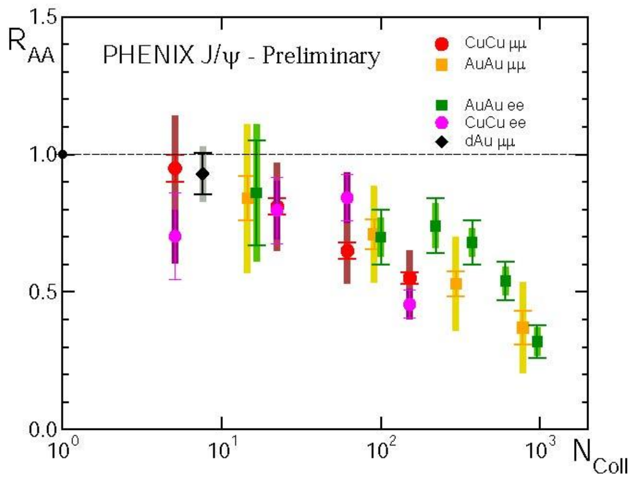

Figure 4.13: The nuclear modification factor R_{AA} for the J/Ψ meson measured at RHIC [79].

For what concerns RHIC results in Fig. (4.13) we plot the nuclear modification factor

$$R_{AA} \equiv \frac{dN/dy(AA)}{N_{\rm coll} dN/dy(pp)} \tag{4.47}$$

measured by the PHENIX collaboration [79]. Since $c\bar{c}$ production is a *hard process* which scales with the number of binary collisions $N_{\rm coll}$, a value $R_{AA} <$ 1 signals medium absorption. Indeed the consideration of this quantity alone does not allow to distinguish between nuclear matter and QGP suppression. An analysis similar to the one performed for the NA50 and NA60 data should be carried on.

This has been very recently attempted in Refs. [80, 81] where the J/Ψ survival probability (normalized to the normal nuclear absorption scenario) was studied, collecting all the available experimental data from SPS and RHIC. We quote their findings in Fig. 4.14. The above analysis seems to support a picture in which the direct J/Ψ survive up to very high energy density, the anomalous suppression being due only to the melting of the higher resonances. This appears to agree with our results.

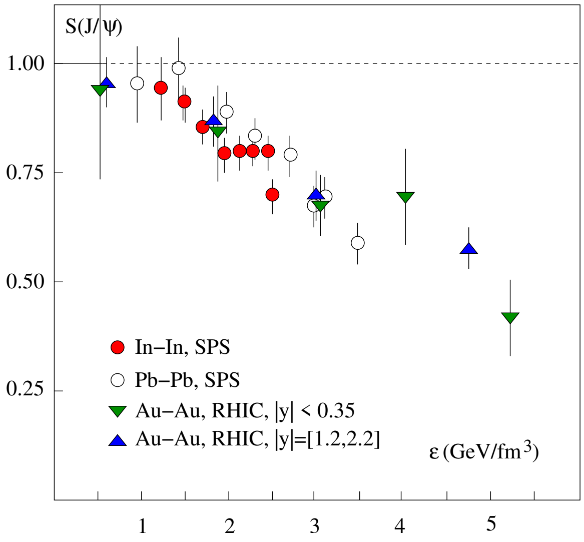

Figure 4.14: The J/Ψ suppression pattern as a function of the energy density.

4.6 Conclusions

The picture of the deconfined phase of QCD for values of the temperature slightly exceeding T_c — that is the ones accessible in the heavy-ion experiments presently performed at RHIC — has substantially evolved in the last few years.

For large values of the temperature ($T > 3T_c$) a description of the QGP in terms of a gas of weakly interacting quasiparticles [82] appears reliable (even in a regime where the coupling g is not so weak) and supported by the lattice data for the QGP thermodynamics [83].

On the other hand, for temperatures up to $T \sim 2T_c$ (namely the ones currently accessible in the experiments), the matter resulting from the heavy-ion collisions is nowadays often described [63] as a strongly interacting QGP (sQGP). In particular, a striking feature of the QGP matter obtained at RHIC is its hydrodynamical behaviour [84, 85] (characterized by a very low viscosity), which manifests itself in particular in the elliptic flow [86] observed in non-central collisions: the plasma obtained at RHIC seems to behave as a nearly ideal fluid whose expansion is driven by pressure gradients.

In order to explain the very small mean free path of the plasma particles required by the hydrodynamical scenario, a picture of the matter obtained at RHIC in terms of a system of hundreds of loosely bound states of *quasi-particles* ($q\bar{q}$, qg, gg...) has been recently proposed [63]. In such a framework one has to resort to some assumptions. Gluons and light quarks are treated as quasiparticles endowed with quite heavy thermal masses obtained from lattice calculations and the potential felt by them in the different color channels is got from the lattice $Q\overline{Q}$ free energy under the hypothesis of *Casimir scaling*.

The presence of such a pattern of bound states in the range of temperatures $T_c < T < 2T_c$ has been recently questioned on the basis of the analysis of the correlation between baryon number (B) and strangeness (S)[87]. The evaluation of the correlation coefficient $C_{BS} = -3\langle BS\rangle/\langle S^2\rangle$ should allow to discriminate between a scenario in which the relevant degrees of freedom in the QGP are weakly interacting quark and gluon *quasiparticles* or loosely bound states of the latters. The lattice data on the off-diagonal quark-number susceptibilities available so far seem to favour the first hypothesis.

Here we followed a different approach, starting from the case of a heavy $Q\overline{Q}$ pair placed in a thermalized QGP and extracting their interaction from the available lattice calculations. Indeed, we have exploited the lattice data for the heavy quark free energies to get information on the existence of $c\bar{c}$ and $b\bar{b}$ bound states above in the deconfined phase. We have examined the cases $N_f = 0$ [56], $N_f = 2$ [59] and also $N_f = 3$ [65], where lattice data are getting available. For the color singlet free energy we have adopted a parameterization which accounts for the effects of asymptotic freedom at short distances and displays an exponential screening at large distances. From the free energy we have then extracted the heavy quark potential, to be inserted into the Schrödinger equation. The latter has been solved numerically for the two interesting cases of charmonium and bottomonium.

For what concerns the charmonium, we have found a dissociation temperature $T_d \sim 2T_c$ for the 1S states (η_c and J/ψ). Also the excited states 1P and 2S appear to melt, but at temperatures slightly exceeding T_c.

On the other hand, the bottomonium spectrum displays a much larger number of bound states above T_c. In particular its ground state turns out to remain bound in the whole range of temperatures covered by our parameterization. By extrapolating the latter at larger T we get a dissociation temperature $T_d \sim 4 \div 6T_c$, depending upon the number of dynamical fermions. At fixed T/T_c, both for the charmonium and for the bottomonium, the system turns out to be more bound when the number of light flavors is increased.

Remarkably, in the range of temperatures of experimental interest covered in this paper a number of loosely bound $Q\overline{Q}$ states exists. Since the existence of states near zero binding energy entails a huge increase of the elastic cross sections at low relative momenta, this can help the approach to thermal equilibrium also of the heavy quarks.

An analogous situation occurs in the cross-over from the BCS theory of superconductivity to the Bose-Einstein condensation, much explored lately in ensembles of alkaline fermionic atoms confined in a magnetic trap. Indeed, by smoothly changing the external magnetic field B, one induces a smooth change of the energy of the two interacting atoms: if this energy is close to the one of a Feshbach resonance, a huge increase in the cross-section occurs [88, 89, 90, 91]. The striking analogy between B and T as control parameters is self-imposing.

In connection with the previous discussion on heavy quark thermalization, it would be highly desirable to have lattice data also for the $Q\bar{q}$ states, which are not yet available.

A phenomenological model has been recently proposed assuming the existence of *resonant* (not bound) D- and B- meson states above T_c [92]. In this scheme the transverse momentum distributions of the charmed quarks (anti-quarks) would approach their thermal equilibrium value much faster, due to isotropic resonant scattering on light anti-quarks (quarks). Indeed, recent PHENIX results for azimuthally averaged transverse momentum spectra of single electrons arising, in Au-Au collisions, from the decay of D- and B-mesons seem to be compatible with a thermalization scenario [93].

Furthermore, preliminary results from PHENIX and STAR on the elliptic flow of the above electrons tend to support a picture in which, due to strong rescattering, charmed quarks reach thermal equilibrium and follow the flow of the fireball [94, 95, 96, 97]. Hence, an extension of the present approach to the $Q\bar{q}$ ($q\bar{Q}$) states might shed light on the mechanism of thermalization of the heavy quarks.

Coming back to the present results, they offer the relevant possibility of evaluating the charmonium (bottomonium) multiplicity produced in heavy ion collisions at the experimental conditions of SPS, RHIC and LHC.

Indeed, a reliable estimate of the dissociation temperature of the different quarkonia is essential in order to predict how many of them, after being produced in the hard initial processes, survive in the QGP phase thus contributing to the final measured yields. The latter of course also contain, e. g., the charmonia that might be thermally produced during the hadronization process by $c\bar{c}$ recombination.

In particular, the knowledge of the in-medium quarkonium wave function and binding energy would allow a hopefully reliable estimate of the gluon-dissociation cross section of the J/ψ (and hence, via a detailed balance analysis, also of the cross section for the inverse process). Thus a kinetic rate equation accounting for both the dissociation and recombination processes can be dealt with: its solution, depending on how many $c\bar{c}$ pairs are produced in the initial state, should provide the number of J/ψ present at the end of the QGP phase. These issues will be addressed in future work.

Appendix A

Running coupling and perturbative potentials at short distances

In this appendix we collect the formulas resulting from the perturbative calculations of Refs. [68, 69, 70] of the heavy quark potential at short distances, where asymptotic freedom guarantees that the perturbative approach is justified.

The static QCD potential turns out to be given by:

$$V(r) = -C_F \frac{\alpha_{\overline{MS}}(\mu)}{r} \left(1 + v_1(r,\mu) \frac{\alpha_{\overline{MS}}(\mu)}{\pi} + v_2(r,\mu) \frac{\alpha^2_{\overline{MS}}(\mu)}{\pi^2} + \ldots \right), \tag{A.1}$$

where [69]

$$\begin{aligned} v_1(r,\mu) &= \frac{1}{4}\left[\frac{31}{9}C_A - \frac{20}{9}T_F n_f + 2\beta_0 \log(\mu r')\right], & \text{(A.2)} \\ v_2(r,\mu) &= \frac{1}{16}\left[\left(\frac{4343}{162} + 4\pi - \frac{\pi^2}{4} + \frac{22}{3}\zeta_3\right) C_A^2 - \left(\frac{1798}{81} + \frac{56}{3}\zeta_3\right) C_A T_F n_f \right. \\ &\quad - \left(\frac{55}{3} - 16\zeta_3\right) C_F T_F n_f + \left(\frac{20}{9} T_F n_f\right)^2 + \beta_0^2 \left(4\log^2(\mu r') + \frac{\pi^2}{3}\right) \\ &\quad \left. +2\left(\beta_1 + 2\beta_0\left(\frac{31}{9}C_A - \frac{20}{9}T_F n_f\right)\right)\log(\mu r')\right]. & \text{(A.3)} \end{aligned}$$

In the above $r' \equiv r\exp(\gamma_E)$ (γ_E is the Euler-Mascheroni constant), $C_A = 3$, $C_F = 4/3$, $T_F = 1/2$ and $\zeta_3 = \zeta_R(3)$ (the Riemann function of argument 3); moreover, $\alpha_{\overline{MS}}(\mu)$ is the QCD running coupling in the $\overline{MS}$ renormalization scheme fixed by the solution of the RGE:

$$\beta(\alpha_s(\mu^2)) = \frac{1}{\alpha_s(\mu^2)}\frac{\partial\alpha_s(\mu^2)}{\partial\log\mu^2} \equiv -\sum_{n=0}^{\infty}\beta_n\left(\frac{\alpha_s(\mu^2)}{4\pi}\right)^{n+1}. \tag{A.4}$$

The one-loop perturbative potential is obtained keeping only the first two terms of Eq. (A.1) and employing for $\alpha_{\overline{MS}}(\mu)$ the expression

$$\alpha_{\overline{MS}}(\mu) = \frac{4\pi}{\beta_0 \ln\dfrac{\mu^2}{\Lambda^2_{\mathrm{QCD}}}}\left(1 - \frac{\beta_1}{\beta_0^2}\frac{\ln\left(\ln\dfrac{\mu^2}{\Lambda^2_{\mathrm{QCD}}}\right)}{\ln\dfrac{\mu^2}{\Lambda^2_{\mathrm{QCD}}}}\right), \tag{A.5}$$

which arises from the solution of Eq. (A.4) with the two-loop beta function (i.e. considering only the first two terms of the series). Indeed the coefficients β_0 and β_1 do not depend on the renormalization scheme and are given by:

$$\beta_0 = 11 - \frac{2}{3}N_f, \qquad \beta_1 = 102 - \frac{38}{3}N_f. \tag{A.6}$$

On the other hand, for the two-loop perturbative potential one has to keep all the terms up to order α_s^3 displayed in Eq. (A.1). The evaluation of the running coupling should include also the three-loop coefficient β_2 of the beta-function, which is no more renormalization scheme independent. In evaluating the two-loop curve in Fig. 4.3 we have used Eq. (13) of Ref. [98], where the $\overline{MS}$ scheme is employed.

Clearly, Eq. (A.1) still depends on the parameters μ and Λ_{QCD}. The scale $\mu \sim r^{-1}$ is quite arbitrary: we chose $\mu = [r\exp(\gamma_E)]^{-1}$ as usually done in the literature. For what concerns Λ_{QCD} we employed the value suggested by a recent lattice collaboration [98] $\Lambda_{\mathrm{QCD}} = 261$ MeV for all the three cases ($N_f = 0, 2, 3$).

Appendix B

T-dependence of the fit parameters

In this appendix we quote the functions employed in fitting the temperature dependence of the parameters $a_0(T)$, $a_2(T)$ and $a_3(T)$ entering into the functional form we have adopted for the $Q\bar{Q}$ free energy (see Sect. 4.3).

As already mentioned in the text, since we have no phenomenological or theoretical hints to the functional form of the T-dependence of these parameters, we have tried to use the simplest expressions yielding a smooth fit and a "reasonable" χ^2 (say, of the order of a few units).

For $a_0(T)$ and $a_2(T)$ we have used the following forms:

$$a_0 = \frac{A_1^{(0)} x^{A_3^{(0)}} \exp[-A_0^{(0)} x]}{A_2^{(0)} x^2 - 1}, \tag{B.1}$$

$$a_2 = A_0^{(2)} \frac{A_1^{(2)} + A_2^{(2)} x^2 + x^4}{A_3^{(2)} + A_4^{(2)} x + x^3}, \tag{B.2}$$

where $x \equiv T/T_c$ and the $A_i^{(0)}$'s and $A_i^{(2)}$'s are fitting parameters.

Only in the case of $a_3(T)$ we have used an expression inspired by perturbative QCD, namely the one for the Debye mass (although, rigorously this parameter does not represent the Debye mass):

$$a_3 = \left(1 + \frac{N_F}{6}\right)^{1/2} x \left(A_0^{(3)} + \frac{A_1^{(3)}}{x^2} + \frac{A_2^{(3)}}{x^4} + \frac{A_3^{(3)}}{x^6} + \frac{A_4^{(3)}}{x^8}\right) g_{2-\text{loop}}(x), \tag{B.3}$$

where $g^2_{2-\text{loop}}/4\pi \equiv \alpha_{\overline{MS}}$ is the 2-loop coupling constant obtained by replacing μ/Λ_{QCD} with $4.8826x \cong (2\pi T_c/\Lambda_{\text{QCD}})x$, having used $T_c = 202$ MeV and $\Lambda_{\text{QCD}} = 261$ MeV. In the case $N_f = 3$, because of the larger errors affecting the parameterization of the free energy, we made the fit of a_3 stiffer by setting $A_4^{(3)} = 0$.

Bibliography

[1] F. Karsch and E. Laermann, Phys. Rev. D **50**, 6954 (1994).

[2] Z. Fodor and S.D. Katz, JHEP **0404**, 050 (2004).

[3] F. Karsch and E. Laermann, hep-ph/0305025, in *Quark Gluon Plasma 3*, edited by R.C. Hwa and X.N. Wang (World Scientific, Singapore, 2003), p. 1.

[4] Abreu *et al.*, Phys. Lett. B **477**, 28 (2000).

[5] Na50 Collaboration, Eur. Phys. J. C **39**, 335 (2005).

[6] X.N. Wang, Nucl.Phys. A **750**, 98 (2005).

[7] D. d'Enterria Eur. Phys. J. C **43**, 295 (2005).

[8] U.W. Heinz, hep-ph/0305025, Lecture Notes for lectures presented at the 2nd CERN - Latin-American School of High-Energy Physics.

[9] F. Becattini, M. Gazdzicki and J. Sollfrank, Eur. Phys. J. C **5**, 143 (1998).

[10] T. Matsui and H. Satz, Phys. Lett. B **178**, 416 (1986).

[11] J. Rafelski and B. Müller, Phys. Rev. Lett. **48**, 1066 (1982).

[12] E. Shuryak, Prog. Part. Nucl. Phys. **53**, 273 (2004).

[13] J.P. Blaizot and E. Iancu, Phys. Rept. **359** (2002), 355.

[14] A. Rebhan Nucl. Phys. B **430**, 319 (1994).

[15] A. Peshier, B. Kampfer, O.V. Pavlenko and G. Soff Phys. Rev. D **54**, 2399 (1996).

[16] M. Le Bellac, Thermal Field Theory, Cambridge University Press, 1996.

[17] B. Vanderheyden and G. Baym, hep-ph/9803300.

[18] E. Braaten, R.D. Pisarski and T.C. Yuan, Phys.Rev.Lett. **64** (1990), 2242.

[19] M.G. Mustafa, M.H. Thoma , Pramana **60** (2003), 711.

[20] F. Karsch, M.G. Mustafa, M.H. Thoma, Phys. Lett. B**497** (2001), 249.

[21] T. Renk, R. Schneider, W. Weise, Phys.Rev. C**66** (2002).

[22] J.P. Blaizot, E. Iancu, A. Rebhan, Eur.Phys.J. C**27** (2003), 433.

[23] J.P. Blaizot and E. Iancu, Phys. Rev. D**63** (2001)

[24] J.P. Blaizot, E. Iancu, A. Rebhan, Phys. Lett. B**523** (2001), 143.

[25] J.P. Blaizot, Lect. Notes Phys. **583** (2002), 117.

[26] J.P. Blaizot, E. Iancu, A. Rebhan, Phys. Lett. B**470** (1999), 181.

[27] S. Datta, F. Karsch, P. Petreczy, and I. Wetzorke, Phys. Rev. D **69**, 094507 (2004).

[28] M. Asakawa, T. Hatsuda, and Y. Nakahara, Nucl. Phys. A **715**, 863 (2003).

[29] M. Asakawa and T. Hatsuda, Phys. Rev. Lett. **92**, 012001 (2004).

[30] E. Shuryak, Prog.Part.Nucl.Phys. **53** (2004), 273-303.

[31] E. Shuryak, hep-ph/0403127.

[32] M. Caselle, M. Hasenbusch, P. Provero, Nucl.Phys.Proc.Suppl. **83** (2000), 715.

[33] M. Caselle, M. Hasenbusch, P. Provero, K. Zarembo, Nucl.Phys. B**623** (2002), 474.

[34] R. Savit, Rev.Mod.Phys. **52** (1980), 453.

[35] M.H. Thoma, Z.Phys. C**66** (1995), 491.

[36] E. Braaten, R.D. Pisarski, Nucl.Phys. B**337** (1990), 569.

[37] F. Karsch, E. Laermann, hep-lat/0305025.

[38] F. Karsch *et al.*, Nucl.Phys. A**715** (2003), 701-704.

[39] F. Karsch *et al.*, Phys.Lett. B**530** (2002) 147-152.

[40] M. Laine, M. Vepsalainen, JHEP 0402 (2004) 004.

[41] A. Peshier, M. Thoma, Phys.Rev.Lett. **84** (2000), 841.

[42] H.A. Weldon, Phys.Rev. D**61** (2000) 036003.

[43] A. Beraudo, A. De Pace, M. Martini and A. Molinari, nucl-th/0409039.

[44] P. Chakraborty, M.G. Mustafa, M.H. Thoma, Phys.Rev. D**67**:114004, 2003.

[45] P. Chakraborty, M.G. Mustafa, M.H. Thoma, Phys.Rev. D**68**:085012, 2003

[46] R.L. Thews, hep-ph/0206179, in *New States of Matter in Hadronic Interactions*, edited by H.T. Elze, E. Ferreira, T. Kodama, J. Rafelski, and R.L. Thews (AIP, New York, 2002).

[47] S. Gupta and H. Satz, Phys. Lett. B **283**, 439 (1992).

[48] S. Digal, D. Petreczy, and H. Satz, Phys. Lett. B **514**, 57 (2001).

[49] S. Digal, D. Petreczy, and H. Satz, Phys. Rev. D **64**, 094015 (2001).

[50] F. Karsch, hep-lat/0502014.

[51] D. Kharzeev, C. Lourenco, M. Nardi, and H. Satz, Z. Phys. C **74**, 307 (1997).

[52] P. Braun-Munzinger and J. Stachel, Phys. Lett. B **490**, 196 (2000).

[53] L. Grandchamp and R. Rapp, Phys. Lett. B **523**, 60 (2001).

[54] L. Grandchamp and R. Rapp, Nucl. Phys. A **709**, 415 (2002).

[55] L.D. McLerran and B. Svetitsky, Phys. Rev. D **24**, 450 (1981).

[56] O. Kaczmarek, F. Karsch, P. Petreczky, and F. Zantow, Phys. Lett. B **543**, 41 (2002).

[57] O. Kaczmarek, F. Karsch, P. Petreczky, and F. Zantow, Nucl. Phys. Proc. Suppl. **129**, 560 (2004).

[58] O. Kaczmarek, S. Ejiri, F. Karsch, P. Petreczky, and F. Zantow, Prog. Theor. Phys. Suppl. **153**, 287 (2004).

[59] O. Kaczmarek and F. Zantow, hep-lat/0503017.

[60] C.Y. Wong, Phys. Rev. C **65**, 034902 (2002).

[61] C.Y. Wong, J. Phys. G **28**, 2349 (2002).

[62] C.Y. Wong, hep-ph/0408020.

[63] E.V. Shuryak and I. Zahed, Phys. Rev. D **70**, 054507 (2004).

[64] R.L. Thews, M. Schroedter, and J. Rafelski, Phys. Rev. C **63**, 054905 (2001).

[65] P. Petreczky and K. Petrov, Phys. Rev. D **70**, 054503 (2004).

[66] S. Nadkarni, Phys.Rev. D **33**, 3738 (1986).

[67] E. Braaten and A. Nieto, Phys. Rev. Lett. **74** (1995), 3530.

[68] M. Peter, Nucl.Phys. B **501**, 471 (1997).

[69] M. Melles, Phys. Rev. D **62**, 074019 (2000).

[70] Y. Schröder, Phys. Lett. B **447**, 321 (1999).

[71] O. Kaczmarek and F. Zantow, hep-lat/0506019.

[72] S. Eidelman em et al. (Particle Data Group), Phys. Lett. B **592**, 1 (2004) (http://pdg.lbl.gov).

[73] E. Eichten, K. Gottfried, T. Kinoshita, K. D. Lane, and T.M. Yan, Phys. Rev. D **21**, 203 (1980).

[74] N. Brambilla *et al.*, hep-ph/0412158.

[75] D. Kharzeev and H. Satz, Phys. Lett. B **366**, 316 (1996).

[76] D. Kharzeev *et al.*, Z. Phys. C **74**, 307 (1997).

[77] B. Alessandro *et al.*, Eur. Phys. J. C **33**, 31 (2004).

[78] R. Arnaldi, talk at QM2005.

[79] Y. Akiba, nucl-ex/0510008.

[80] H. Satz, hep-ph/0512217.

[81] F. Karsch, D. Kharzeev and H. Satz, hep-ph/0512239

[82] J.P. Blaizot, E. Iancu, and A. Rebhan, hep-ph/0303185, in *Quark Gluon Plasma 3*, edited by R.C. Hwa and X.N. Wang (World Scientific, Singapore, 2003), p. 60.

[83] F. Karsch, E. Laermann, and A. Peikert, Phys. Lett. B **478**, 447 (2000).

[84] D. Teaney, J. Laueret, and E. Shuryak, nucl-th/0110037.

[85] P.F. Kolb and U.W. Heinz, nucl-th/0305084, in *Quark Gluon Plasma 3*, edited by R.C. Hwa and X.N. Wang (World Scientific, Singapore, 2003), p. 634.

[86] J.Y. Ollitrault, Phys. Rev. D **46**, 229 (1992).

[87] V. Koch, A. Majumder, and J. Randrup, nucl-th/0505052.

[88] E. Timmermans, P. Tommasini, M. Hussein, and A. Kerman, Phys. Rep. **315**, 199 (1999).

[89] A.J. Leggett, Rev. Mod. Phys. **73**, 307 (2001).

[90] R.A. Duine and H.T.C. Stoof, Phys. Rep. **396**, 115 (2004).

[91] K.M. O Hara, S.L. Hemmer, M.E. Gehm, S.R. Granade, and J.E. Thomas, Science **298**, 2179 (2002).

[92] H. van Hees and R. Rapp, Phys. Rev. C **71**,034907 (2005).

[93] S. Batsouli, S. Kelly, M. Gyulassy, and J.L. Nagle, Phys. Lett. B **557**, 26 (2003).

[94] PHENIX Collaboration (S. Kelly *et al.*), J. Phys. G **30**, S1189 (2004).

[95] PHENIX Collaboration (S.S. Adlet *et al.*), nucl-ex/0502009.

[96] STAR Collaboration (F. Laue *et al.*), J. Phys. G **G31**, S27 (2005).

[97] V. Greco, C.M. Ko, and R. Rapp, Phys. Lett. B **595**, 202 (2004).

[98] M. Gockeler *et al.*, hep-ph/0502212.